

University of Hohenheim
Institute of Soil Science and Land Evaluation
Department of Biogeophysics (310d)

**Towards a better understanding of land surface exchange processes
over agricultural crop stands**

Dissertation to obtain the doctoral degree of Agricultural Sciences

Faculty of Agricultural Sciences

Presented by

Kristina Bohm

born Imukova

from Voronezh, Russia

2020

This thesis was accepted as a doctoral thesis (Dissertation) in fulfillment of the regulations to acquire the doctoral degree "Doktor der Agrarwissenschaften" by the Faculty of Agricultural Sciences at University of Hohenheim on 13.12.2019

Date of the oral examination: 1.07.2020

Examination Committee

Chairperson of the oral examination	Prof. Dr. Andrea Knierim
Supervisor and Reviewer	Prof. Dr. Thilo Streck
Co-Reviewer	Prof. Dr. Volker Wulfmeyer
Additional examiner	Prof. Dr. Andreas Fangmeier

Contents

1 Summary	1
2 Zusammenfassung	3
3 General Introduction	6
3.1 Land Surface Models	6
3.2 Eddy covariance method.....	7
3.3 Croplands	8
3.3 Scope of the thesis.....	10
4 Energy balance closure on a winter wheat stand: comparing the eddy covariance technique with the soil water balance method	12
Abstract	13
4.1 Introduction.....	13
4.2 Materials and methods	14
4.3 Results.....	19
4.4 Discussion	21
4.5 Conclusions.....	23
References.....	24
5 Determining the Spatial and Temporal Dynamics of the Green Vegetation Fraction of Croplands using high-resolution RapidEye satellite images	26
Abstract	27
5.1 Introduction.....	27
5.2 Materials and methods	28
5.3 Results.....	30
5.4 Discussion	35
5.5 Conclusions.....	36
References.....	37
6 Distinguishing between early and late covering crops in the land surface model Noah-MP: Impact on simulated surface energy fluxes and temperature	38
Abstract	39
6.1 Introduction.....	39
6.2 Materials and methods	40
6.3 Results.....	44
6.4 Discussion	46
6.5 Conclusions.....	51
References.....	52
7 General Discussion and Conclusions	54
8 References	57
Acknowledgments	61
Curriculum Vitae	63

1 Summary

Weather and climate models are useful tools for projecting the influence of global climate change on the regional scale. These models are critically dependent on an accurate representation of soil-plant-atmosphere interactions, which are simulated by Land Surface Models (LSMs). The present PhD thesis was designed to improve the representation of land surface exchange processes of croplands in the Noah-MP land surface model. My thesis aims: a) to elucidate the nature of the energy imbalance over a winter wheat stand and to identify the appropriate post-closure method for the study region Kraichgau, southwest Germany; b) to improve the representation of the green vegetation fraction (GVF) dynamics of croplands in the Noah-MP for a more accurate computation of surface energy and water fluxes; and c) to determine the effect of aggregating different crop types with various shares into a single generic cropland class on the simulation of water and energy exchange between land surface and atmosphere. In order to achieve these goals, I performed several experimental and modeling studies.

The eddy covariance (EC) technique is a widely used method for assessing the turbulent exchange of water and energy between the land surface and atmosphere. The energy balance of fluxes measured with the EC method is typically not closed. The sum of the turbulent fluxes of latent heat (LE) and sensible heat (H) measured with the EC technique is systematically lower than the available energy estimated as the difference between net radiation and ground heat flux. The nature of the missing energy is usually unknown, which hampers using EC data for calibrating and validating LSMs. Several post-closure methods are used to achieve energy balance closure. The measured turbulent fluxes are usually adjusted with either LE flux, H flux or the Bowen ratio (BR) post-closure method. The first method adds the missing energy fully to the latent heat flux. The second method, in contrast, assigns the energy residual fully to the measured sensible heat flux, while the latent heat flux remains unchanged. The third method assumes the energy residual has the same Bowen ratio ($Bo=H/LE$) as the measured turbulent fluxes. In the present research, I compared evapotranspiration rates measured with the EC technique against measurements conducted using the soil water balance method. I tested the above-described post-closure methods and provided recommendations on the post-processing of the EC data. Our results show that the EC method reliably measures the evapotranspiration rate at our study site and, therefore, the H post-closure method is recommended for calibrating and

parametrizing the Noah-MP at our site. Nevertheless, further investigation of the energy imbalance problem of the EC data was recommended.

In Noah-MP, the earth's surface is presented as a set of different land use classes, one of them being “cropland” or “generic cropland class”. At the regional scale, this class may cover a considerable part of the simulation domain. The generic cropland class is a combination of different crops varying in phenology, planting and harvesting dates, canopy and rooting characteristics, senescence dynamics, etc. In the Noah-MP, the vegetation dynamics and its seasonal development are described by GVF and the leaf area index (LAI). GVF and LAI are key input plant variables for forcing evapotranspiration schemes of the LSM. In standard applications of Noah-MP, the GVF is obtained from a global map with a coarse resolution ($15 \times 15 \text{ km}^2$ grid cell size). In the present research I improved the representation of the GVF dynamics of croplands by deriving the gridded GVF data of a study region at a high spatial resolution ($5 \times 5 \text{ m}^2$) using RapidEye satellite data. The analyses of the new data showed that, at the regional scale, GVF has a bimodal distribution during the growing seasons. This distribution is formed by two different crop types varying in phenology and growth dynamics: early covering crops (ECC, ex.: winter wheat, winter rapeseed, winter barley) and late covering crops (LCC, ex.: corn, silage maize, sugar beet). The present PhD thesis implemented a new parametrization for ECC and LCC and studied its effect on the simulation of the land surface exchange processes. The results were compared against fluxes simulated using a generic cropland class of Noah-MP. The present research shows that ECC and LCC vary significantly in the seasonal dynamics of energy- and water exchange between land surface and atmosphere. Merging both crop groups into one land use class, as introduced in Noah-MP, is an oversimplification. The current thesis recommends splitting the generic cropland class of Noah-MP into ECC and LCC because this approach has the potential to improve the simulation of land surface exchange processes, particularly during transition periods and late in the vegetation period.

2 Zusammenfassung

Wetter- und Klimamodelle sind nützliche Werkzeuge, um den Einfluss des globalen Klimawandels auf die regionale Ebene zu projizieren. Diese Modelle sind entscheidend von einer genauen Darstellung der Wechselwirkungen zwischen Boden, Pflanzen und Atmosphäre abhängig, welche durch „Land Surface Models“ (LSMs) simuliert werden. Die Dissertation wurde erstellt, um die Darstellung von Landoberflächenaustauschprozessen von Ackerland im Noah-MP-Landoberflächenmodell zu verbessern. In meiner Doktorarbeit geht es um: a) die Art des Energiegleichgewichts über einem Winterweizenbestand aufzuklären und die geeignete Post-Closure-Methode für die Region Kraichgau (Südwestdeutschland) zu identifizieren; b) die Darstellung der Dynamik der Grünen Vegetationsfraktion (*GVF*) von Anbauflächen im Noah-MP für eine genauere Berechnung der Oberflächenenergie und der Wasserflüsse zu verbessern; und c) um die Auswirkungen der Aggregation verschiedener Kulturarten mit unterschiedlichen Anteilen zu einer einzigen generischen Ackerflächenklasse auf die Simulation des Wasser- und Energieaustauschs zwischen Landoberfläche und Atmosphäre zu bestimmen. Damit diese Ziele erreicht werden, habe ich mehrere experimentelle und Modellierungsstudien durchgeführt.

Die Eddy Covariance (EC)-Technik ist eine weit verbreitete Methode zur Beurteilung des turbulenten Austauschs von Wasser und Energie zwischen Landoberfläche und Atmosphäre. Die Energiebilanz der mit der EC-Methode gemessenen Flüsse ist in der Regel nicht geschlossen. Die Summe der turbulenten Ströme von latenter Wärme (*LE*) und sensibler Wärme (*H*), gemessen mit der EC-Technik, ist systematisch niedriger als die verfügbare Energie, die als Differenz zwischen Netto-Strahlung und Erdwärmestrom geschätzt wird.

Die Art der fehlenden Energie ist in der Regel unbekannt, was die Verwendung von EC-Daten zur Kalibrierung und Validierung von LSMs erschwert. Um den Abschluss der Energiebilanz zu erreichen, werden mehrere Nachverschlussmethoden eingesetzt. Die gemessenen turbulenten Ströme werden in der Regel entweder mit *LE*-Fluss, *H*-Fluss oder dem Bowen-Ratio (*BR*) Post-Closure-Verfahren eingestellt. Die erste Methode addiert die fehlende Energie vollständig zum latenten Wärmestrom. Das zweite Verfahren hingegen ordnet den Energierückstand vollständig dem gemessenen fühlbaren Wärmestrom zu, während der Latentwärmestrom unverändert bleibt. Die dritte Methode geht davon aus, dass der Energierückstand das gleiche Bowen-Verhältnis ($Bo=H/LE$) aufweist wie die gemessenen turbulenten Strömungen. In der vorliegenden Studie

habe ich die mit der EC-Technik gemessenen Evapotranspirationsraten mit Messungen nach der Bodenwasserbilanz-Methode verglichen. Ich habe die oben beschriebenen Post-Closure-Methoden getestet und Empfehlungen zur Nachbearbeitung der EC-Daten gegeben. Unsere Ergebnisse zeigen, dass die EC-Methode die Evapotranspirationsrate an unserem Studienort zuverlässig misst und daher die H-Post-Verschlussmethode für die Kalibrierung und Parametrierung des Noah-MP an unserem Standort empfohlen wird. Dennoch wurde eine weitere Untersuchung des Energiegleichgewichtsproblems der EC-Daten empfohlen.

In Noah-MP wird die Erdoberfläche als eine Reihe von verschiedenen Landnutzungsklassen dargestellt, von denen eine "Ackerland" oder "allgemeine Ackerlandklasse" ist. Auf regionaler Ebene kann diese Klasse einen erheblichen Teil der Simulationsdomäne abdecken. Die generische Ackerlandklasse ist eine Kombination verschiedener Kulturen, die sich in der Phänologie, dem Pflanz- und Erntezeitpunkt, den Eigenschaften von Kronen und Wurzeln, der Seneszenzdynamik usw. unterscheiden. Im Noah-MP wird die Vegetationsdynamik und ihre saisonale Entwicklung durch den GVF und den Blattflächenindex (LAI) beschrieben. GVF und LAI sind wichtige Input-Pflanzenvariablen für die Forcierung von Evapotranspirationsverfahren der LSM. In Standardanwendungen von Noah-MP wird das GVF aus einer globalen Karte mit einer groben Auflösung ($15 \times 15 \text{ km}^2$ Rasterzellgröße) gewonnen. In der vorliegenden Forschung habe ich die Darstellung der GVF-Dynamik von Ackerland verbessert, indem ich die gitterförmigen GVF-Daten einer Untersuchungsregion mit hoher räumlicher Auflösung ($5 \times 5 \text{ m}^2$) unter Verwendung von RapidEye-Satellitendaten abgeleitet habe. Die Analysen der neuen Daten zeigten, dass die GVF auf regionaler Ebene eine bimodale Verteilung während der Vegetationsperiode aufweist. Diese Verteilung wird durch zwei verschiedene Kulturarten gebildet, die sich in Phänologie und Wachstumsdynamik unterscheiden: frühe Deckkulturen (ECC, z.B.: Winterweizen, Winterraps, Wintergerste) und späte Deckkulturen (LCC, z.B.: Mais, Silomais, Zuckerrüben). Die vorliegende Dissertation implementierte eine neue Parametrisierung für ECC und LCC, und studierte ihre Auswirkungen auf die Simulation der Landoberflächenaustauschprozesse. Die Ergebnisse wurden mit Flussmitteln verglichen, die mit einer generischen Ackerlandklasse von Noah-MP simuliert wurden. Die vorliegende Studie zeigt, dass ECC und LCC in der saisonalen Dynamik des Energie- und Wasseraustauschs zwischen Landoberfläche und Atmosphäre stark variieren. Die Zusammenführung beider

Kulturgruppen zu einer Landnutzungs-kategorie, wie sie in Noah-MP eingeführt wurde, ist eine übertriebene Vereinfachung. Die aktuelle Arbeit empfiehlt die Aufteilung der generischen Anbauflächen-kategorie von Noah-MP in ECC und LCC, da dieser Ansatz das Potenzial hat, die Simulation von Landoberflächen-austauschprozessen zu verbessern, insbesondere in Übergangszeiten und am Ende der Vegetationsperiode.

3 General Introduction

3.1 Land Surface Models

The present PhD thesis was prepared in the frame of the project P2 “Soil-Plant-Atmosphere Interactions at the Regional Scale” of the DFG Research Unit (RU) 1695 “Agricultural Landscapes under Global Climate Change. Processes and feedbacks on a regional scale”. The major goal of RU 1695 was to assess the impact of global climate change on agricultural landscapes in southwest Germany. This work was designed to improve existing atmosphere-, land surface-, crop growth- and land use decision models and to integrate them into one land system model. The new model system would help to better predict and analyze future effects of climate change on the structure and functions of agricultural land use as well as on human-environmental interactions at a high spatial and temporal resolution.

Land surface models simulate the exchange of energy, water, and momentum between soil, vegetation and atmosphere. LSMs are generally coupled to weather and climate models, providing them with key information on the partitioning of net radiation into sensible (H), latent (LE) and soil heat fluxes (G). The energy partitioning between turbulent fluxes H and LE depends on the physical and physiological properties of the land surface. Physical properties include variables such as albedo, roughness and soil texture. Physiological properties are plant-specific variables such as leaf area index, green vegetation fraction and rooting depth. Energy partitioning significantly influences the evolution of the atmospheric boundary layer (ABL), which in turn strongly influences the initiation of convection, cloud formation, and ultimately the location and strength of precipitation (Crawford et al. 2001, Koster et al. 2006, Santanello Jr. et al. 2013, van Heerwaarden et al. 2009, Milovac et al. 2016).

A widely used LSM is Noah (Chen and Dudhia 2001). This model was developed several decades ago and has been continuously improved and tested in recent years. Later, Noah was extended to Noah-MP by introducing multi-physics options and a semi-tile approach (bare and vegetated tile) to better represent land surface heterogeneities (Niu et al. 2011). Noah was developed to be coupled with the Mesoscale Meteorology Model 5 (Dudhia 1993) and was later coupled with the Weather Research and Forecasting (WRF) model (Skamarock et al. 2008).

3.2 Eddy covariance method

The eddy covariance (EC) technique is a widely used method for developing and testing LSMs. The EC technique is the only one that enables a direct and continuous measurement of the energy and water vapor fluxes near the land surface, in real time, *in situ*, and without disturbing the crop environment. These advantages make the EC method more attractive for the scientific community than other common micrometeorological and ecological methods such as the chamber method, Bowen ratio method, etc. Several networks of EC stations (ex. FLUXNET, Ameriflux, NEON, etc.) have been installed worldwide to obtain a detailed image of the exchange of energy, water and trace gases between land surface and atmosphere over different land use types and crop groups at a high temporal resolution. Despite the great importance and actuality of the EC technique, it is not perfect. One problem of the EC method is the lacking energy balance closure (EBC). Accordingly, the law of conservation of energy often cannot be fulfilled by EC measurements. The sum of the EC-determined turbulent fluxes LE and H is systematically lower than the available energy computed as the difference between net radiation (R_n) and ground heat flux (G). Various studies reported EBC ranges between 70 to 90% over various land use types (Oncley et al. 2007, Wilson et al. 2002, Twine et al. 2000). Low EBCs (60-80 %) were mainly observed at various agricultural sites and bare soil, whereas over forest they were typically higher (80-90 %) (Charuchittipan et al. 2014, Stoy et al. 2013, Foken, 2008, Panin and Bernhofer 2008, Wilson et al. 2002). The uncertainty arising from the energy imbalance hampers the use of EC data for model parameterization and testing (Ingwersen et al. 2011, Ingwersen et al. 2015, El Maayar et al. 2008, Falge et al. 2005). Numerous studies were conducted to investigate the reasons for this imbalance, but the nature of the energy gap is still not fully understood. Most researchers concluded that a calibration of field instruments and other tool errors as well as data-processing errors cannot be a major reason for the imbalance (Oncley et al. 2007, Foken 2008, Mauder et al. 2006). The nature of the gap is apparently site-specific, and the missing energy could consist of either LE or H or both or other neglected storage terms. Several authors reported that underestimated G and neglected minor storage terms such as the air heat storage, biomass heat storage and energy consumption by photosynthesis can also contribute to closing the energy balance (Eshonkulov et al. 2019, Guo et al. 2009; Jacobs et al. 2008; Meyers and Hollinger 2004).

Various methods are available for achieving energy balance closure for use in land surface models. The measured turbulent fluxes are usually adjusted with either H flux, LE flux or, most often, the Bowen ratio (BR) post-closure method. These methods fully add the missing energy to the measured turbulent fluxes, assuming that the available energy is measured correctly. The H post-closure method adds the lacking energy fully to the measured H flux (Ingwersen et al. 2011, Ingwersen et al. 2015, Gayler et al. 2013). In contrast, the LE flux post-closure method assigns the energy residual fully to LE , leaving the sensible heat flux unaltered (Falge et al. 2005). The BR post-closure method assumes that the missing energy has the same Bowen ratio ($B_o=H/LE$) as the measured turbulent fluxes (Twine et al. 2000, Barr et al. 1994).

3.3 Croplands

In LSMs, the earth's surface is presented as a combination of various land use classes such as “urban”, “forest”, “grassland”, “cropland” and others. In the regional LSMs, cropland may cover a considerable part of the simulation domain. In 2015, agricultural land accounted for 41.1% of the total area in the European Union (Eurostat 2018). On the regional scale, the share of cropland can be much higher. For example, in Denmark it was reported at 62% of the total area in 2016 according to the World Bank collection of development indicators, compiled from officially recognized sources. In Germany, in 2016, agricultural land covered 47.7 % of the total area (Worldbank 2019).

The cropland land use classes, as defined in LSMs, stand for a combination of different crops varying in phenology, planting and harvesting dates, canopy structure, plant rooting, senescence dynamics, etc. It can include different crop types such as summer and winter crops, legumes and non-legumes, and/or C3 and C4 plants. Within the cropland class, the combination of crops and their share can vary significantly from season to season and from region to region. Each entity of this land use type shows distinct seasonal dynamics. Some crops develop early in spring, achieve maturity and already become senescent in mid-summer; whereas other crops are planted in spring and harvested in mid-autumn. During the germination stage, roots are normally a few centimeters long, whereas at the end of the growing season the root system of some plants may reach a depth of one or more meters. The leaf area index (LAI) is zero after sowing and may

attain a value of ~6 during the season, returning to close to zero after harvest. Depending on the crop rotation, the fields may be cropped or left bare over winter.

In Noah-MP, the agricultural area is represented by general land use classes such as “Dryland Cropland and Pasture”, “Irrigated Cropland and Pasture” or “Mixed Dryland/Irrigated Cropland and Pasture”. For simplification, in this manuscript these classes are referred to as “generic cropland classes”. The plant variables, green vegetation fraction (GVF) and LAI are used in the Noah-MP to describe the vegetation dynamics over the season. GVF is a grid-cell fraction covered by a green canopy and thus represents the horizontal density of the vegetation in each grid cell (Rundquist 2002, Gutman and Ignatov 1998). LAI describes the vertical density of the canopy in the LSM. GVF and LAI vary significantly during the vegetation period, altering the physical parameters of the surface such as albedo, roughness and emissivity. These, in turn, have a considerable effect on water and energy fluxes at the land-atmosphere interface. Accurately representing LAI and GVF is therefore considered essential for better estimates of surface fluxes (Chen and Xie 2011, Crawford et al. 2001, Refslund et al. 2014). In Noah-MP, GVF and LAI are prescribed in lookup tables, i.e. they do not depend on the preceding weather conditions during a simulation.

Noah-MP offers different options to parameterize the dynamics of GVF. Depending on data availability the user can select between several options. One of the preferable options is to use remotely sensed gridded GVF data. If gridded GVF data are absent, GVF is estimated from LAI, which are predefined for each land cover in Noah-MP or set up as maximum possible GVF.

In standard applications, Noah-MP uses GVF values derived from normalized difference vegetation index (NDVI) obtained from the NESDIS/NOAA satellite data. These data have a 0.15° spatial resolution ($15 \times 15 \text{ km}^2$ grid cell size). This means that different land use classes are merged within one grid cell, for example, a combination of agricultural, forest and urban areas. Such a coarse resolution cannot properly characterize the land cover elements, yielding major uncertainties when computing physiological variables of the grid-cell elements. Seasonal GVF and LAI dynamics derived from these maps are strongly smoothed compared to the actual dynamics. Several authors have shown that LSMs are highly sensitive to physical, biological

parameters and state variables of the landscape. They emphasize the need for finer GVF grid data for use in the Noah-MP LSM, given their importance for ABL evolution. (Milovac et al. 2016, Nielsen et al. 2013).

3.3 Scope of the thesis

The scientific aim of my research was to improve our understanding and description of soil-plant-atmosphere interactions of croplands in the Noah-MP land surface model. My thesis aims

- a) to elucidate the nature of the energy balance gap over a winter wheat stand and to identify the appropriate post-closure method for the study region Kraichgau, Southwest Germany;
- b) to improve the representation of the GVF dynamics of croplands in Noah-MP for a more accurate simulation of water and energy exchange between the land surface and atmosphere;
- c) to determine the effect of aggregating different crop types with various shares into a single generic cropland class on the simulation of energy and water fluxes.

The thesis contains three published papers:

The first study compares the evapotranspiration measured using the EC method (ET_{EC}) with the evapotranspiration determined using the soil water balance method (ET_{WB}); the latter does not depend on an a priori assumption on the composition of the energy residual. During two growing seasons, we continuously measured (in a half-hourly resolution) the latent heat and sensible heat fluxes at winter wheat stands using the EC technique. Measured fluxes were adjusted with either the Bowen ratio, H or LE post-closure method and compared with ET_{WB} . ET_{WB} was computed based on rainfall, seepage and soil water storage measurements. The soil water storage term was measured over a soil depth of 1.5 m. The soil water content was measured at sixteen locations within the footprint of an EC station. In the second growing season, the volumetric soil water content was additionally continuously measured with sixteen capacitance soil moisture sensors. The measurements were conducted in 15 min resolution in 10 cm intervals down to 90 cm depth. Details are given in the Chapter 4.

The second study derives gridded GVF data of Kraichgau region in a high spatial resolution (5 m x 5 m) from RapidEye satellite images. The GVF dynamics were determined based on the

Normalized Difference Vegetation Index (NDVI) calculated from the red and near-infrared bands of the satellite images. The satellite GVF data were calibrated and validated against ground truth measurements. Based on the obtained calibration scheme, we derived GVF maps in a monthly resolution for the study region and studied the GVF dynamics of different crops over the growing season. For details see Chapter 5.

The third study quantifies the effect of splitting the generic cropland class “Cropland and Pasture” of Noah-MP into early covering crops (ECC, e.g.: winter wheat, winter rapeseed, winter barley) and late covering crops (LCC, ex.: corn, silage maize, sugar beet) on surface energy fluxes and temperature. We further studied the influence of increasing the share of late covering crops (driven by the growth of biomass production in the study region) on energy partitioning at the land surface. For the simulations we used the GVF data derived in the previous study and measured LAI data. For more information see Chapter 6.

4 Energy balance closure on a winter wheat stand: comparing the eddy covariance technique with the soil water balance method

Kristina Imukova, Joachim Ingwersen, Michael Hevart and Thilo Streck

Institute of Soil Science and Land Evaluation, Department of Biogeophysics, University of Hohenheim, 70593 Stuttgart, Germany

Chapter 4 is published with the consent of the Copernicus Publications on behalf of the European Geosciences Union under the Creative Commons Attribution 4.0 License. The original publication was in: Journal of Biogeosciences (2016), Volume 13, Pages 63–75. It can be found under the following link: <https://doi.org/10.5194/bg-13-63-2016>

Biogeosciences, 13, 63–75, 2016
www.biogeosciences.net/13/63/2016/
doi:10.5194/bg-13-63-2016
© Author(s) 2016. CC Attribution 3.0 License.



Energy balance closure on a winter wheat stand: comparing the eddy covariance technique with the soil water balance method

K. Imukova, J. Ingwersen, M. Hevart, and T. Streck

Institute of Soil Science and Land Evaluation, University of Hohenheim, 70593 Stuttgart, Germany

Correspondence to: K. Imukova (kristina.imukova@uni-hohenheim.de)

Received: 26 March 2015 – Published in Biogeosciences Discuss.: 6 May 2015

Revised: 15 November 2015 – Accepted: 11 December 2015 – Published: 15 January 2016

Abstract. The energy balance of eddy covariance (EC) flux data is typically not closed. The nature of the gap is usually not known, which hampers using EC data to parameterize and test models. In the present study we cross-checked the evapotranspiration data obtained with the EC method (ET_{EC}) against ET rates measured with the soil water balance method (ET_{WB}) at winter wheat stands in southwest Germany. During the growing seasons 2012 and 2013, we continuously measured, in a half-hourly resolution, latent heat (LE) and sensible (H) heat fluxes using the EC technique. Measured fluxes were adjusted with either the Bowen-ratio (BR), H or LE post-closure method. ET_{WB} was estimated based on rainfall, seepage and soil water storage measurements. The soil water storage term was determined at sixteen locations within the footprint of an EC station, by measuring the soil water content down to a soil depth of 1.5 m. In the second year, the volumetric soil water content was additionally continuously measured in 15 min resolution in 10 cm intervals down to 90 cm depth with sixteen capacitance soil moisture sensors. During the 2012 growing season, the H post-closed LE flux data ($ET_{EC} = 3.4 \pm 0.6 \text{ mm day}^{-1}$) corresponded closest with the result of the WB method ($3.3 \pm 0.3 \text{ mm day}^{-1}$). ET_{EC} adjusted by the BR ($4.1 \pm 0.6 \text{ mm day}^{-1}$) or LE ($4.9 \pm 0.9 \text{ mm day}^{-1}$) post-closure method were higher than the ET_{WB} by 24 and 48 %, respectively. In 2013, ET_{WB} was in best agreement with ET_{EC} adjusted with the H post-closure method during the periods with low amount of rain and seepage. During these periods the BR and LE post-closure methods overestimated ET by about 46 and 70 %, respectively. During a period with high and frequent rainfalls, ET_{WB} was in-between ET_{EC} adjusted by H and BR post-closure methods. We conclude that, at most observation

periods on our site, LE is not a major component of the energy balance gap. Our results indicate that the energy balance gap is made up by other energy fluxes and unconsidered or biased energy storage terms.

1 Introduction

The eddy covariance (EC) method is a widely used, long-standing method to directly measure turbulent energy and matter fluxes near the land surface. As a quality check, the energy balance closure (EBC) of eddy covariance flux measurements may be computed. According to the first law of thermodynamics, energy must be conserved. At the land surface, the surface energy budget equation, written here for its major components, must be fulfilled:

$$R_n = LE + H + G. \quad (1)$$

Here, R_n (W m^{-2}) is net radiation, and LE (W m^{-2}) and H (W m^{-2}) denote the latent heat and sensible heat flux, respectively. The symbol G (W m^{-2}) stands for the ground heat flux. Minor flux terms such as energy storage in the canopy or energy conversion by photosynthesis are generally neglected (see e.g., Leuning et al., 2012). However, several studies, where minor energy fluxes were carefully investigated as potential sources for the imbalance, show that considering these minor terms is relevant (Lamaud et al., 2001; Meyers and Hollinger, 2004; Oncley et al., 2007) and could even in some cases help to achieve a nearly perfect EBC (Jacobs et al., 2008).

Usually the sum of the two turbulent fluxes measured with the EC method is systematically lower than the so-called available energy: the difference between net radiation (R_n)

and ground heat flux (G). As a consequence, the energy balance at the Earth's surface usually cannot be closed with the EC technique. The quotient of turbulent fluxes and available energy expresses the energy balance closure:

$$\text{EBC} = \frac{(H + \text{LE})}{(R_n - G)}. \quad (2)$$

In general, EBC ranges between 70 and 90 % as observed over different types of surface ranging from bare soil to a forest (Onckley et al., 2007; Wilson et al., 2002; Twine et al., 2000). Low EBCs (60–80 %) were mainly observed at various agricultural sites and bare soil, whereas over forest they were typically higher (80–90 %) (Charuchittipan et al., 2014; Wilson et al., 2002; Foken, 2008a; Panin and Bernhofer, 2008; Stoy et al., 2013). The imbalance usually occurs during day time, particularly around noon, whereas during the night when fluxes are low EBC is often close to unity (Onckley et al., 2007).

It was long thought that the energy balance gap originates from the instrumental errors of the EC-measurements. However, the accuracy of the energy flux measurements and data quality has significantly increased during the last years. According to Foken (2008a), measuring errors cannot explain the problem of the imbalance provided that measurements and data processing were performed carefully. In a more recent paper, Foken et al. (2010) investigated the EBC of the LITFASS-2003 experimental data. He concluded that the observed lack of EBC on the local scale in heterogeneous landscape can be explained only by deficits in measurement concepts and methodologies. This conclusion is supported by Heusinkveld et al. (2004); they found a perfect EBC over a homogeneous surface: a desert in Israel. Tsvang et al. (1991) and Stoy et al. (2013) also concluded that the heterogeneities of the surrounding area are an important factor contributing to the lack of EBC. Several authors (Klaassen and Sogachev, 2006; Friedrich et al., 2000) reported an increase of the turbulent fluxes at forest edges. Kanda et al. (2004) and Inagaki et al. (2006) used large eddy simulations (LES) to study the contribution of large eddies to energy exchange. They found out that the energy balance can be significantly improved by considering contributions from secondary circulations or turbulent organized structures. The secondary circulations are large-scale eddies, they are relatively stationary and are induced, for example, by surface heterogeneities (Foken, 2008a). Due to their large size and slow motion, their transport of heat, water or gas is not detectable by a single EC station. Energy transfer by such large eddies has to be modeled or measured with an area-averaging method (Foken, 2008a; Stoy et al., 2013). Mauder et al. (2007) analyzed airborne flux measurements over a boreal ecosystem in Canada in order to quantify secondary circulation fluxes. They found that these fluxes were in the same order of magnitude as energy balance residuals observed at EC stations close to the flight track. However, this large eddy theory has not been fully embraced by the scientific community. Leun-

ing et al. (2012), for instance, evaluated EBC of the La Thuile data set. He concluded that unrealistically large and positive horizontal gradients in temperature and humidity would be needed for advective flux divergences in order to explain the EBC problem at half-hourly timescale. Other potential reasons for the imbalance discussed in the literature relate to the possible loss of low- and/or high-frequency components (Wolf et al., 2007; Sakai et al., 2001; Barr et al., 1994). A small fraction of the energy balance gap may also be explained by energy storage in the canopy and photosynthetic energy flux. Both components are normally neglected due to their alleged small contribution (Foken, 2008a; Guo et al., 2009; Jacobs et al., 2008).

The uncertainty arising from the energy balance gap hampers the use of EC data for model parameterization and testing (Ingwersen et al., 2011; El Maayar et al., 2008; Falge et al., 2005). In these types of studies, in order to achieve an energy balance closure, the measured turbulent fluxes are usually adjusted with either H flux, LE flux or the Bowen ratio (BR) post-closure method. These methods fully add the residual to the measured turbulent fluxes, assuming that the available energy is measured correctly. The H post-closure method, letting the latent heat flux unaltered, adds the gap fully to the measured H flux (Ingwersen et al., 2011; Gayler et al., 2013). Oppositely, the LE flux post-closure method assigns the lacking energy fully to LE (Falge et al., 2005). The BR post-closure method assumes that the energy residual has the same Bowen ratio ($\text{Bo} = H / \text{LE}$) as the measured turbulent fluxes (Twine et al., 2000; Barr et al., 1994). In this case, the adjusted LE flux (LE^* , Wm^{-2}) is computed as follows:

$$\text{LE}^* = \frac{R_n - G}{\text{Bo} + 1}. \quad (3)$$

The present study elucidates the nature of the energy balance gap over winter wheat in southwest Germany. For this purpose we (a) evaluated the energy balance of EC flux measurements over two vegetation seasons, additionally measuring evapotranspiration with the soil water balance method (ET_{WB}), which does not depend on an a priori assumption on the composition of the energy residual, and (b) tested ET_{EC} adjusted by the BR, H or LE post-closure method against the ET_{WB} .

2 Materials and methods

2.1 Study site

The present study was performed in the region Kraichgau (Fig. 1), one of the warmest regions in Germany. Mean annual temperature ranges between 9–10 °C, and precipitation between 730 and 830 mm per year. The rivers Neckar and Enz form the borders in the east. In the north and in the south, Kraichgau is bounded by the low mountain ranges of Odenwald and the Black Forest. In the west, Kraichgau borders on the Upper Rhine plain. The Kraichgau area is about

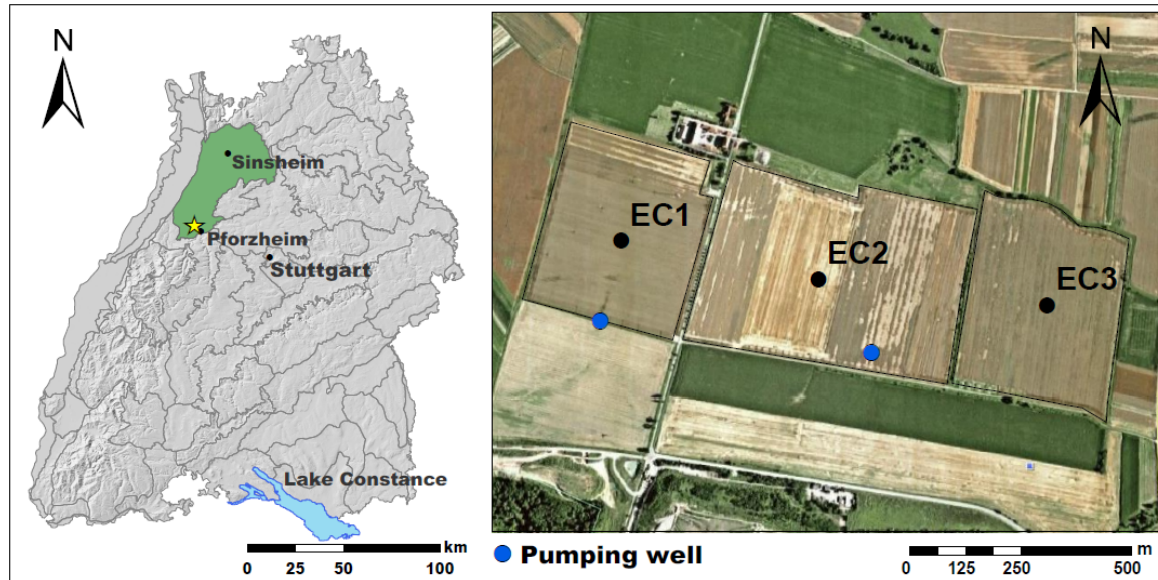


Figure 1. The study region “Kraichgau” (green) on the map of the federal state Baden-Württemberg. Location of the central study site is indicated by a yellow star. The right panel shows a close-up of the central study site. That site consists of three fields (EC1-3). An eddy covariance station (black full point) is installed in the center of each field.

1600 km² and has a gently sloping landscape. Elevations vary between 200 and 320 m above sea level (a.s.l.). Soils, predominantly classified as Luvisols (IUSS Working Group WRB, 2007), were mostly formed here from periglacial loess, which accumulated during the last ice age. Today, the region is intensively used for agriculture. Around 53 % of the total area is used for crop production. Winter wheat, winter rape, summer barley, maize and sugar beet are the predominant crops.

The measurements were performed at the agricultural fields EC1 and EC3 belonging to the farm “Katharinentalerhof” (Fig. 1). The fields are located north of the city of Pforzheim (48.92° N, 8.70° E). The fields EC1 and EC3 are 14 and 15 ha in size, respectively. The terrain is flat (elevation a.s.l.: 319 m). The predominant wind direction is south-west. Both fields are surrounded by other agricultural fields, which are separated partly by tree-hedges. Two permanent pumping wells (installation depth 3 m) were used to monitor the groundwater table (see Fig. 1). The soil type at both fields is Stagnic Luvisol (IUSS Working Group WRB, 2007). Basic soil properties are given in Table 1. In both 2012 and 2013, fields were cropped with winter wheat (*Triticum aestivum* L. cv. Akteur). In both years, winter wheat was drilled on 17 October.

2.2 Measurement of evapotranspiration

2.2.1 Eddy covariance technique

Using the EC technique, we measured the land surface exchange fluxes in a 30 min resolution at two study fields (EC1 and EC3). Both sites were cropped with winter wheat. The

EC method enables measuring the heat, energy and momentum exchange between land surface and atmosphere without disturbing the crop environment. Provided that the land surface is sufficiently flat and homogeneous, the exchange fluxes are one-dimensional and can be calculated from the covariance between vertical wind speed and the scalar of interest. In the case of the LE flux (W m⁻²) this leads to

$$LE = \lambda \rho \overline{q'w'}, \quad (4)$$

where λ (J kg⁻¹) and ρ (kg m⁻³) are the heat of vaporization and the density of air, respectively. The symbol q (kg kg⁻¹) stands for the specific humidity of the air, and w (m s⁻¹) denotes the vertical wind speed. The term $\overline{q'w'}$ is the covariance between the fluctuations of the two quantities.

The EC stations were installed in the center of each study field in April 2009. The stations were equipped with an open path infrared CO₂/H₂O gas analyzer (Licor 7500, LI-COR Biosciences, USA) and a 3-D sonic anemometer (CSAT3, Campbell Scientific, UK). At EC3 (2012) the turbulent complex was installed at a height of 2.63 m. The Licor-CSAT3 separation distance was 0.22 m. The direction of Licor 7500 was 25° against north, CSAT3 orientation was 170°. At EC1 (2013), the turbulent complex was installed at a height of 3.10 m with a sensor separation of 0.12 m. Orientations of Licor 7500 and CSAT3 were 0 and 170°, respectively. Vertical wind speed and specific humidity were measured with 10 Hz frequency. All other sensors recorded data in 30 min intervals. Net radiation was measured with a NR01 4-component sensor (NR01, Hukseflux Thermal Sensors, The Netherlands). Air temperature and humidity were measured in 2 m height (HMP45C, Vaisala Inc., USA). Rainfall was

Table 1. Basic soil properties of the fields EC1 and EC3. At both sites the soil type is Stagnic Luvisol (IUSS Working Group WRB, 2007).

Depth (cm)	Bulk density (g cm ⁻³)	Texture S/U/C* (% by weight)	Organic matter content (% by weight)	Carbonate content (% by weight)	pH (0.01 M CaCl ₂)
EC1					
0–30	1.49	3.4/81.2/15.4	1.54	0.21	6.9
30–60	1.50	3.4/81.6/15.0	0.31	0.29	6.7
60–90	1.47	2.8/81.6/15.6	0.27	0.31	6.6
90–120	1.47	2.8/81.1/16.1	0.53	0.27	6.6
120–150	1.48	2.4/80.0/17.6	0.33	0.37	6.6
EC3					
0–30	1.43	3.4/81.2/15.4	1.60	0.13	6.4
30–60	1.49	3.7/80.6/15.7	0.31	0.10	6.5
60–90	1.47	2.3/80.9/16.7	0.62	0.12	6.6
90–120	1.51	1.8/80.5/17.7	0.40	0.13	6.6
120–150	1.55	1.5/80.3/18.2	0.34	0.05	6.6

* Fraction of sand (S), silt (U), clay (C).

measured using a tipping bucket (resolution: 0.2 mm per tip). The rain gauge (ARG100, Campbell Scientific Ltd., UK) was located close to the EC station. The rain gauge readings (R , in mm h⁻¹) were corrected for catching, wetting and evaporation losses according to WMO (2009, p. 57):

$$R_{\text{cor}} = 1.21 R^{0.92} \quad (5)$$

Soil sensors were also installed close to the EC station. Temperature probes (107 Thermistor probe, Campbell Scientific Inc., UK) were installed in 2, 6, 15, 30 and 45 cm depth. The volumetric water content was measured with TDR probes (CS616, Campbell Scientific Inc., UK) at 5, 15, 30, 45 and 75 cm depth. Three soil heat flux plates (HFP01, Huskeflux Thermal Sensors, the Netherlands) were installed in 8 cm depth. For measuring the hydraulic gradient at the lower boundary of the water balance domain, two matric potential sensors (257-L, Campbell Scientific Inc., UK) were installed in 130 cm and three sensors in 150 cm depth. The horizontal distance between sensors was about 50 cm.

The EC flux data were processed with the TK3.1 software (Mauder and Foken, 2011). Surface energy fluxes were computed from 30 min covariances. Data points exceeding 4.5 standard deviations in a window of 15 values were labeled as spikes and were excluded from the time series. The planar fit coordinate rotation was applied to time periods of 10–14 days. Spectral losses were corrected according to Moore (1986). The fluctuation of sonic temperature was converted into actual temperature according to Schotanus et al. (1983). Density fluctuations were corrected by WPL (Webb et al., 1980). For data quality analysis we used the flag system after Foken (Mauder and Foken, 2011). Half-hourly values with flags from 1 to 6 (high and moderate quality data) were used to calculate the energy balance closure and evapotranspiration. Gap filling of EC flux data was performed with the mean diurnal variation method using an averaging window of 14 days (Falge et al., 2001). Additionally we com-

puted the random error of the fluxes, which consist of the instrumental noise error of the EC station and the stochastic (sampling) error (Mauder et al., 2013).

The EC ET (L m⁻² or mm) per half hour was estimated with the following equation:

$$ET_{\text{EC}} = \frac{LE}{\lambda} \times 1800s, \quad (6)$$

where the heat of vaporization λ (J L⁻¹) as a function of temperature T (°C) (Foken, 2008b) was taken as

$$\lambda = 2501000 - 2370 \times T. \quad (7)$$

Subsequently, ET_{EC} values were adjusted by the H , LE or Bowen ratio post-closure method.

Ground heat flux was calculated as the sum of measured soil heat flux using the mean of the three heat flux plates and the heat storage change (ΔS_G) (Eq. 8) between the surface and the plates (Foken, 2008b)

$$\Delta S_G = \frac{C_v \times \Delta T \times L}{\Delta t}, \quad (8)$$

where C_v (J m⁻³ °C⁻¹) is the volumetric heat capacity of the soil, ΔT (°C) denotes the soil temperature change during the period of time, Δt , considered, and L (m) is the thickness of the soil layer above the soil heat flux plates. The heat capacity of the soil was computed according to de Vries (1963) using the volumetric water content measured in 5 cm depth.

2.2.2 Soil water balance method

The water balance equation of a soil volume of a unit area and given depth reads as follows:

$$ET_{\text{WB}} = R - SP - SR - \Delta S. \quad (9)$$

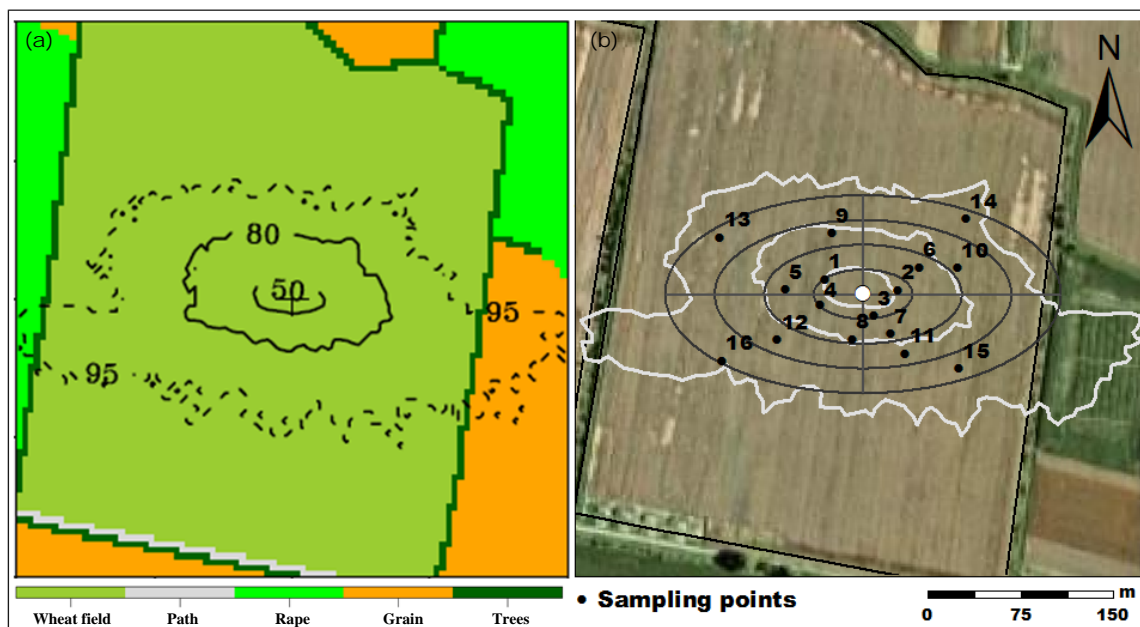


Figure 2. (a) Footprint of the eddy covariance station EC 3 in 2012. Black isolines indicate the fraction of the source area of 50, 80 and 95 % of measured EC fluxes. (b) Positions of sampling points within the footprint of EC3 used to measure soil water storage.

Here, R stands for rainfall, and SP is seepage (negative: capillary rise, positive: vertical drainage). The symbol SR denotes surface runoff and ΔS stands for the change in soil water storage over the balancing period. Based on our field observations, SR was negligible at the study sites during the periods considered.

ΔS was measured at sixteen positions. Sampling positions were distributed across the footprint of the EC station using a stratified random sampling design (Figs. 2b and 3b). To check whether the measured ΔS values are uncorrelated (independent) we computed semi-variograms and spatially interpolated ΔS over the footprint. The geostatistical analysis was performed with ArcGIS (Version 10.3, ESRI Inc.). The point data were interpolated with the Ordinary Kriging method. No trend removal was applied and isotropy was assumed.

The footprint area of the EC station was determined with the forward Lagrangian stochastic footprint model described by Göckede et al. (2006) based on EC flux data in 2010 (EC3) and 2011 (EC1). In these years, the fields were also cropped with winter wheat (*Triticum aestivum* cv. Cubus (EC3) and cv. Akteur (EC1)). The model estimates the footprint for different atmospheric stratifications (stable, neutral and unstable). In the present study, we used the weighted average footprint of these atmospheric stratifications. Footprint analyses were processed for periods from mid-May to late July, when the average plant height was about constant, on average 0.77 and 0.83 m at EC3 and EC1, respectively. The installation height of CSAT was 2.5 m at EC3 and 3.10 m at EC1 over the entire periods. The footprint model requires a land use and a roughness matrix as input files. Based on the satellite remote-

sensing data, we produced land use matrices of the surroundings of the EC stations. The special spatial resolution of matrices was 5 m and their areal coverage $500 \times 500 \text{ m}^2$. The subsequent land use types were counted: winter wheat, path, rape, grain, trees and suburban. Roughness values of the land use classes were taken from Foken (2008b) (Figs. 2a and 3a).

In 2012, we performed three soil sampling campaigns over the growing season: late April (25–27), mid-June (14–15) and late July (24–27). In 2013, four sampling campaigns were performed: mid-April (15–16), early June (3–4), mid-June (18–19) and late July (30–31). Soil samples were taken in 10 cm intervals down to 150 cm. For this purpose, three augers with a length of 60 cm ($\varnothing = 2.885 \text{ cm}$), 100 cm ($\varnothing = 2.386 \text{ cm}$) and 150 cm ($\varnothing = 1.763 \text{ cm}$) were used. The 60 cm auger was used for taking soil samples down to 60 cm. The 100 cm auger was used for sampling the 60–100 cm depth, and the 150 cm auger was taken for sampling between 100 to 150 cm. Soil samples were filled in plastic bags and transported to the lab within less than 10 h. Field wet soil samples were weighed, put into a ventilated oven and dried at 105°C . Final weights were usually reached within 12 h. Based on mass balance, the gravimetric water content was calculated. It was converted to volumetric water content by multiplication with the bulk density. Bulk density of the top-soil layers (0–30 cm) was determined at each sampling position using a cylindrical steel core cutter (diameter: 7.92 cm, volume for a 10 cm sampling depth: 492.7 cm^3) on 4 May in 2012 and on 30 April in 2013. In three 10 cm intervals the core cutter was inserted into the soil by careful turning. The soil sample was stored in a plastic bag and in the lab the soil dry weight was determined by drying the sample at 105°C .

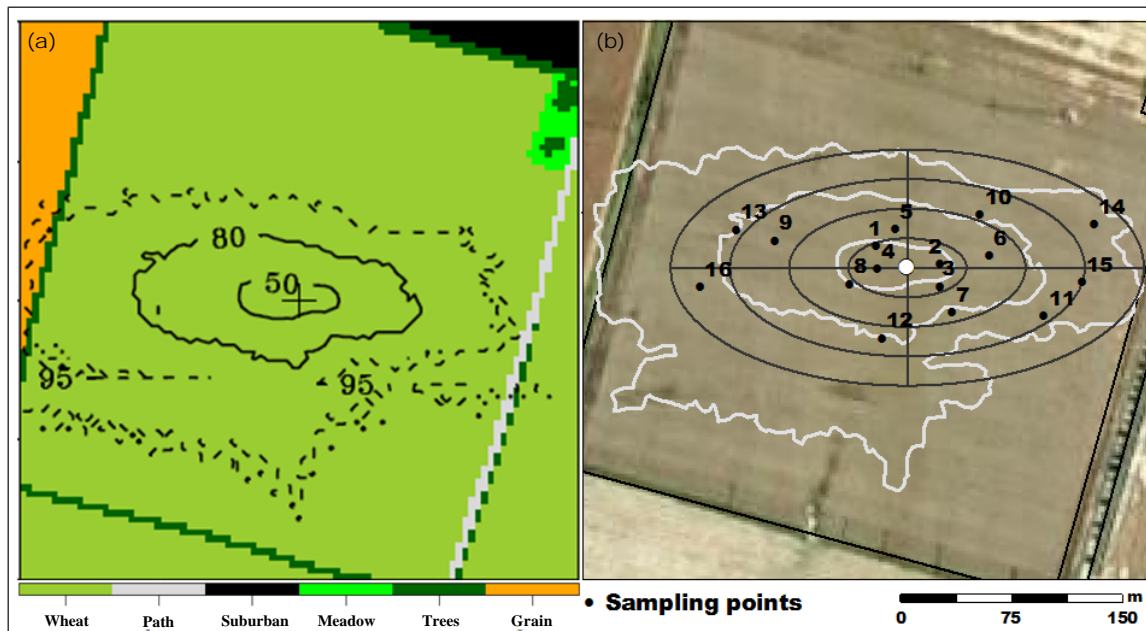


Figure 3. (a) Footprint of the eddy covariance station EC 1 in 2013. Black isolines indicate the fraction of the source area of 50, 80 and 95 % of measured EC fluxes. (b) Positions of sampling points within the footprint of EC3 used to measure soil water storage.

Close to the EC station a pit was dug down to 150 cm. In the center of every 10 cm layer, 100 cm³ of soil was sampled in triplicates using cylindrical cores ($\varnothing = 5.50$ cm, height 4.21 cm). Bulk density was determined by drying the soil at 105 °C and determining its mass by weighing.

At the 140 cm depth we took soil samples to measure the water retention curve and the hydraulic conductivity function. Samples ($V = 250$ cm³, $\varnothing = 8$ cm, 5 cm height) were taken in triplicates using sampling rings (UMS GmbH, Germany).

Additionally, soil texture was determined at each sampling position. Three layers (0–30, 30–60, 60–90, 90–120, and 120–150 cm) were pooled to one composite sample and soil texture was determined with the standard pipette method (Dane and Topp, 2002).

The seepage flux was computed from the Darcy-Buckingham law:

$$q_w = -K(h) \frac{\Delta H}{\Delta z}. \quad (10)$$

Here, q_w (cm d⁻¹) is the water flux density, $K(h)$ (cm d⁻¹) denotes the hydraulic conductivity as a function of the matric potential h (cm), and H (cm) is the hydraulic potential, the sum of matric and gravitational potentials. The hydraulic gradient $\Delta H/\Delta z$ was computed from the matric potential measurements performed at 130 and 150 cm depth and the vertical separation distance Δz (cm) of the matric potential sensors.

The hydraulic conductivity function $K(h)$ was determined with the evaporation method according to Wind/Schindler using the HYPROP lab system (UMS GmbH, Germany).

First, soil samples taken from the 140 cm depth were slowly saturated for 5–6 days. Afterwards soil samples were placed on a balance and exposed to evaporation. The matric potential was measured with micro-tensiometers in 1.25 and 3.75 cm depth. The soil sample weight and the matric potential were recorded automatically every minute at the first hour and every 10 min in the next hours. After 4 to 5 days, the tensiometers fell dry and the measurement was stopped. The initial water content of soil samples was computed from their dry weight. Based on the acquired data, a water retention curve and hydraulic conductivity function were fitted to the data. Parameters of the functions were fitted with the robust, non-linear optimizing procedure developed by Durner and Peters (2006) (User Manual HYPROP, 2012). Among the available hydraulic models, the bimodal van Genuchten parameterization (Durner, 1994) yielded the lowest Akaike information criterion and was used in the following to model $K(h)$:

$$K(h) = K_s \cdot \left[\sum_{j=1}^2 w_j [1 + (a_j |h|)^{n_j}]^{1/n_j - 1} \right]^\tau$$

$$\left[\frac{\sum_{j=1}^2 w_j a_j \left\{ 1 - (a_j |h|)^{n_j - 1} [1 + (a_j |h|)^{n_j}]^{1/n_j - 1} \right\}}{\sum_{j=1}^2 w_j a_j} \right]^2$$

$j = (1, 2)$ (11)

In Eq. (10), K_s (cm d⁻¹) is saturated hydraulic conductivity, w_j is the weighting factors of the two van Genuchten func-

tions and a_j, n_j are the shape parameters of the two retention curves. The tortuosity factor τ was set to 0.5. K_s was measured on soil samples taken at EC1 from 140 cm depth by the falling head technique using a KSAT system (UMS GmbH, Germany). The methodology of the device follows the German standard DIN 18130-1 and is based on the inversion of the Darcy law (Operation Manual KSAT, 2013). Measurement of K_s was repeated five times with each of three samples. The average value of K_s was 39.3 cm day^{-1} .

In 2013, we additionally measured the volumetric soil water content with capacitance soil moisture probes (SM1, Adcon Telemetry, Austria). The probes were installed on 17 and 18 December 2012. The soil moisture network consisted of sixteen stations located at the same positions where soil samples were taken (Fig. 3b). Every station was situated in the middle between two machine tracks, so the farmer could easily pass the station during fertilization and pesticide application. Each station consisted of a nine-level SM1 capacitance probe, remote transfer unit (RTU) (addIT A723 Series 4, Adcon Telemetry, Austria) and a solar panel for power supply.

Adcon SM1 sensors measure the capacitance and are characterized by low power consumption. Their radius of influence is about 10 cm. In order to install the SM1 probes, we removed the soil with a screw auger and then carefully installed the moisture sensors. To avoid air voids between sensor and soil, the bore hole was carefully filled up with soil slurry. The RTU and solar panel were mounted to an aluminum mast and installed about 2 m away from the SM1 sensor.

The volumetric water content was measured for 15 min intervals at 10 cm resolution down to 90 cm depth. Soil moisture content was measured from 1 April to 4 August 2013. Each RTU stored and transmitted the data to the so-called master station (RA440, Adcon Telemetry, Austria) mounted on the EC mast. The master station transferred the data via GSM modem to the central data server (A850 Telemetry Gateway, Adcon Telemetry GmbH, Austria) located at the University of Hohenheim.

The SM1 sensors were calibrated separately using the data of the four sampling campaigns in 2013 described above. Soil samples were taken about 30–50 cm away from the sensor. The calibration line was derived by regressing volumetric water content measured by the sensor to that of measured in the lab.

Mean diurnal ET_{WB} and ET_{EC} , adjusted by the BR, H or LE post-closure methods, were estimated and compared in 6 OPs (OP) (Tables 2 and 3). In OP-1, OP-2, OP-3 and OP-6, ET_{WB} was estimated based on data obtained during the soil sample campaigns, whereas in OP-4 and OP-5 it was estimated based on the data of SM1 sensors. The latter two periods are characterized by low precipitation and seepage, which helps minimize uncertainties in drainage calculations (Fig. 4).

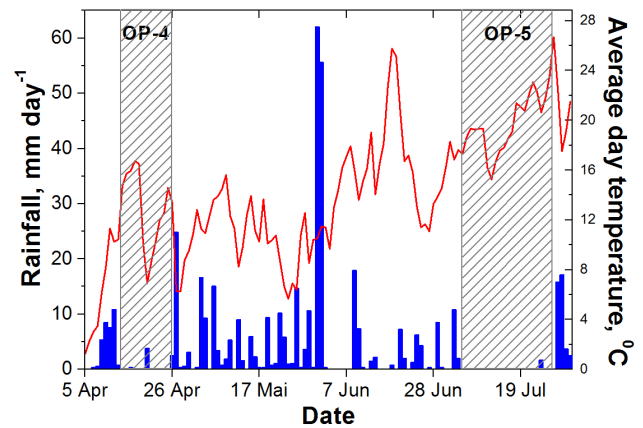


Figure 4. Diurnal rainfall and mean temperature during the 2013 growing season. Hatched zones (OP-4, OP-5) indicate periods with low amount of rain and seepage.

2.3 Error estimation

The error of measured ET_{WB} was estimated based on the Gaussian error propagation law (Currell and Dowman, 2009):

$$s_{ET_{WB}} = \sqrt{s_R^2 + s_{SP}^2 + s_{\Delta S}^2}. \quad (12)$$

Here, s is the standard error of the corresponding variables R , SP or ΔS . The standard error of rainfall was calculated based on the observations of the three rain gauges (EC1-3) ($n = 3$). The standard error of ΔS was computed from the soil water content measurements that were performed every campaign at 16 positions ($n = 16$). In order to evaluate an error of SP estimates, we used the three sets of the bimodal van Genuchten parameterization, which were determined in the lab (see chapter 2.2.2). For each parameterization the drainage and capillary rise were estimated ($n = 3$).

3 Results

3.1 Energy balance closure of eddy covariance data

The EBC of high-quality data (1–3 flags after Foken) and excluding low LE fluxes ($-25 \text{ W m}^{-2} < LE < 25 \text{ W m}^{-2}$) was 73 % during the growing season 2012 and 67 % from mid-June to late July in 2013. The average random error was 16 % for both LE and H in 2012. In 2013, the random error of LE was 12 % and that of H was 14 %. In total, 43 % of the data fulfilled the above quality criteria. Allowing in addition for moderate quality data (4–6 flags after Foken), EBC decreased on average by about 2 and 4 % in 2012 and 2013, respectively. Table 3 summarizes the EBC in different OPs estimated based on high and moderate quality data. In 2012, from late April to late July the average EBC was about

70

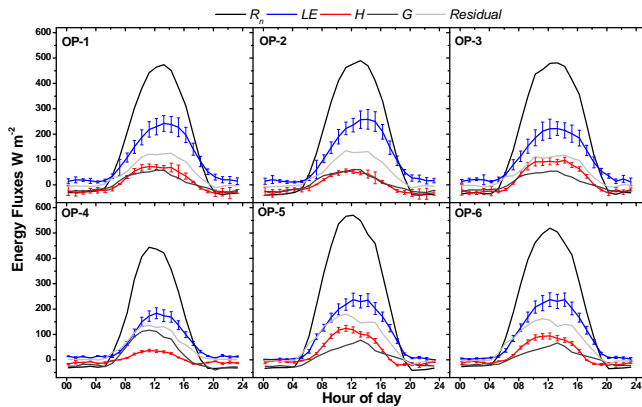


Figure 5. Averaged diurnal cycles of net radiation R_n , latent LE, sensible H and ground heat fluxes G in the observation periods (OPs) of 2012 (OP 1–3) and 2013 (OP 4–6).

71 %. This EBC was uniform during different OPs. The average residual was 68.5 W m^{-2} . The random error of LE was 18 %, that of H 19 %. In 2013, we observed a lower EBC of about 60 %. The average residual was 86.1 W m^{-2} . The average random error of flux measurements was 16.5 % for LE and 18 % for H . The lowest EBC of about 57 % was measured from mid-April to early June. During this period, 55 % of days were rainy days (Fig. 4) resulting in a large amount of rainfall (250 mm) – about 50 % higher than in 2012 (Table 2). In this period we also measured the lowest net radiation and vapor pressure deficit (data not shown). At the end of the growing season, EBC increased. Figure 5 shows the diurnal cycles of the energy fluxes as well as energy residual during the different OPs. Figure 6 shows graphically EBC in both years. The slope of the regression line, forced through the origin, of the available energy on the turbulent energy was 0.71 in 2012. In 2013 it was 0.64.

3.2 Evapotranspiration measurements

3.2.1 Growing season 2012

The results of the geostatistical analysis, performed for the OPs in which soil was sampled down to 1.5 m, showed that the 16 ΔS sampling points were not or only weakly spatially correlated. Computing the footprint-averaged ΔS with Ordinary Kriging instead of using simply the arithmetic mean of the 16 sampling points resulted in differences between 0.4 and 1.7 mm, what corresponds to a relative error below 0.5 %. Therefore, the arithmetic mean was used in the following.

Applying the rain gauge correction proposed by the WMO (1999) (see Eq. 5) increased total rainfall on average by 12 % in both years. In 2012, the two pumping wells stayed dry during the whole growing season (OP-1), i.e., the groundwater level was always deeper than 3 meters. Total rainfall was 305 mm and seepage amounted to 38 mm (Ta-

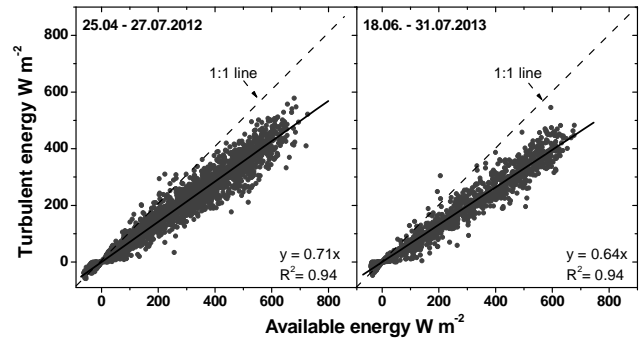


Figure 6. Scatter plots and linear regressions between turbulent and available energy in the periods from April to July 2012 and 2013. The 1 : 1 line indicates perfect energy balance closure.

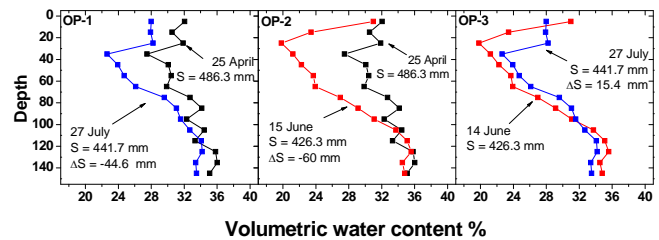


Figure 7. Vertical soil water profiles and change in water storage over three observation periods (OPs) at winter wheat stands at EC3 in 2012.

ble 3). During the first soil sample campaign, 486.3 mm of water was stored in the upper 150 cm of soil (Fig. 7). The soil water stock decreased by 44.6 to 441.7 mm. During OP-2, soil water storage was depleted to 426.3 mm. During OP-3, rainfall refilled the soil water stock by 15.4 mm. The vertical soil water profiles showed the largest differences within the upper 100 cm of the soil profile. Below 100 cm the soil water content changed only very little (Fig. 7). The components of the soil water balance and the resulting ET are compiled and compared with ET_{EC} in Table 3. In all OPs, the best agreement of the EC technique with WB method was achieved without adjusting the LE flux data (H post-closure method). The ET_{EC} computed with the Bowen ratio method was on average about 28 % higher than ET_{WB} . The ET_{EC} computed with the LE flux post-closure method was on average about 54 % higher than ET_{WB} .

In 2012, standard error of rainfall measurements ranged from 2 to 4 mm depending on the observation period. Standard error of ΔS ranged from 6 (1.3 %) to 9 (2 %) mm. Standard error of SP ranged from 2 to 5 mm.

3.2.2 Growing season 2013

Between mid-April and early June 2013, rainfall was more than twice as high as in 2012 (data not shown). The water level in the pumping wells rose to the surface for several days during this period (8 May and 3–5 June), and surface runoff

71

Table 2. Weather conditions during the vegetation periods 2012 and 2013. The numbers in brackets give the anomaly over an observation period with regard to the 5-year average from 2009 to 2013.

Growing season, year	2012				2013			
	25/04–27/07 OP-1	25/04–15/06 OP-2	14/06–27/07 OP-3	13/04–26/04 OP-4	05/07–27/07 OP-5	18/06–31/07 OP-6	15/04–04/06 OP-0	
BBCH stage	30–89	30–65	65–89	20–30	75–89	65–89	20–60	
Mean Net Radiation, $W m^{-2}$	148.9 (+0.7)	146.9 (+8.5)	152.6 (–8.8)	119.1 (–5.1)	192.7 (+33.8)	173.3 (+12.5)	108.5 (–23.7)	
Mean temperature, $^{\circ}C$	16.1 (+0.6)	14.6 (+1.0)	17.9 (+0.1)	12.8 (+2.6)	19.9 (+1.5)	18.6 (+0.6)	11.1 (–1.3)	
Average wind speed, $m s^{-1}$	1.6 (–0.1)	1.7 (–0.1)	1.5 (–0.1)	2.3 (+0.2)	1.4 (–0.3)	1.6 (–0.0)	2.3 (+0.3)	
VPD, hPa	6.4 (+0.5)	5.9 (+1.1)	6.9 (–0.1)	6.1 (+1.1)	10.2 (+2.3)	8.2 (+1.1)	3.6 (–1.2)	
Bowen Ratio (H/LE)*	0.44 (+0.07)	0.19 (–0.01)	0.44 (–0.16)	0.17 (–0.09)	0.56 (–0.53)	0.5 (–0.34)	0.15 (–0.05)	
Rainfall, mm	305.0 (–8.6)	140.0 (–50.7)	166.0 (+38.9)	6.7 (–10.3)	1.6 (–71.3)	75.0 (–59.1)	282.7 (+117.8)	

* The Bowen ratio was computed for the period 09:00 a.m. to 03:00 p.m.

Table 3. Evapotranspiration measured with the water balance (WB) method and the eddy covariance (EC) technique at winter wheat stands in 2012 and 2013.

Growing season, year	2012				2013		
	25/04–27/07 OP-1	25/04–15/06 OP-2	14/06–27/07 OP-3	13/04–26/04 OP-4	05/07–27/07 OP-5	18/06–31/07 OP-6	
Length of the period, days	94	52	44	14	23	44	
Rainfall, mm	305	140	166	6.7	1.6	75	
Water storage, mm	–44.6	–60	15.4	–24.5	–67.9	–105.2	
Drainage/capillary rise, mm	40.2/2.0	12.7/2.0	28.5/0	0.3/0.2	1.4/0	4.8/0.2	
Average evapotranspiration, $mm day^{-1}$							
WB method	3.3 ± 0.3	3.6 ± 0.3	2.8 ± 0.5	2.3 ± 0.5	3.1 ± 0.3	3.9 ± 0.4	
EC method with sensible heat flux post-closure method	3.4 ± 0.6	3.5 ± 0.6	3.3 ± 0.6	2.3 ± 0.4	3.1 ± 0.5	3.2 ± 0.5	
EC method with Bowen ratio post-closure method	4.1 ± 0.6	4.3 ± 0.7	3.9 ± 0.6	3.3 ± 0.5	4.6 ± 0.7	4.5 ± 0.7	
EC method with latent heat flux post-closure method	4.9 ± 0.9	5.1 ± 1.0	4.8 ± 0.8	3.8 ± 0.7	5.4 ± 0.9	5.3 ± 0.9	
Energy balance closure (EBC)							
Average EBC, %	71	70	72	55	62	63	
Average residual, $W m^{-2}$	68.5	72.4	65.1	70.6	98.8	89.1	
Number of data	2542 (57.0 %)	1426 (57.7 %)	1170 (56.1 %)	391 (58.2 %)	695 (63.0 %)	1269 (60.7 %)	

was observed at the field. In this period, temperatures and vapor pressure deficits were low (data not shown). During this period, marked on Fig. 8 as OP-0, the soil water stock was filled up by 57.9 mm. Due to exceptionally high rainfall and surface runoff, which was not measured, the calculation of ET_{WB} is unreliable for this period, which hampered comparing the EC and WB methods.

In OP-6, soil water storage decreased by 105.2 to 398.7 mm (Fig. 8). The total rainfall for this period was about 50 % less than that in 2012 (Table 2). Seepage was low, about 4.6 mm, over this period. Table 3 compares ET_{WB} with ET_{EC} . In OP-6, better agreement of the EC technique with WB method was achieved by adjusting the LE flux data with the BR and H post-closure method. The ET_{EC} post-closed with the BR method was about 15 % higher than the ET_{WB} . The ET_{EC} computed with the H post-closure method was about 18 % lower than the ET derived from the WB method. The ET_{EC} adjusted with the LE post-closure method was 36 % higher than the ET_{WB} .

Soil water profiles of OP-4 and OP-5 are shown in Fig. 8. ET_{WB} agreed best with non-adjusted raw ET_{EC} (H post-closure method), while BR and LE post-closure methods significantly overestimated ET by about 46 and 70 %, respectively (Table 3).

In 2013, standard error of rainfall measurements ranged from 0.1 to 3.5 mm depending on the observation period. Standard error of ΔS was 8 mm (1.7 %). The standard error of the water storage measured with SM1 sensors was on average 3 mm (1.0 %), and the standard error of SP was up to 1 mm.

4 Discussion

The EBCs of the present study agree with those of other studies performed over agricultural land, where EBCs are typically characterized by high energy residuals (20–40%) (Charuchittipan et al., 2014; Foken, 2008a; Panin and Bernhofer, 2008; Stoy et al., 2013). The random errors of our EC

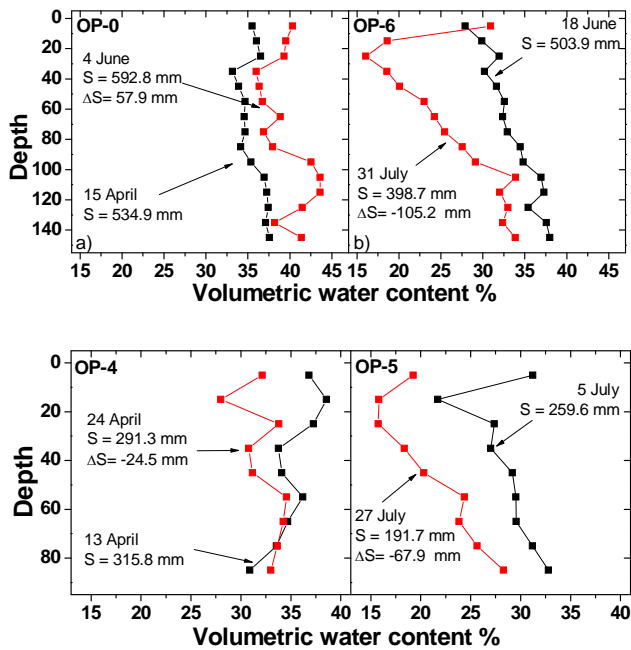


Figure 8. Vertical soil water profiles and change in water storage over four observation periods (OPs) at winter wheat stands at EC1 in 2013. The upper row shows the results of the soil sample campaigns. The soil water contents measured with capacitance soil moisture probes (SM1, Adcon Telemetry, Austria) are shown in the lower row.

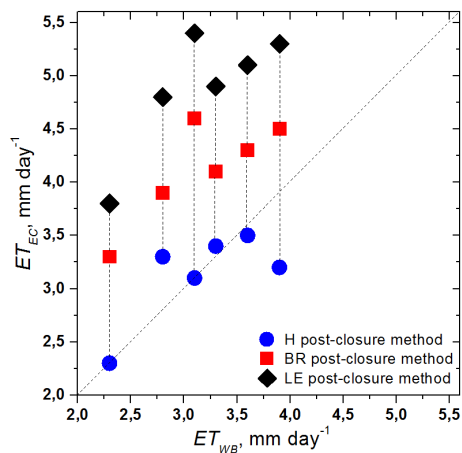


Figure 9. Scatter plots between evapotranspiration assessed from the soil water balance, ET_{WB} , and evapotranspiration measured by the eddy covariance technique, ET_{EC} , adjusted by the sensible heat flux (H), the Bowen ratio (BR) and the latent heat flux (LE) post-closure method.

fluxes are also in a good agreement with random errors reported by Mauder et al. (2013) and Foken (2008a). They are typically between 5 and 20 % for high-quality data.

Our experiment showed the limits of the WB method imposed by the prevailing weather conditions. It was not pos-

sible to reliably estimate ET_{WB} in periods with heavy rain due to the uncertainties in drainage calculation and surface runoff. Ideal conditions for performing the WB method are periods with low precipitation and low or absent seepage, and with soil water contents below field capacity (Schume et al., 2005; Wilson et al., 2001). These conditions were well fulfilled during OP 4 and 5. During OP4 and OP5 we found a nearly perfect match between the WB method and the non-adjusted ET data. The results that we obtained during OPs with higher seepage fluxes (OP1–3) are in line with the findings of OP4 and 5. Therefore, we are confident that the estimated seepage fluxes are in the right order of magnitude and that the total error, which is relatively low due to the small absolute flux, is in an acceptable range.

The comparison of the two methods shows that the EC method reliably measures evapotranspiration when no adjustment is applied (Fig. 9). Similar results were obtained in other experimental studies. Schume et al. (2005) cross-checked ET measured with the EC technique against the soil water balance method over a mixed European beech – Norway spruce forest. The observed EBC ranged between 73 and 92 % at their study site. They demonstrated that ET was adequately measured with the EC technique. They concluded that the proportional distribution of the residual between the energy balance components would lead to an overestimation of LE. Wilson et al. (2001) compared non-adjusted ET_{EC} with ET measured by various other measurement techniques. EBC was 80 %. They reported a good agreement between ET_{EC} and ET assessed by the catchment water balance method. Both methods estimated nearly equal annual ET over a 5-year period. They also observed a high correlation ($R^2 = 0.8$) between ET_{EC} and ET assessed by the soil water budget method. Nonetheless, the data were highly variable during periods with rainfall and rapid water movement within the soil profile.

Contrasting results were obtained in other similar studies, i.e., where independently measured ET was compared with ET_{EC} . For instance, Barr et al. (2012) compared measured streamflow from the watershed with streamflow, estimated from seven flux towers in this watershed, over a 10-year period. The annual EBC was about 85 % across sites and years. His results showed that measured streamflow better agreed with outflow estimated based on the ET_{EC} adjusted with the BR method, whereas outflow based on the raw ET_{EC} flux was about 40 % higher. In several other experimental studies, independently measured ET agreed better with ET_{EC} adjusted by one of the post-closure methods. Wohlfahrt et al. (2010) cross-checked ET_{EC} against ET determined using micro-lysimeters and an approach scaling up leaf-level stomatal conductance to canopy-level transpiration. The observed EBC was about 85 %. The best correspondence between EC and the independent methods was achieved with the LE post-closure method. Gebler et al. (2015) found that ET_{EC} adjusted with BR post closure method yielded the best fit with ET measured by lysimeters, while raw ET_{EC}

was 16 % smaller and ET_{EC} adjusted with LE post-closure method was 15.7 % higher. Cuenca et al. (1997) conducted intensive field campaigns (IFC) in spring and summer using a neutron probe and time domain reflectometry to evaluate the soil water content at a boreal forest. During IFC-1 he reported a good agreement between unadjusted ET_{EC} (2.9 mm day^{-1}) and ET estimated based on the soil water profile analysis (2.6 mm day^{-1}). During IFC-2, however, the difference between the two methods was extremely high: 3.6 mm day^{-1} against 2.1 mm day^{-1} , respectively. They related this difference to the spatial differences and sampling volume of the measurement techniques. They also suggested that the ET_{WB} versus ET_{EC} difference could be due to the underestimation by the turbulent complex of the downward (negative) LE flux at night, which would overestimate the LE flux.

Our results synthesized with the findings from literature suggest that there is no universal approach to post-close the energy balance gap, and that the composition of the energy residual is site-specific. Therefore, it is advisable in case of long-term experiments to perform for each site at the very beginning an independent measurement of LE to identify the most suitable post-closure method. Moreover, if EC flux data are intended to be used to calibrate and parameterize, for example, a land surface model, as in our case, biased measured turbulent fluxes would directly affect the outcome of these calibration efforts and lead to systematically biased simulated turbulent fluxes. Therefore, an elaborated study on the energy residual and its major components measured by the EC system should be mandatory in such research studies.

The energy residual was higher at EC1 (40 %) in comparison with EC3 (29 %). This might be partly assigned to the heterogeneity of the EC station surrounding (Stoy et al., 2013). A hilly forested area is situated about 500 m south from the EC1 station (Figs. 1 and 3) which might have led to formation of stationary large eddies over the field. Their transport of energy and matter cannot be detected by the EC station leading to lower EBC at this study field. However, as already stressed in the Introduction, the large eddy theory has not been fully embraced by the scientific community (see e.g., Leuning et al., 2012). The worst closure during OP-4 could be assigned to additional spatial heterogeneity caused by differences in phenological development of crops in the landscape. OP-4 was performed early in the growing season. In Kraichgau region during this time some fields are already well covered with vegetation (e.g., winter cereals and winter rape) while others are still bare, prepared for late-covering crops, i.e., corn, potato, sugar beet (Imukova et al. 2015). Later in the growing season fields are more evenly covered with vegetation.

One of the possible components, which may be partly responsible for the energy imbalance at our study site, is the loss of fluxes in the low- and/or high-frequency range. Mauder and Foken (2006) estimated the low-frequency loss of EC flux data. They reported that the commonly used

30 min averaged interval of the covariances does not cover the entire spectrum of the turbulent fluxes. Extending the average time substantially reduced the residual, considerably increasing H flux leaving LE practically unaltered. H changed from 40.1 W m^{-2} with a 5 min averaging interval to 66.9 W m^{-2} with 24 h. LE, in contrast, decreased from 73.9 W m^{-2} with 5 min averaging interval to 66.9 W m^{-2} with 24 h, although with an averaging time of multiple days, LE was about 75 W m^{-2} . Wolf and Laca (2007) performed a cospectra analysis of the ET_{EC} measured over short-grass steppes. They found that H flux was underestimated by 14 % due to the lack of measurement resolution in the high-frequency range. The LE loss was only half of the H loss. They concluded that this must lead to a bias in the measured Bowen ratio.

Other possible candidates of the energy imbalance at our study site are underestimated ground heat flux and neglected terms such as energy storage in the canopy and energy consumption by photosynthesis. Accounting for these fluxes would probably help to improve the EBC at our study site. Jacobs et al. (2008), for example, showed that EBC could be improved at a grassland site by 15 % by elaborate estimation of ground heat flux (9 %) and considering energy consumption by photosynthesis and other minor storage terms such as enthalpy storage in the air layer between turbulent complex and the land surface (6 %). Meyers and Hollinger (2004) demonstrated that combining soil heat storage with canopy heat and photosynthetic energy flux improved the EBC by 15 and 7 % for a fully developed maize and soybean site, respectively. They found that photosynthetic energy flux can reach, on a half-hourly basis, up to 30 W m^{-2} at midday. A maximum of the canopy heat storage was observed in the early morning hours (up to 20 W m^{-2}). Oncley et al. (2007) report that the average heat storage by the canopy was about 10 W m^{-2} on a flood-irrigated cotton field, whereas the photosynthetic energy flux peaked at 48 W m^{-2} with a diurnal average of 8 W m^{-2} . Guo et al. (2009) observed a decrease of EBC with the physiological development of maize. EBC was about 89 % on bare soil and 67 % during the senescence phase of the maize at the same field. Accordingly, the study concluded that heat storage and photosynthesis energy of the vegetation canopy play a non-negligible role in energy balance closure. In summary, our results imply that at our study site during most observation periods of the growing season (OP 1–5), the energy balance residual was not made up by latent heat. At our study site, the energy balance residual most probably consists of a combination of underestimated heat fluxes and neglected storage terms.

5 Conclusions

We cross-checked the evapotranspiration (ET) data obtained with the eddy covariance (EC) method against ET data measured with the soil water balance (WB) method. Both mea-

surements were performed at winter wheat stands in southwest Germany in 2 years, 2012 and 2013. At the study site, both the Bowen-ratio and the LE post-closure method led to substantially higher ET than the WB method. In general, ET measured with the WB method agreed best with the raw non-adjusted ET fluxes (sensible heat flux (H) post-closure method). Only at the end of the vegetation season 2013, during a period with high and frequent rainfall, ET_{WB} was in-between the ET_{EC} adjusted by the H and Bowen ratio method, respectively. The LE post-closure method strongly overestimated LE during all OPs is not suitable for this site. Our study also illustrates the limits of the WB method. The lower the rainfall and seepage, the more reliable the method. At our study site, during most observation periods (OP 1–5), the energy balance gap was not made up by latent heat. This calls for considering other fluxes and storage terms to even out the energy balance.

Acknowledgements. The present study was supported by the German Research Foundation (DFG) in the framework of the Research Unit (RU) 1695 “Structure and function of agricultural landscapes under global climate change – Processes and projections on regional scale” and in part by Erasmus Mundus grant SGA 2010-2361. We thank Benedikt Prechter and Maxim Poltoradnev for the great help in conducting the soil sampling campaigns and installing the soil moisture network.

Edited by: P. Stoy

References

- Barr, A. G., King, K. M., Gillespie, T. J., den Hartog, G., and Neumann, H. H.: A comparison of Bowen ratio and eddy correlation sensible and latent heat flux measurements above deciduous forest, *Bound.-Lay. Meteorol.*, 71, 21–41, 1994.
- Barr, A. G., van der Kamp, G., Black, T. A., McCaughey, J. H., and Nesic, Z.: Energy balance closure at the BERMS flux towers in relation to the water balance of the White Gull Creek watershed 1999–2009, *Agr. Forest Meteorol.*, 153, 3–13, 2012.
- Charuchittipan, D., Babel, W., Mauder, M., Leps, J.-P., and Foken, T.: Extension of the Averaging Time in Eddy-Covariance Measurements and Its Effect on the Energy Balance Closure, *Bound.-Lay. Meteorol.*, 152, 303–327, 2014.
- Cuenca, R. H., Stangel, D. E., and Kelly, S. F.: Soil water balance in a boreal forest, *J. Geophys. Res.-Atmos.*, 102, 29355–29365, 1997.
- Currell, G. and Dowman, A.: *Essential mathematics and statistics for science*, The University of the West of England, UK, 2009.
- Dane, J. H. and Topp, G. C.: *Methods of soil analysis, Part 4 – Physical methods*: Soil Science Society of America Book Series No. 5, Soil Science Society of America, Madison, Wisconsin, 2002.
- de Vries, D. A.: Thermal properties of soils, in: *Physics of Plant Environment*, edited by: W. R. van Wijk, North-Holland Publishing Co., Amsterdam, 210–235, 1963.
- Durner, W.: Hydraulic conductivity estimation for soils with heterogeneous pore structure, *Water Resour. Res.*, 30, 211–223, 1994.
- El Maayar, M., Chen, J. M., and Price, D. T.: On the use of field measurements of energy fluxes to evaluate land surface models, *Ecol. Model.*, 214, 293–304, 2008.
- Falge, E., Baldocchi, D., Olson, R., Anthoni, P., Aubinet, M., Bernhofer, C., Burba, G., Ceulemans, R., Clement, R., Dolman, H., Granier, A., Gross, P., Grünwald, T., Hollinger, D., Jensen, N.-O., Katul, G., Keronen, P., Kowalski, A., Lai, C. T., Law, B. E., Meyers, T., Moncrieff, J., Moors, E., Munger, J. W., Pilegaard, K., Rannik, Ü, Rebmann, C., Suyker, A., Tenhunen, J., Tu, K., Verma, S., Vesala, T., Wilson, K., and Wofsy, S.: Gap filling strategies for defensible annual sums of net ecosystem exchange, *Agr. Forest Meteorol.*, 107, 43–69, 2001.
- Falge, E., Reth, S., Brüggemann, N., Butterbach-Bahl, K., Goldberg, V., Oltchev, A., Schaaf, S., Spindler, G., Stiller, B., Queck, R., Köstner, B., and Bernhofer, C.: Comparison of surface energy exchange models with eddy flux data in forest and grassland ecosystems of Germany, *Ecol. Model.*, 188, 174–216, 2005.
- Foken, T.: The energy balance closure problem: An overview, *Ecol. Appl.*, 18, 1351–1367, 2008a.
- Foken, T.: *Micrometeorology*, Heidelberg, Springer, 308 pp., 75 cloth, ISBN: 978 3 540 74665 2, 2008b.
- Foken, T., Mauder, M., Liebethal, C., Wimmer, F., Beyrich, F., Leps, J.-P., Raasch, S., DeBruin, H. A. R., Meijninger, W. M. L., and Bange, J.: Energy balance closure for the LITFASS-2003 experiment, *Theor. Appl. Climatol.*, 101, 149–160, 2010.
- Friedrich, K., Mölders, N., and Tetzlaff, G.: On the influence of surface heterogeneity on the Bowen-Ratio: A theoretical case study, *Theor. Appl. Climatol.*, 65, 181–196, 2000.
- Gayler, S., Ingwersen, J., Priesack, E., Wöhling, T., Wulfmeyer, V., and Streck, T.: Assessing the relevance of subsurface processes for the simulation of evapotranspiration and soil moisture dynamics with CLM3.5: Comparison with field data and crop model simulations, *Environ. Earth Sci.*, 69, 415–427, 2013.
- Gebler, S., Hendricks Franssen, H.-J., Pütz, T., Post, H., Schmidt, M., and Vereecken, H.: Actual evapotranspiration and precipitation measured by lysimeters: a comparison with eddy covariance and tipping bucket, *Hydrol. Earth Syst. Sci.*, 19, 2145–2161, doi:10.5194/hess-19-2145-2015, 2015.
- Göckede, M., Markkanen, T., Hasager, C. B., and Foken, T.: Update of a footprint-based approach for the characterisation of complex measurement sites, *Bound.-Lay. Meteorol.*, 118, 635–655, 2006.
- Guo, J. X., Bian, L. G., and Dai, Y. J.: Multiple time scale evaluation of the energy balance during the maize growing season, and a new reason for energy imbalance, *Sci. China Ser. D*, 52, 108–117, 2009.
- Heusinkveld, B. G., Jacobs, A. F. G., Holtslag, A. A. M., and Berkowicz, S. M.: Surface energy balance closure in an arid region: Role of soil heat flux, *Agr. Forest Meteorol.*, 122, 21–37, 2004.
- Imukova, K., Ingwersen, J., and Streck, T.: Determining the spatial and temporal dynamics of the green vegetation fraction of croplands using high-resolution RapidEye satellite images, *Agr. Forest Meteorol.*, 206, 113–123, 2015.
- Inagaki, A., Letzel, M. O., Raasch, S., and Kanda, M.: Impact of surface heterogeneity on energy imbalance: A study using LES, *J. Meteorol. Soc. Jpn.*, 84, 187–198, 2006.

- Ingwersen, J., Steffens, K., Högy, P., Warrach-Sagi, K., Zhunusbayeva, D., Poltoradnev, M., Gäbler, R., Wizemann, H.-D., Fangmeier, A., Wulfmeyer, V. and Streck, T.: Comparison of Noah simulations with eddy covariance and soil water measurements at a winter wheat stand, *Agr. Forest Meteorol.*, 151, 345–355, 2011.
- IUSS Working Group WRB.: World Reference Base for Soil Resources 2006, First Update 2007, World Soil Resources Reports, FAO, Rome, 2007.
- Jacobs, A. F. G., Heusinkveld, B. G., and Holtslag, A. A. M.: Towards closing the surface energy budget of a mid-latitude grassland, *Bound.-Lay. Meteorol.*, 126, 125–136, 2008.
- Kanda, M., Inagaki, A., Letzel, M. O., Raasch, S., and Watanabe, T.: Les study of the energy imbalance problem with eddy covariance fluxes, *Bound.-Lay. Meteorol.*, 110, 381–404, 2004.
- Klaassen, W. and Sogachev, A.: Flux footprint simulation downwind of a forest edge, *Bound.-Lay. Meteorol.*, 121, 459–473, 2006.
- Lamaud, E., Ogée, J., Brunet, Y., and Berbigier, P.: Validation of eddy flux measurements above the understorey of a pine forest, *Agr. Forest Meteorol.*, 106, 187–203, 2001.
- Leuning, R., van Gorsel, E., Massman, W. J., and Isaac, P. R.: Reflections on the surface energy imbalance problem, *Agr. Forest Meteorol.*, 156, 65–74, 2012.
- Mauder, M. and Foken, T.: Impact of post-field data processing on eddy covariance flux estimates and energy balance closure, *Meteorol. Z.*, 15, 597–609, 2006.
- Mauder, M. and Foken, T.: Documentation and Instruction Manual of the Eddy-Covariance Software Package TK3, Arbeitsergebnisse Nr. 46, Universität Bayreuth, Abteilung Mikrometeorologie, ISSN 1614-8916, Bayreuth, 2011.
- Mauder, M., Desjardins, R. L., and MacPherson, I.: Scale analysis of airborne flux measurements over heterogeneous terrain in a boreal ecosystem, *J. Geophys. Res.-Atmos.*, 112, D13112, doi:10.1029/2006JD008133, 2007.
- Mauder, M., Cuntz, M., Drüe, C., Graf, A., Rebmann, C., Schmid, H. P., Schmidt, M., and Steinbrecher, R.: A strategy for quality and uncertainty assessment of long-term eddy-covariance measurements, *Agr. Forest Meteorol.*, 169, 122–135, 2013.
- Meyers, T. P. and Hollinger, S. E.: An assessment of storage terms in the surface energy balance of maize and soybean, *Agr. Forest Meteorol.*, 125, 105–115, 2004.
- Moore, C. J.: Frequency response corrections for eddy correlation systems, *Bound.-Lay. Meteorol.*, 37, 17–35, 1986.
- Oncley, S. P., Foken, T., Vogt, R., Kohsiek, W., DeBruin, H. A. R., Bernhofer, C., Christen, A., van Gorsel, E., Grantz, D., Feigenwinter, C., Lehner, I., Liebethal, C., Liu, H., Mauder, M., Pitacco, A., Ribeiro, L., and Weidinger, T.: The energy balance experiment EBEX-2000. Part I: Overview and energy balance, *Bound.-Lay. Meteorol.*, 123, 1–28, 2007.
- Panin, G. N. and Bernhofer, C.: Parametrization of turbulent fluxes over inhomogeneous landscapes, *Izv. Atmos. Ocean Phy.*, 44, 701–716, 2008.
- Peters, A. and Durner, W.: Improved estimation of soil water retention characteristics from hydrostatic column experiments, *Water Resour. Res.*, 42, W1140, doi:10.1029/2006WR004952, 2006.
- Sakai, R. K., Fitzjarrald, D. R., and Moore, K. E.: Importance of low-frequency contributions to eddy fluxes observed over rough surfaces, *J. Appl. Meteorol.*, 40, 2178–2192, 2001.
- Schotanus, P., Nieuwstadt, F. T. M., and De Bruin, H. A. R.: Temperature measurement with a sonic anemometer and its application to heat and moisture fluxes, *Bound.-Lay. Meteorol.*, 26, 81–93, 1983.
- Schume, H., Hager, H., and Jost, G.: Water and energy exchange above a mixed European Beech – Norway Spruce forest canopy: A comparison of eddy covariance against soil water depletion measurement, *Theor. Appl. Climatol.*, 81, 87–100, 2005.
- Stoy, P. C., Mauder, M., Foken, T., Marcolla, B., Boegh, E., Ibrom, A., Arain, M. A., Arneth, A., Aurela, M., Bernhofer, C., Cescatti, A., Dellwik, E., Duce, P., Gianelle, D., van Gorsel, E., Kiely, G., Knohl, A., Margolis, H., Mccaughy, H., Merbold, L., Montagnani, L., Papale, D., Reichstein, M., Saunders, M., Serrano-Ortiz, P., Sottocornola, M., Spano, D., Vaccari, F., and Varlagin, A.: A data-driven analysis of energy balance closure across FLUXNET research sites: The role of landscape scale heterogeneity, *Agr. Forest Meteorol.*, 171–172, 137–152, 2013.
- Tsvang, L. R., Fedorov, M. M., Kader, B. A., Zubkovskii, S. L., Foken, T., Richter, S. H., and Zeleny, Y.: Turbulent exchange over a surface with chessboard-type inhomogeneities, *Bound.-Lay. Meteorol.*, 55, 141–160, 1991.
- Twine, T. E., Kustas, W. P., Norman, J. M., Cook, D. R., Houser, P. R., Meyers, T. P., Prueger, J. H., Starks, P. J., and Wesely, M. L.: Correcting eddy-covariance flux underestimates over a grassland, *Agr. Forest Meteorol.*, 103, 279–300, 2000.
- UMS GmbH: User Manual HYPROP, Germany, 2012.
- UMS GmbH: Operation Manual KSAT, Germany, 2013.
- Webb, E. K., Pearman, G. I., and Leuning, R.: Correction of flux measurements for density effects due to heat and water vapour transfer, *Q. J. Roy. Meteor. Soc.*, 106, 85–100, 1980.
- Wilson, K., Goldstein, A., Falge, E., Aubinet, M., Baldocchi, D., Berbigier, P., Bernhofer, C., Ceulemans, R., Dolman, H., Field, C., Grelle, A., Ibrom, A., Law, B. E., Kowalski, A., Meyers, T., Moncrieff, J., Monson, R., Oechel, W., Tenhunen, J., Valentini, R., and Verma, S.: Energy balance closure at FLUXNET sites, *Agr. Forest Meteorol.*, 113, 223–243, 2002.
- Wilson, K. B., Hanson, P. J., Mulholland, P. J., Baldocchi, D. D., and Wullschlegel, S. D.: A comparison of methods for determining forest evapotranspiration and its components: Sap-flow, soil water budget, eddy covariance and catchment water balance, *Agr. Forest Meteorol.*, 106, 153–168, 2001.
- Wohlfahrt, G., Irschick, C., Thalinger, B., Hörtnagl, L., Obojes, N., and Hammerle, A.: Insights from independent evapotranspiration estimates for closing the energy balance: A grassland case study, *Vadose Zone J.*, 9, 1025–1033, 2010.
- Wolf, A. and Laca, E. A.: Cospectral analysis of high frequency signal loss in eddy covariance measurements, *Atmos. Chem. Phys. Discuss.*, 7, 13151–13173, doi:10.5194/acpd-7-13151-2007, 2007.
- World Meteorological Organization (WMO): Instruments and Observing Methods – WMO Field intercomparison of rain intensity gauges, Report No. 99, 2009.

5 Determining the Spatial and Temporal Dynamics of the Green Vegetation Fraction of Croplands using high-resolution RapidEye satellite images

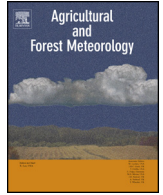
Kristina Imukova, Joachim Ingwersen and Thilo Streck

Institute of Soil Science and Land Evaluation, Department of Biogeophysics, University of Hohenheim, 70593 Stuttgart, Germany

Chapter 5 is published with the consent of the Elsevier B.V. The original publication was in: Journal of Agricultural and Forest Meteorology (2015), Volume 206, Pages 113–123. It can be found under the following link: <https://doi.org/10.1016/j.agrformet.2015.03.003>

Contents lists available at [ScienceDirect](http://www.sciencedirect.com)

Agricultural and Forest Meteorology

journal homepage: www.elsevier.com/locate/agrformet

Determining the spatial and temporal dynamics of the green vegetation fraction of croplands using high-resolution RapidEye satellite images



Kristina Imukova^{*}, Joachim Ingwersen, Thilo Streck

Institute of Soil Science and Land Evaluation, University of Hohenheim, 70593 Stuttgart, Germany

ARTICLE INFO

Article history:

Received 15 July 2014

Received in revised form 3 March 2015

Accepted 7 March 2015

Available online 26 March 2015

Keywords:

Green vegetation fraction

RapidEye

NOAH-MP

Land surface model

Crop phenology

Digital camera

Winter wheat

Silage maize

Winter rape

ABSTRACT

The green vegetation fraction (GVF) is a key input variable of the evapotranspiration scheme applied in the widely used NOAH-MP land surface model (LSM). In standard applications of the NOAH-MP, the GVF is taken from a global map with a 15 km × 15 km resolution. The central objective of the present study was (a) to derive gridded GVF data of a region in Southwest Germany in a high spatial resolution (5 m × 5 m) from RapidEye satellite images, and (b) to improve the representation of the GVF dynamics of croplands in the NOAH-MP for a more accurate simulation of water and energy exchange between land surface and atmosphere. The GVF dynamics were determined based on the normalized difference vegetation index (NDVI) calculated from the red and near-infrared bands of the satellite images. The satellite GVF data were calibrated and validated against ground truth measurements. Based on the obtained calibration scheme, GVF maps were derived in a monthly resolution for the region. Our results confirm a linear relationship between GVF and NDVI and demonstrate that it is possible to determine the GVF of croplands from RapidEye images based on a simple two end-member mixing model. Our data highlight the high variability of the GVF in time and space. At the field scale, variability was mainly caused by soil heterogeneities and management differences. At the regional scale, the GVF showed a bimodal distribution formed by the different phenology of crops. We suggest to divide croplands according to their distinctly different temporal dynamics of the GVF into “early-covering” (winter rape, winter wheat, spring barley) and “late-covering” crops (sugar beet, silage maize). Based on our results, we recommend that simulations with LSM should take into account this differentiation of croplands, since it is to be expected that these two crop groups produce pronounced differences in energy partitioning at the land surface.

© 2015 Elsevier B.V. All rights reserved.

1. Introduction

Weather and climate simulations are essential to assess the impact of global climate change on agriculture. The quality of weather and climate simulations critically depends on the accurate representation of land surface exchange processes, which are simulated by so-called land surface models (LSMs). The central purpose of a LSM is to partition the net radiation at the land surface into sensible and latent heat flux. This partitioning controls the extent of the boundary layer, the formation of clouds and the distribution of rainfall. A widely used LSM is NOAH (Chen and Dudhia, 2001). Its development has been started about 25 years ago. Since then, it has undergone continuous improvement. Recently, NOAH has been

extended to NOAH-MP by implementing multi-physics options and a semi-tile approach (bare and vegetated tile) for an improved description of land surface heterogeneities (Niu et al., 2011). NOAH was designed to be coupled with the Mesoscale Meteorology Model 5 (Dudhia, 1993) and was later coupled with the Weather Research and Forecasting (WRF) model (see, e.g., Skamarock et al., 2008). The WRF model is intended for use from the large eddy simulation scale up to the global scale.

In local to regional weather forecast simulations, NOAH-MP is typically applied with grid cell sizes from 3 × 3 km² to 20 × 20 km². At such resolutions, the model design must be a compromise between the detailedness of process description and data availability. As a consequence, NOAH-MP, like other LSMs, relies on simplified modelling parameterizations. Rather than explicitly simulating plant growth and the seasonal dynamics of the physiological properties of the crop canopy, NOAH-MP uses external data of vegetation development, typically by a satellite-derived map of the

^{*} Corresponding author. Tel.: +49 711 459 22327; fax: +49 711 459 23117.

E-mail address: Kristina.Imukova@uni-hohenheim.de (K. Imukova).

green vegetation fraction (GVF). GVF is defined as the grid-cell fraction that is covered with green canopy (Gutman and Ignatov, 1998). GVF is a two-dimensional property of the upper canopy (Rundquist, 2002) and represents the horizontal density of vegetation in each grid cell (Gutman and Ignatov, 1998). NOAH-MP computes net longwave, latent, sensible and ground heat flux separately for a bare soil (1- green fraction cover (FVEG)) and vegetated tile (FVEG) within each grid cell, while short-wave radiation fluxes are computed over the entire grid cell (semi-tile approach; Niu et al., 2011). In NOAH-MP, one option to parameterize FVEG is to use gridded GVF data. In standard applications, gridded GVF data are taken from a global map with a 0.15° resolution ($15 \times 15 \text{ km}^2$ grid cell size). This global map was derived from normalized difference vegetation index (NDVI) data derived from NOAA advanced very high resolution radiometer (AVHRR) (Gutman and Ignatov, 1998).

At the plot scale, the GVF is usually estimated visually (Liu et al., 2009) or derived from digital color photographs (Zerger et al., 2012; Lukina et al., 1999; Crimmins and Crimmins, 2008; Rundquist, 2002; Hirano et al., 2004). An advantage of evaluating digital photographs is that this eliminates the subjectivity in visual estimations. The GVF based on digital photographs is usually determined by subtracting the red and the green band of the images and counting pixels below a certain threshold as green pixel or by applying a supervised pixel-based classification method (e.g., Rundquist, 2002). At the field and regional scale, the GVF is usually derived from multispectral satellite images. The approach used most widely is to estimate the GVF from the normalized difference vegetation index (NDVI) (Gutman and Ignatov, 1998; Qi et al., 2000; Xiao and Moody, 2005; Yue et al., 2013; Carlson and Ripley, 1997). The NDVI is computed from the reflectance at the NIR (ρ_{NIR}) and red (ρ_{red}) bands:

$$\text{NDVI} = \frac{(\rho_{\text{NIR}} - \rho_{\text{red}})}{(\rho_{\text{NIR}} + \rho_{\text{red}})}, \quad (1)$$

The GVF can then be computed from the NDVI with the help of commonly used spectral mixture analysis (SMA) (Xiao and Moody, 2005). The assumption is that each pixel signal of the satellite data results from a mixture of two endmembers: bare soil and vegetation. The computed NDVI value is then taken as a linear combination of the NDVIs of the two components according to their proportion. In the present study, we will call this method, the two-point approach. The NDVI of bare soil depends on soil organic matter content, soil water content etc. The NDVI of vegetation is a function of chlorophyll content. The relation between NDVI and GVF is

therefore usually region- and season-specific (Qi et al., 2000; Price, 1992; Gutman and Ignatov, 1998).

The accuracy of GVF data derived from satellite data highly depends on the resolution of the latter (Jiang et al., 2006). Low-resolution data such as those routinely used with the NOAH model represent mixtures of different land uses within one pixel leading to mixed GVF pixel values, which may seriously compromise the quality of regional and climate simulations. In our study, for the first time we derived GVF data with high spatial resolution using RapidEye satellite images with a cell grid size of $5 \times 5 \text{ m}^2$. The RapidEye system consists from five satellites and is operated by BlackBridge (Berlin, Germany, <http://web-dev.rapideye.de>). The system produces multispectral images with five bands: blue (440–510 nm), green (520–590 nm), red (630–685 nm), red-edge (690–730 nm) and near infrared (NIR) (760–850 nm) (RapidEye AG, 2012). A further advantage of high-resolution data is that they can easily be compared to ground measurements.

In the present study, we will derive and test high-resolution GVF data for a 1500 km^2 region in Southwest Germany over two vegetation periods (April–October 2012 and 2013). Based on these data, we quantify and analyze the temporal and spatial variability of the GVF at the field and regional scale. Finally, we discuss possible implications of our findings for the parameterization of LSMs.

2. Material and methods

2.1. Study site

The present study was performed in Southwest Germany within the Kraichgau region (Fig. 1). The Kraichgau covers about 1523 km^2 and has a mild climate with a mean annual temperature of $9\text{--}10^\circ\text{C}$ and annual precipitation between 730 and 830 mm. The rivers Neckar and Enz form the borders in the East. In the North and in the South, the region is bounded by the low mountain ranges Odenwald and Black Forest. In the West, Kraichgau is adjacent to the Upper Rhine Plain (Oberrheinischen Tiefland). Kraichgau region is a gently sloping hilly territory with elevations between 100 and 400 m above sea level (a.s.l.). Soils have mostly been formed from loess material. The region is intensively used for agriculture. Around 46% of the total area is used for crop production. Winter wheat, winter rape, spring barley, corn, silage maize and sugar beet are the predominant crops.

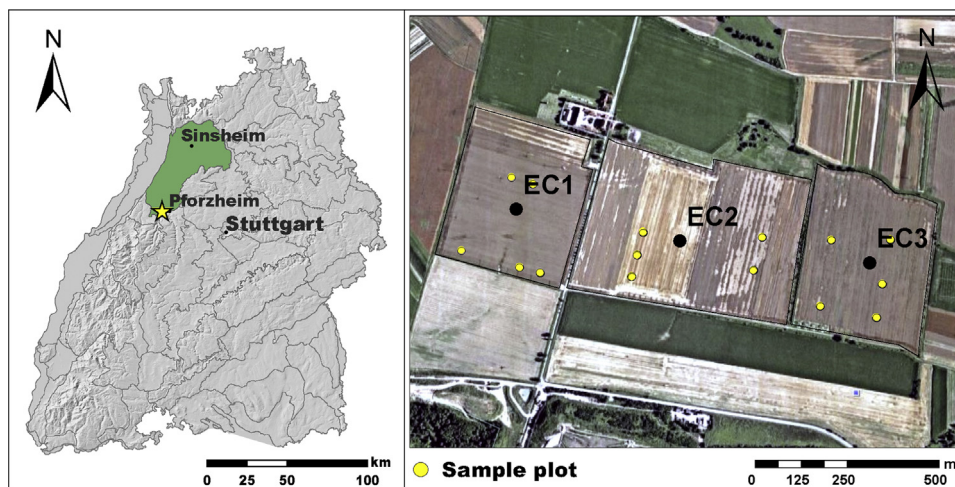


Fig. 1. The study region “Kraichgau” (green) on the map of Baden-Württemberg state. The location of the central study site is marked by a yellow star. On the right, the scene of Google map shows the scaled-up central study site with sample plots (ground truth). (For interpretation of the references to color in this figure legend, the reader is referred to the web version of this article.)

Ground truth measurements were performed at three agricultural fields (EC1–EC3) belonging to the farm “Katharinentalerhof”. The fields are situated in north of the city of Pforzheim (48°55′44″N, 8°42′36″E, 318 m a.s.l.) and managed by a local farmer. The fields EC1–EC3 are 14, 23 and 15 ha large, respectively. Soil type is stagnic cambisol (WRB) at all three sites. In 2012, at EC1 winter rape (*Brassica napus* L. ssp. *napus*; cv. Artoga), at EC2 silage maize (*Zea mays* L., cv. Cannavaro), and at EC3 winter wheat (*Triticum aestivum* L. cv. Akteur) were grown. In 2013, at EC1 and EC2 winter wheat (*Triticum aestivum* L. cv. Akteur) and at EC3 winter rape (*Brassica napus* L. ssp. *napus* cv. Alabaster and Fregat) were cropped.

In the center of each field, an eddy covariance station was operated. Global radiation was determined with a NR01 4-component sensor (NR01, Hukseflux Thermal Sensors, The Netherlands). Air temperature and humidity (HMP45C, Vaisala Inc., USA) were measured in 2 m height. Rainfall was measured with a tipping bucket (resolution: 0.2 mm per tip). Meteorological data were recorded at half-hour intervals. The weather conditions in 2012 and 2013 are summarized in Table 1.

2.2. Ground measurement of GVF

Ground truth measurements of GVF were conducted at five permanently marked plots (1 m × 1 m) within each field (Fig. 1). Their exact position (±0.02 m) was determined with a Differential Global Positioning System (APS-3, Altus Positioning Systems, USA). From these plots canopy, photos were taken with a Nikon COOLPIX P7000 digital camera (Nikon Corporation, Tokyo, Japan). The camera was mounted to a portable custom-made mast. Photos were taken from one meter above the canopy (nadir sampling). During the vegetation period (April–October), photos were taken in almost weekly resolution. Using the automatic mode of the camera, we took color images with and without flash. The resolution of the photos was 3648 × 2736 pixels. In parallel to the ground truth measurements, at each acquisition day, the principal growth stages of crops were determined using the BBCH scale (Meier et al., 2009).

The green area (GV, see Eq. (2)) of the photographs was determined by calculating the difference between red and green pixel values (Rundquist, 2002) as follows:

$$GV = \text{Red} - \text{Green}, \tag{2}$$

Resulting pixels below the certain threshold (GV_{th}) were counted as green pixels. The ratio between green pixels and the total amount of pixels gives the GVF. All photographs were processed with ArcGIS 10 (ArcGIS 10, Esri, USA). The threshold GV_{th} was derived from a comparison between Rundquist’s approach and a supervised classification scheme implemented in ArcGIS 10 (ArcGIS 10, Esri, USA). In ArcGIS, for selected photos, we defined training areas of green pixels and non-green pixels including bare soil and senescent parts. Based on the spectral signature of each class, a maximum-likelihood estimation classified the remaining

pixels into these two classes. We found the best agreement between both methods for a GV_{th} of –10. A visual inspection of 30 randomly selected images confirmed the robustness of this threshold.

2.3. RapidEye data and processing

RapidEye satellite images with radiometric and geometric corrections were obtained from the German Aerospace Center (DLR). Due to the sensitivity of NDVI to atmospheric conditions (Song et al., 2001; McDonald et al., 1998; Myneni and Asrar, 1994; Qi et al., 2000) and to allow for a proper comparison of the scenes of different months, atmospheric effects were removed from the images using the ATCOR2 atmospheric correction model (Richter, 1996a,b). Corrected images were merged into one scene according to their acquisition day.

In 2012, RapidEye images for the whole study region were available for the months May–July, September, and October. In 2013, images were acquired from the DLR in April, May, July and August. Scenes containing all ground truth sites for comparison with the ground measurements of GVF, were available for five days in 2012 (24.05.12, 30.06.12, 23.07.12, 05.09.12, and 21.10.12) and for two days in 2013 (13.04.13 and 18.05.13).

2.3.1. Computing the GVF from RapidEye satellite images

As mentioned above, the SMA approach assumes a linear relationship between GVF and NDVI:

$$GVF = \frac{(NDVI - NDVI_0)}{(NDVI_\infty - NDVI_0)} \tag{3}$$

where $NDVI_0$ and $NDVI_\infty$ are the NDVI of bare soil and of dense vegetation, respectively. This equation can be rewritten as:

$$GVF = aNDVI - b \tag{4}$$

where a and b are slope and intercept of the linear function given by:

$$a = \frac{1}{NDVI_\infty - NDVI_0} \tag{5}$$

$$b = \frac{NDVI_0}{NDVI_\infty - NDVI_0} \tag{6}$$

According to the literature (Montandon and Small, 2008; Yue et al., 2013; Jiménez-muñoz et al., 2009; Gutman and Ignatov, 1998), $NDVI_\infty$ and $NDVI_0$ can be calculated as maximum and minimum observed NDVI, respectively, provided that it is possible to find pure pixels with full vegetation cover and pure pixels with bare soil. As discussed in several studies (Qi et al., 2000; Price, 1992; Gutman and Ignatov, 1998), the NDVI value of bare soil and dense vegetation is site- and season-specific, because NDVI depends on, among others, soil and vegetation type as well as soil water and chlorophyll content. The high resolution of the RapidEye satellite images together with the field observations allowed to precisely determine $NDVI_\infty$ and $NDVI_0$ at the field scale. For the three study crops, $NDVI_\infty$ was determined when the maximum GVF was reached.

In an alternative approach, the parameters a and b were determined by linearly regressing GVF derived from ground truth against the NDVI data derived from the RapidEye images. Because the number of available scenes was unevenly distributed between the two years (5 acquisition dates in 2012 and 2 acquisition dates in 2013), the two-year dataset ($N = 105$) was randomly split into a calibration and validation subset before performing the regression. This procedure was repeated 10 times, and the means of the slopes and intercepts were computed.

Table 1
Mean temperature, mean global radiation and rainfall during the vegetation periods 2012 and 2013.

Month	Mean global radiation, $W m^{-2}$		Mean temperature, C°		Rainfall, mm	
	2012	2013	2012	2013	2012	2013
March	144.5	113.5	7.2	1.9	13.0	27.2
April	174.3	160.5	9.6	9.7	48.0	56.6
May	262.4	168.5	15.3	10.9	51.5	169.1
June	236.1	254.2	16.5	15.8	111.1	103.7
July	213.7	272.2	17.7	19.7	105.7	46.4
August	225.4	211.4	19.3	18.1	33.5	73.6
September	166.6	136.9	13.9	14.3	65.9	115.8

2.3.2. Generation of regional GVF maps

For each acquisition date, regional maps were derived by joining 4–12 scenes into one mosaic. Twelve scenes covered the whole Kraichgau region, but for some months, not all scenes could be collected by the satellite system at one gangway. To restrict the evaluation to croplands, each mosaic was overlaid with a land used map processed and provided by the Federal State Office (LUBW, 2010). This map is based on the image of Landsat 7 of the year 2000. Areas obscured by clouds were excluded from the analysis. These areas were identified with the interactive supervised classification tool of ArcGIS (ArcGIS 10, Esri, USA), which uses a maximum-likelihood algorithm. Pixels with negative values (less than 1% per map) were excluded. Negative NDVIs are usually related to water surface, snow or artificial materials like concrete or asphalt. Table 2 summarizes the different acquisition dates, number of available scenes and size and fraction of cropland area included in the analysis.

2.4. Statistical analysis

The quality of regressions for deriving GVF from satellite was evaluated based on the criteria model efficiency (EF), root mean square error (RMSE) and bias. EF is defined as the proportion of the total variance explained by a model:

$$EF = 1 - \frac{\sum_{i=1}^N (P_i - O_i)^2}{\sum_{i=1}^N (O_i - \bar{O})^2}, \tag{7}$$

where P_i denotes predicted values, O_i and \bar{O} – observed values and their mean, respectively, while N is the number of observations. RMSE and bias were calculated as:

$$RMSE = \sqrt{\frac{1}{N} \sum_{i=1}^N (P_i - O_i)^2} \tag{8}$$

and

$$bias = \frac{1}{N} \sum_{i=1}^N (P_i - O_i). \tag{9}$$

Student's t -test was used to test if slopes and intercepts of the linear regression were significantly different from zero at $\alpha=0.05$. The GVF distributions were checked for normality with the Shapiro–Wilk test. All statistical tests were performed using RStudio (Version 0.98.490, RStudio Inc.).

For each regional map, we computed a histogram of GVF. To the received bi-modal data, we fitted a combination of two Gaussian peak functions (Fig. 9), assuming a normal distribution for each peak. This was performed with a help of the fitting tool of the Origin 7.5 (Origin 7.5, OriginLab Corporation, USA). This tool considers for each distribution an own width (w_1, w_2), center (xc_1, xc_2) and

amplitude (A_1, A_2), but uses a shared y offset (y_0) (Eq. (10)), which we set to zero in the present case.

$$y = y_0 + \frac{A_1}{w_1 \sqrt{\pi/2}} e^{-2 \frac{(x-xc_1)^2}{w_1^2}} + \frac{A_2}{w_2 \sqrt{\pi/2}} e^{-2 \frac{(x-xc_2)^2}{w_2^2}} \tag{10}$$

3. Results

3.1. GVF dynamic of crops

The majority of photos was taken on sunny days without clouds at Middle European Time between 11 am and 1 pm, when the effect of shadow is minor (Duggin and Philipson, 1982). For comparison, the photos were taken with and without flash. In photos taken without flash, leaves in the understory of the canopy were often shadowed by leaves above, so that the corresponding pixels were identified as non-green pixels. Therefore, photos taken without flash tended to underestimate the actual GVF. The flash reduced this effect by resulting in a better illumination of the different canopy stories, thus, yielding higher GVF values. All results presented in the following are based on photos taken with flash.

Figs. 2 and 3 show time-sequences of selected photographs of the canopies taken in 2012 and 2013, respectively. Due to wide row spacing (~0.7 m), the leaf coverage of maize never exceeded 90%. Due to late drilling, the maize field achieved maximum GVF much later in the year than the other crops. Maize was green on the field, while winter wheat and rape were fully senescent and later already harvested. The most homogeneous leaf coverage was achieved by winter wheat. During spring and early summer, leaf coverage of rape was patchy, so that some spots of bare soil can be seen. During May, yellow rape flowers made up for a significant fraction of the photographs hampering to some degree, the computation of the GVF during that period (see below). GVF of winter wheat and winter rape reached their maxima nearly at the same period. Afterwards, the greenness of winter wheat decreased drastically, while winter rape stayed green for about three weeks longer.

Fig. 4 shows the seasonal dynamics of GVF for winter rape, maize and winter wheat over the vegetation periods 2012 and 2013. In 2012, the GVF of winter wheat increased during the tillering and stem elongation stages [day of the year (DOY): 76–139]. Maximum GVF of winter wheat was observed at the end of the stem elongation stage and during booting stage [DOY: 139]. In June, during heading, flowering and grain filling [DOY: 153–188] GVF sharply declined to 50–55%. In the ripening and senescence periods, green vegetation cover was close to zero [DOY: 195–202]. In 2013, we observed similar dynamics but due to the colder weather conditions in the beginning of the season, phenological development, and with that the GVF dynamics were delayed by around 10 days compared with

Table 2 Overview of the RapidEye satellite images that were used in the present to determine the green vegetation fraction in Kraichgau (southwest Germany) in 2012 and 2013. The Kraichgau region covers in total 12 scenes, and the total area of croplands is 706.6 km².

Acquiring date	Number of RapidEye scenes in Mosaic	Cropland area included in the analysis	
		km ²	%
24 May 2012 ^a	12	692.2	98.0
30 June 2012 ^a	10	659.6	93.3
23 July 2012 ^a	12	703.2	99.5
05 September 2012 ^a	12	498.1	70.5
21 October 2012 ^a	11	620.4	87.8
14 April 2013	6	352.0	49.8
24 April 2013 ^a	11	596.6	84.4
18 May 2013 ^a	12	547.9	77.5
19 July 2013	7	377.9	53.5
29 August 2013	4	223.90	31.7
03 September 2013	10	577.3	81.7

^a Mosaic that contains a RapidEye scene used for comparison between satellite data and ground-truth measurements of the green vegetation fraction.

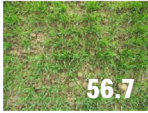


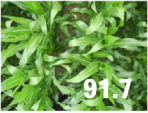

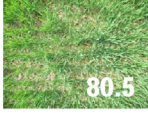

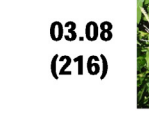

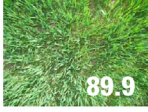



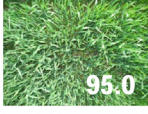


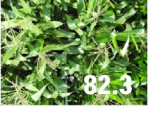


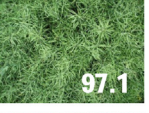
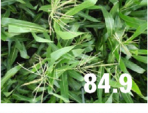

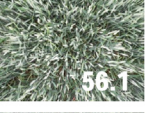
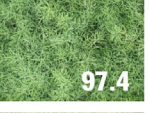

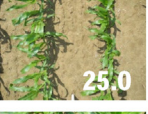
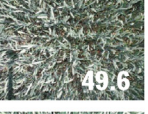


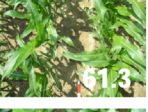

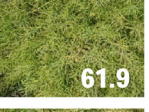



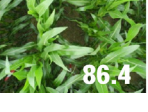


Date (DOY)	Maize	Wheat	Rape	Date (DOY)	Maize	Wheat
10.04 (101)				20.07 (202)		
27.04 (118)				03.08 (216)		
02.05 (123)				10.08 (223)		
18.05 (139)				17.08 (230)		
01.06 (153)				22.08 (235)		
08.06 (160)				05.09 (249)		
22.06 (174)				14.09 (258)		
29.06 (181)						
06.07 (188)						
13.07 (195)						

Fig. 2. Time sequence of digital color images from the canopy-top of maize, winter wheat and winter rape. The photographs were taken at the central study site of the Kraichgau region in 2012. Numbers in the photographs give the green vegetation fraction (GVF) in percentage. The number in brackets below the data is, the day of the year (DOY).

2012. In 2013, on DOY: 156, the crop was still in the booting stage, and heading and flowering were shifted to DOY:163–171 (Fig. 5). At harvest time, about 5% of the pixels were still classified as “green”. Moreover, in 2013, the transition of the GVF from booting to ripening period was smoother than in 2012 (Figs. 4 and 5).

During inflorescence emergence of winter rape in March and April 2012 [DOY: 76–118], we observed a continuous increase of the GVF. During flowering [DOY: 118–139], estimated GVF declined due to the large number of yellow flowers, while based on a visual estimation, the green vegetation cover was close to 100%. Yellow flowers made the underlying green leaves invisible for the camera. The maximum GVF close to 100% was reached in June during fruit development [DOY: 153–181]. Similar as for cereals, the GVF dropped sharply during ripening and senescence in July [DOY: 188–195]. As with wheat, the general pattern of the GVF dynamic

was similar in both years, but due to the colder weather in 2013, flowering [DOY: 120–148] was prolonged by around one week in comparison with the year 2012. During ripening, the GVF value was higher than in the preceding year was observed [DOY: 190–204]. At a harvest time, the green cover was still about 23% (Fig. 5). In contrast to winter wheat, winter rape stayed longer green. While the GVF of winter wheat declined during heading, flowering and grain filling (DOY: 153–188 in 2012, DOY: 163–190 in 2013), the GVF of winter rape remained constant during these phenological stages. Consequently, the ripening/senescence phase of winter rape was much shorter than that of winter wheat.

GVF of silage maize was very different from that of winter wheat and winter rape. The GVF of the two winter crops reached their maxima already in the end of May. At this time, the GVF of silage maize was still close to zero. In the end of June, all three crops


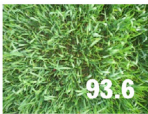
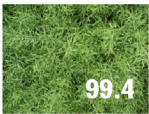










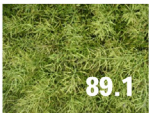



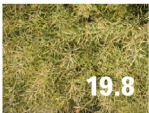






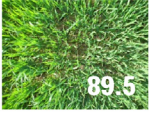

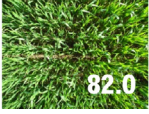
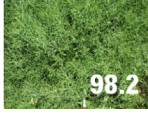
Date (DOY)	Wheat	Rape	Date (DOY)	Wheat	Rape
21.03 (80)		 45.6	12.06 (163)	 93.6	 99.4
10.04 (100)		 68.9	20.06 (171)	 87.7	 99.0
17.04 (107)	 71.1	 81.0	26.06 (177)	 58.5	 99.1
23.04 (113)	 88.7	 93.1	09.07 (190)	 45.4	 89.1
30.04 (120)	 92.7	 98.2	17.07 (198)	 13.5	 19.8
08.05 (128)	 93.9	 72.6	23.07 (204)	 0.0	 18.6
14.05 (134)	 94.0	 69.6			
28.05 (148)	 89.5	 93.2			
05.06 (156)	 82.0	 98.2			

Fig. 3. Time sequence of digital color images from the canopy-top of winter wheat and winter rape. The photographs were taken at the central study site of the Kraichgau region in 2013. Numbers in the photographs give the green vegetation fraction (GVF) in percentage. The number in brackets below the data is the day of the year (DOY).

approach the same GVF of about 50%, and the three GVF lines cross around DOY: 181. Afterwards, the GVF of the winter crops diverge again from that of the summer crop. While the winter crops enter their ripening phase accomplished with a strong decline of GVF, silage maize moves toward its GVF maximum. The GVF of the silage maize continuously increased from germination over stem elongation to the heading stage [DOY: 202] toward a maximum value of about 90%. During flowering and fruit development, GVF slightly went down [DOY: 216–249]. At harvest, silage maize had still a high GVF of about 70%.

3.2. GVF–NDVI relationship

NDVIs of bare soil and dense vegetation are needed to estimate GVF with the two-point approach (see Eq. (3)). The NDVI of bare soil was determined based on the scenes of 24 May 2012, 5 September 2012, and 3 September 2013. On 24 May 2012, the maize at EC2 was shortly before emergence. On 5 September 2012, at EC3, winter rape was harvested and the soil was ploughed. At these two days,

NDVI of bare soil ranged between 0.05 and 0.20. On 3 September 2013, the NDVI of bare soil was between 0.1 and 0.2 on the fields EC1 and EC2, where winter wheat had been harvested and the soil ploughed. Based on the above ground truth observations, we selected images from the days at which the highest GVFs have been observed in the ground observations during the entire vegetation period for deriving maximum NDVI values from RapidEye images. Maximum NDVIs of winter rape, winter wheat and silage maize were 0.95 [24.05.12], 0.94 [18.05.13], and 0.88 [23.07.12], respectively. Based on these measurements, we derived (see Eq. (4)) the following equation ($NDVI_{max} = 0.95$; $NDVI_{mi} = 0.05$):

$$GVF = 1.11 \times NDVI - 0.06 \quad (11)$$

Based on the ground truth data, the modeling efficiency (EF) of the two-point approach was 0.86, while RMSE was 0.15 and the bias 0.084. Additionally, we performed a linear regression of GVF derived from ground truth data and on NDVI determined from RapidEye images. The results are given in Table 3. The modeling efficiency of the general regression was slightly higher than that

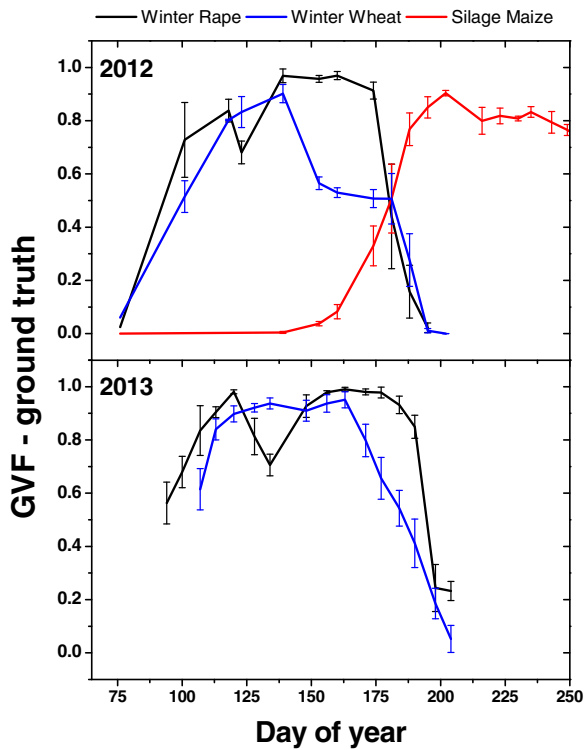


Fig. 4. Dynamics of the green vegetation fraction (GVF) based on photographs taken from 1 m above the canopy at the central study sites of Kraichgau in 2012 and 2013. (For interpretation of the references to color in this figure legend, the reader is referred to the web version of this article.)

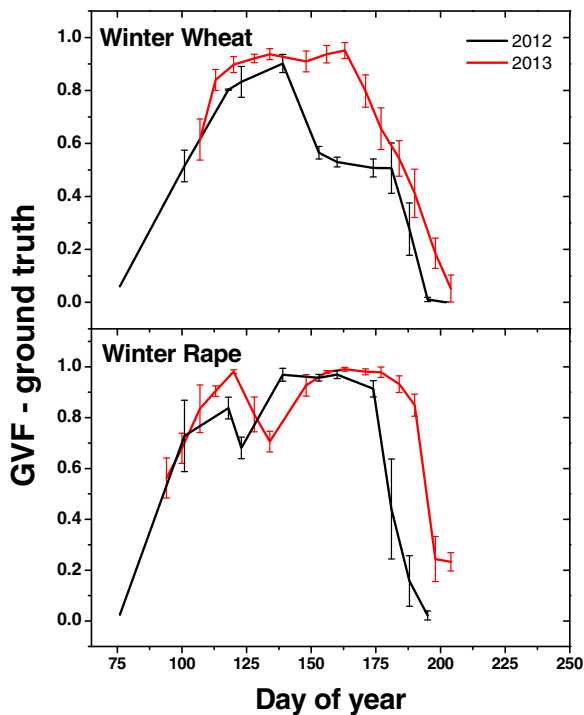


Fig. 5. Comparison of green vegetation fraction (GVF) dynamics of winter wheat and the winter rape in 2012 and 2013 based on photographs taken from 1 m above the canopy at the central study sites of Kraichgau.

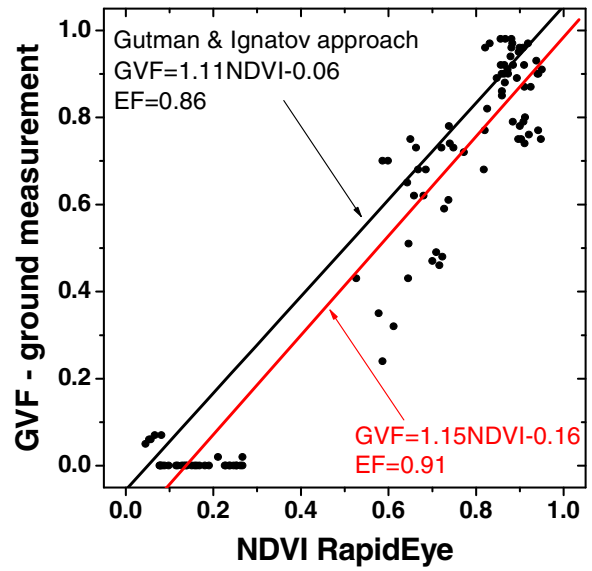


Fig. 6. Relationship between measured GVF and NDVI calculated from RapidEye images. The black line shows the relationship between both variables following the Gutman and Ignatov (1998) approach. The red line shows the linear regression of GVF from ground truth measurements on NDVI calculated from RapidEye images. (For interpretation of the references to color in this figure legend, the reader is referred to the web version of this article.)

of the two-point approach (EF = 0.91). Regression results were, of course, non-biased, RMSE was 0.12. Fig. 6 compares the result of the regression analysis and the two-point approach. The linear regression was validated against the second subset that had not been used in the regression (see Section 2.3.1). The statistical criteria for the regression equation (EF = 0.91, RMSE = 0.11, bias = 0.008) were similar to those of the calibration data. The regression equation was used to generate the gridded GVF data of the Kraichgau region. We repeated the linear regression crop-wise. Mean slopes and intercepts are summarized in Table 3. Based on Student's *t*-test, the regression parameters of maize were significantly different from those of the winter crops, while the differences between those of the latter were not ($\alpha = 0.05$).

The high intercepts in case of winter wheat and winter rape is a result of senescence. NDVI of senescent plants was higher than NDVI of bare soil, while GVF for both of them equals to zero. Shortly before harvest, both crops lost their chlorophyll, thus, the greenness cover was about zero and the soil was covered with dry vegetation like it is shown on the photographs of Figs. 2 and 3 on DOY: 195 and 202 in 2012 and DOY: 204 in 2013. In this case, the average NDVI of the winter wheat was 0.25 ± 0.01 and that of the winter rape was 0.23 ± 0.01 . The mean NDVI of bare soil of sample plots remained the same in all three fields in both years. It was about 0.13 with a standard deviation around 0.01.

Table 3
Results of regressing GVF on NDVI ($GVF = a \text{ NDVI} + b$). Numbers in bracket give standard errors.

Crop	Mean slope (a)	Mean intercept (b)	EF
Winter rape	1.38 (0.09) ^a	-0.30 (0.07) ^a	0.89
Winter wheat	1.35 (0.07) ^a	-0.34 (0.06) ^a	0.91
Silage maize	0.92 (0.05) ^b	-0.005 (0.03) ^b	0.95
All	1.15 (0.05) ^c	-0.16 (0.03) ^c	0.91

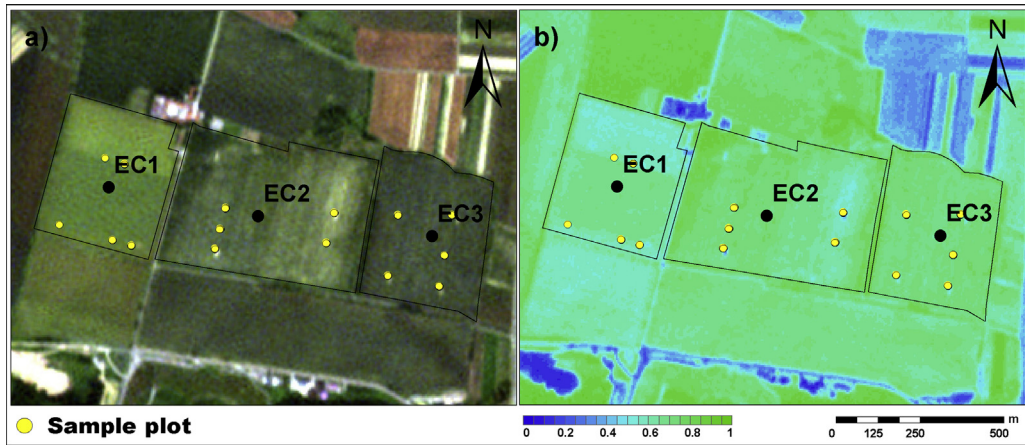


Fig. 7. (a) RapidEye image (RGB) of the central study site Katharinentalerhof taken on June 30, 2012 [DOY: 182]. (b) Green vegetation fraction (GVF) map derived from the same RapidEye image. The more green the pixel, the higher the GVF. Bluish pixels indicate areas almost void of vegetation.

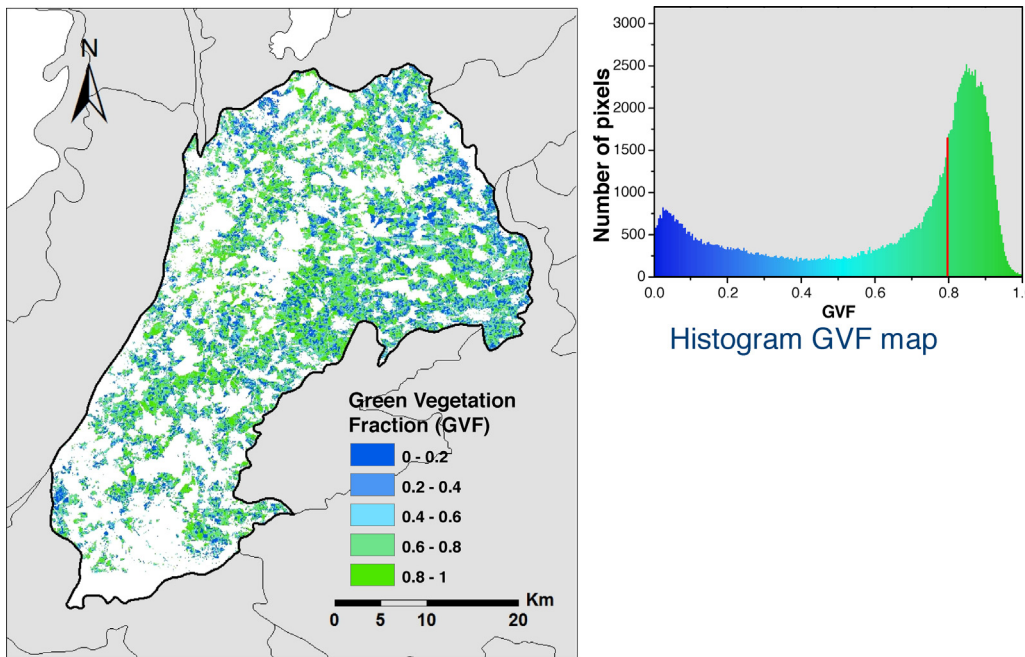


Fig. 8. Map of the green vegetation fraction (GVF) of Kraichgau region calculated from RapidEye data on 24 May 2012. The inset shows the histogram of the GVF. The red line indicates the GVF used by the NOAA-MP land surface model in large-scale simulations.

3.3. High-resolution 2D GVF fields

3.3.1. Field scale

Fig. 7 shows, by way of example, a RapidEye scene of the central study site acquired on 30 June 2012 and the derived GVF map. The bright green color indicates areas with a high green vegetation cover. The dense blue color is related to bare soil or sparsely vegetated areas. Buildings and asphalt roads were not excluded from the scene and show up in the graph as bluish pixels. During both vegetation periods, we observed in most cases that the distribution of GVF in each field was bell-shaped (data are not shown). The most homogeneous spatial distribution of GVF was observed at EC3. In June 2012, the distribution of the green cover was normal at EC3 ($\alpha=0.05$). In 2012, we observed at EC1 (winter rape), larger contiguous zones of lower and higher GVF. In the north of the field, there was a strip with GVF lower than in the southern part of the field, which resulted in a bi-modal distribution. In June

2012, we observed in the eastern part of the EC2 field (silage maize) a north–south strip of lower GVF, while in July and September 2012, the GVF distribution had a bell shape at this field. These differences were mostly related to differences in management (see Section 4).

3.3.2. Regional scale

At the regional scale, the GVF data showed bi-modal distributions (Figs. 8 and 9). In the scene of 24 May 2012, for example, the histogram shows two clearly distinct peaks in the low (blue color) and the high (green color) range. The dense dark blue color covers around 17% of the total area. Highest GVF values (80–100%; dark green) contribute 38% of the total area. At 28% of the total area, GVF was between 0.6 and 0.8. To each histogram, we fitted a bi-modal Gaussian distribution (red and green lines in Fig. 9). In nearly all months, both distributions were clearly separated from each other. Only in June, both distributions distinctly overlapped.

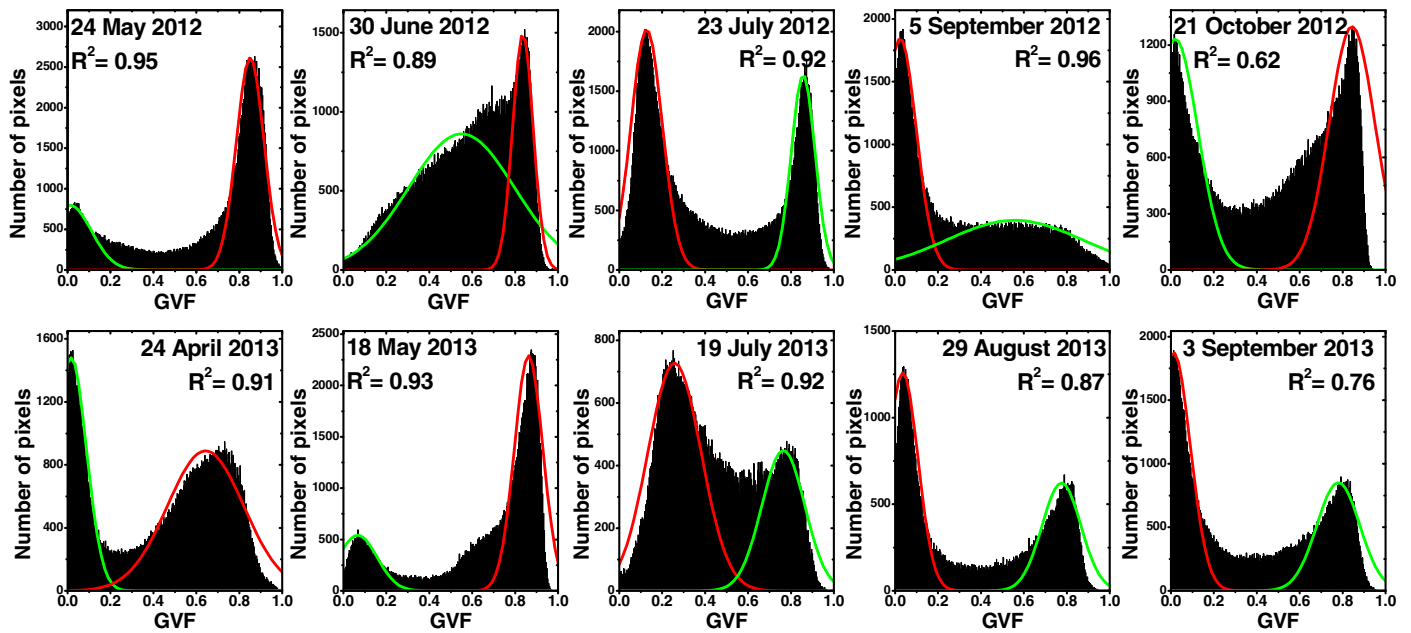


Fig. 9. Histograms of the green vegetation fractions over croplands at the Kraichgau region in 2012 and 2013. GVF data were derived from RapidEye satellite images (resolution: 5 m \times 5 m). The red and green lines show fitted Gaussian distributions. (For interpretation of the references to color in this figure legend, the reader is referred to the web version of this article.)

4. Discussion

In the present study, we successfully used color images from a digital camera to measure the dynamics of GVF for different crops over two seasons. Rundquist's method is simple and allows for automating the evaluation process thereby reducing human subjectivity. In our study, we found a linear relationship between NDVI derived from RapidEye data and GVF ground truth data. A linear relationship was observed across different development stages and for three crops. The relationship of maize was closer ($EF=0.95$) than that of winter wheat ($EF=0.91$) and winter rapeseed ($EF=0.89$). The linear relationships support, at least in principle, the approach of estimating GVF from NDVI data using a two-endmember mixing model. Rundquist (2002), Lukina (1999) and Hurcom and Harrison (1998) also found a linear relationship between NDVI and GVF, with NDVI computed from spectral measurements and GVF based on digital color images. Linearity is confirmed by further studies in which an NDVI-SMA approach was used (Qi et al., 2000; Xiao and Moody, 2005; Wittich and Hansing, 1995).

Both methods used to estimate GVF, i.e., regression of GVF on NDVI and the two-endmember mixing model, performed similarly well. Model efficiencies were $EF=0.91$ and $EF=0.86$, respectively. The regression model showed a slightly lower RMSE (0.12) than the NDVI-SMA approach ($RMSE=0.15$). The validation of linear regression against the independent dataset resulted in a comparable model efficiency ($EF=0.91$) revealing that the regression is robust. When performing the regression crop-wise, we found significant differences, in particular, between winter wheat and maize. This suggests that the estimation of GVF may be further improved by performing the regression crop by crop, but this would require a detailed mapping of the crop species in the region. Both methods yielded better estimates of GVF when green cover was above 40%. Observed variation at high GVFs relates to the crop differences. Estimation of GVF was problematic during flowering of winter rapeseed, when model efficiency was low.

Particularly at low GVF, the GVF-NDVI data showed a large scatter (Fig. 6). The reason for this scatter is that at low GVF, the NDVI is strongly affected by the reflectance of soil or senescent non-green

vegetation. GVF measurements are considerably affected by soil reflectance, particularly when vegetation is sparse (Smith et al., 1990; Huete et al., 1985; García-haro et al., 1996; Elmore et al., 2000). Soil reflectance depends on soil texture, soil organic matter content and moisture conditions (Huete et al., 1985; Liu and Huete, 1995; Myneni et al., 1992; Qi et al., 2000). At our study site, the observed NDVI of bare soil was between 0.05 and 0.20. The variation was probably mainly caused by different moisture conditions and led to a systematical overestimation of GVF (Carlson and Ripley, 1997; Huete and Jackson, 1988). Furthermore, we found that the regression method tends to overestimate the GVF at fields covered with senescent crops ($GVF=0$) because the NDVI of the senescent plants was on average by 0.11 higher than that of bare soil. This issue has also been addressed by other authors (Purevdorj et al., 1998; Xiao and Moody, 2005).

At the field scale, the distribution of GVF was in most cases bell-shaped with a coefficient of variation (CV) between 2% and 50%. High CVs were observed at fields with low GVF. In the fields with $GVF > 0.15$, the CV was on average 5.1%. In 2012, at EC1, we observed a bi-modal distribution, which was mainly caused by management differences. For instance, in the northern part of the EC1 field, the winter rapeseed had been drilled some days later than in the southern part. The two different drilling dates resulted in a bi-modal distribution. Both parts are clearly distinguishable on the GVF maps. The development of winter rapeseed in the northern part of the field was delayed leading to a lower green vegetation cover. A similar situation was observed at the EC2 field in June 2012 (Fig. 7). In the western part, silage maize was drilled on 1 May, while in the eastern part it was drilled two days later. This small time difference in drilling date caused a distinct variation of GVF at a field scale. Soil heterogeneity may have led to additional variability in the GVF.

Our ground observations show that each crop has a distinct crop-specific seasonal dynamics of GVF. Moreover, we clearly observed intra-annual differences. Due to the cold and wet summer in 2013, development of wheat and rapeseed was delayed by about two weeks. This makes clear that running a LSM with an averaged prescribed constant, seasonal, GVF dynamics will fall short of accounting for the feedback between weather and

vegetation development. Among others, this must lead to inaccuracies in assessing evapotranspiration and convective precipitation.

At the regional scale, the GVF showed a bi-modal distribution during the vegetation period (Fig. 9). The bi-modal shape was mainly caused by differences in crop phenology. According to the land use data from the Statistical Office of the Federal State of Baden-Württemberg (<http://www.statistik.baden-wuerttemberg.de>), in 2010, the shares of the major crops in the municipality Sinsheim, which is located in the center of Kraichgau, were as follows: 34.9% winter wheat, 20.8% spring and winter barley, 16.1% corn and silage maize, 9.5% winter rape, and 8.7% sugar beet. These crops can be basically divided into two groups: early- and late-covering crops. The first group includes crops such as winter wheat, winter rape, winter barley and spring barley. These crops develop early in spring, achieve maximum GVF usually between end of May and mid of June and become senescent in July. The second group includes corn, silage maize, and sugar beet. They are drilled in spring, and will have a developed ground-covering canopy only as late as in June or July. Leaves of these crops are still green in August and September, while the early covering crops are already harvested. Both phenological types show very pronounced differences with regard to the Bowen ratio or rather energy partitioning in the course of the season (Wizemann et al., 2014). Fig. 10 shows the GVF dynamics of the early- and late-covering crops based on the Gaussian fits shown in Fig. 9. The early-covering crops have quite high GVFs in April and May and reach their maxima in June. In July, the GVF declines strongly until it is in the range of 0.1 in August and September. In contrast, the late-covering crops have low GVF in April and May, while the maximum is reached in July, and it stays relatively constant until September.

Based on the modal values of the Gaussian fits, we derived the GVF dynamics of early- and later covering crops for the Kraichgau region (Fig. 10). These satellite-derived GVF dynamics were close to the ground measurements. In the NOAH-MP LSM, croplands of our study region would be classified as one land cover type ("Dryland cropland and pasture"). Our results imply that merging early- and late-covering crops in regional climate simulations into one land-use type as recommended in the NOAH, LSM is an oversimplification, because they will show distinct differences with regard to energy and water fluxes over the vegetation period.

For the municipality of Sinsheim, we calculated based on the ground measurements the area-weighted average GVF dynamics on the basis of varying land use and compared with that of used in

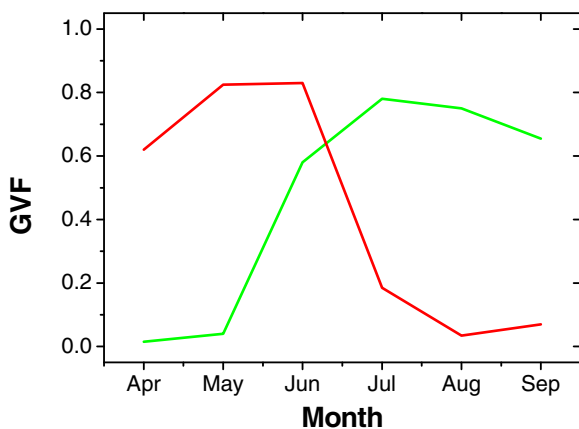


Fig. 10. Seasonal dynamics of the green vegetation fraction (GVF) of early covering crops (red line) and the later covering crops (green line) in Kraichgau region. Early covering crops are, e.g., winter wheat, winter rape, and summer barley. Late covering crops are mainly maize and sugar beet. (For interpretation of the references to color in this figure legend, the reader is referred to the web version of this article.)

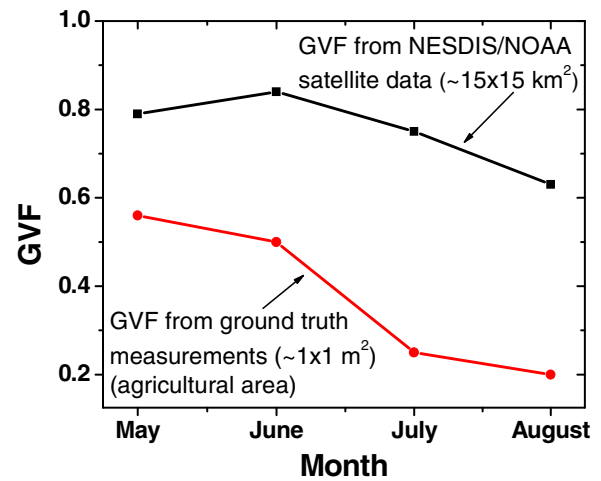


Fig. 11. Comparison of ground truth data with satellite data for the municipality Sinsheim. The black line belongs to the GVF dynamics which is used in the NOAH model by default. In this case, GVF was derived from satellite images with low resolution ($15 \times 15 \text{ m}^2$) what leads to mixed GVF pixel values because the pixel cover different land-use types. The red line is the areal weighted average GVF which was calculated with account of spatial distribution of croplands for the municipality Sinsheim. (For interpretation of the references to color in this figure legend, the reader is referred to the web version of this article.)

the default settings of NOAH-MP LSM (Fig. 11). The land use data were taken from the Statistical Office of the Federal State of Baden-Württemberg (<http://www.statistik.baden-wuerttemberg.de>) as described above. In the default settings of NOAH-MP LSM, GVF values are taken from the NESDIS/NOAA satellite. The NESDI/NOAH data have a resolution of $15 \times 15 \text{ km}^2$. Due to the mixing of croplands, forest and urban areas in practically all pixels, the overall GVF is too high. Moreover, the seasonal dynamics are strongly smoothed (Fig. 11) in comparison with the actual GVF dynamic.

5. Conclusions

For the first time, we presented high-resolution data ($5 \times 5 \text{ m}^2$) on the GVF dynamics of croplands derived from RapidEye satellite data at the field and regional scale. GVF is highly variable in time and space. As to be expected, its seasonal dynamics are affected by the prevailing weather conditions. At the field scale, the variability of GVF depends, among others, on management (drilling, soil tillage etc.). At the regional scale, the variability was impacted by the distinct differences in the phenological development of crops. The observed bi-modal distribution of GVF suggests to distinguish at least between early- and late-covering crops (e.g., winter wheat vs. silage maize), because seasonal dynamics of energy- and water exchange between land surface and atmosphere are very different between these. Concomitantly, we conjecture that splitting the land uses class "croplands" as used by NOAH-MP and other land surface models into two classes (early-covering vs. late-covering crops) have the potential to improve simulations of land surface processes in heterogeneous agricultural landscapes.

Acknowledgments

The present study was supported by the German Research Foundation (DFG) in the framework of the Research Unit (RU) 1695 "Structure and function of agricultural landscapes under global climate change – processes and projections on regional scale" and in part by Erasmus Mundus grant SGA 2010-2361. The authors acknowledge the German Aerospace Center (DLR) for the

delivery of RapidEye satellite images as a part of the RapidEye Science Archive (proposal 505).

References

- Carlson, T.N., Ripley, D.A., 1997. On the relation between NDVI, fractional vegetation cover, and leaf area index. *Remote Sens. Environ.* 62 (3), 241–252.
- Chen, F., Dudhia, J., 2001. Coupling and advanced land surface-hydrology model with the Penn State-NCAR MM5 modeling system. Part I: model implementation and sensitivity. *Mon. Weather Rev.* 129 (4), 569–585.
- Crimmins, M.A., Crimmins, T.M., 2008. Monitoring plant phenology using digital repeat photography. *Environ. Manage.* 41 (6), 949–958.
- Dudhia, J., 1993. A nonhydrostatic version of the Penn State-NCAR mesoscale model: validation tests and simulation of an Atlantic cyclone and cold front. *Mon. Weather Rev.* 121 (5), 1493–1513.
- Duggin, M.J., Philipson, W.R., 1982. Field measurement of reflectance: some major considerations. *Appl. Opt.* 21 (15), 2833–2840.
- Elmore, A.J., Mustard, J.F., Manning, S.J., Lobell, D.B., 2000. Quantifying vegetation change in semiarid environments: precision and accuracy of spectral mixture analysis and the normalized difference vegetation index. *Remote Sens. Environ.* 73 (1), 87–102.
- García-haro, F.J., Gilabert, M.A., Meliá, J., 1996. Linear spectral mixture modelling to estimate vegetation amount from optical spectral data. *Int. J. Remote Sens.* 17 (17), 3373–3400.
- Gutman, G., Ignatov, A., 1998. The derivation of the green vegetation fraction from NOAA/AVHRR data for use in numerical weather prediction models. *Int. J. Remote Sens.* 19 (8), 1533–1543.
- Hirano, Y., Yasuoka, Y., Ichinose, T., 2004. Urban climate simulation by incorporating satellite-derived vegetation cover distribution into a mesoscale meteorological model. *Theor. Appl. Climatol.* 79 (3–4), 175–184.
- Huete, A.R., Jackson, R.D., 1988. Soil and atmosphere influences on the spectra of partial canopies. *Remote Sens. Environ.* 25 (1), 89–105.
- Huete, A.R., Jackson, R.D., Post, D.F., 1985. Spectral response of a plant canopy with different soil backgrounds. *Remote Sens. Environ.* 17 (1), 37–53.
- Hurcom, S.J., Harrison, A.R., 1998. The NDVI and spectral decomposition for semi-arid vegetation abundance estimation. *Int. J. Remote Sens.* 19 (16), 3109–3125.
- Jiang, Z., Huete, A.R., Chen, J., Chen, Y., Li, J., Yan, G., Zhang, X., 2006. Analysis of NDVI and scaled difference vegetation index retrievals of vegetation fraction. *Remote Sens. Environ.* 101 (3), 366–378.
- Jiménez-muñoz, J.C., Sobrino, J.A., Plaza, A., Guanter, L., Moreno, J., Martínez, P., 2009. Comparison between fractional vegetation cover retrievals from vegetation indices and spectral mixture analysis: case study of PROBA/CHRIS data over an agricultural area. *Sensors* 9 (2), 768–793.
- Liu, H.Q., Huete, A., 1995. Feedback based modification of the NDVI to minimize canopy background and atmospheric noise. *IEEE Trans. Geosci. Remote Sens.* 33 (2), 457–465.
- Liu, L., Jing, X., Wang, J., Zhao, C., 2009. Analysis of the changes of vegetation coverage of western Beijing mountainous areas using remote sensing and GIS. *Environ. Monit. Assess.* 153 (1–4), 339–349.
- LUBW, 2010. Landesanstalt für Umwelt, Messungen, Naturschutz Baden-Württemberg.
- Lukina, E.V., Stone, M.L., Raun, W.R., 1999. Estimating vegetation coverage in wheat using digital images. *J. Plant Nutr.* 22 (2), 341–350.
- McDonald, A.J., Gemmill, F.M., Lewis, P.E., 1998. Investigation of the utility of spectral vegetation indices for determining information on coniferous forests. *Remote Sens. Environ.* 66 (3), 250–272.
- Meier, U., Bleiholder, H., Buhr, L., Feller, C., Hack, H., Hess, M., Lancashire, P.D., Schnock, U., Stauss, R., Van den Boom, T., Weber, E., Zwerger, P., 2009. The BBCH system to coding the phenological growth stages of plants—history and publications. *J. Kulturpflanzen* 61, 41–52.
- Montandon, L.M., Small, E.E., 2008. The impact of soil reflectance on the quantification of the green vegetation fraction from NDVI. *Remote Sens. Environ.* 112 (4), 1835–1845.
- Myneni, R.B., Asrar, G., 1994. Atmospheric effects and spectral vegetation indices. *Remote Sens. Environ.* 47 (3), 390–402.
- Myneni, R.B., Asrar, G., Tanre, D., Choudhury, B.J., 1992. Remote sensing of solar radiation absorbed and reflected by vegetated land surfaces. *IEEE Trans. Geosci. Remote Sens.* 30 (2), 302–314.
- Niu, G.-Y., Yang, Z.-L., Mitchell, K.E., Chen, F., Ek, M.B., Barlage, M., Kumar, A., Manning, K., Niyogi, D., Rosero, E., Tewari, M., Xia, Y., 2011. The community Noah land surface model with multiparameterization options (Noah-MP): 1. Model description and evaluation with local-scale measurements. *J. Geophys. Res. D: Atmos.* 116 (12).
- Price, J.C., 1992. Estimating vegetation amount from visible and near infrared reflectances. *Remote Sens. Environ.* 41 (1), 29–34.
- Purevdorj, T., Tateishi, R., Ishiyama, T., Honda, Y., 1998. Relationships between percent vegetation cover and vegetation indices. *Int. J. Remote Sens.* 19 (18), 3519–3535.
- Qi, J., Marsett, R.C., Moran, M.S., Goodrich, D.C., Heilman, P., Kerr, Y.H., Dedieu, G., Chehbouni, A., Zhang, X.X., 2000. Spatial and temporal dynamics of vegetation in the San Pedro River basin area. *Agric. For. Meteorol.* 105 (1–3), 55–68.
- RapidEye AG, 2012. Satellite imagery product specifications. Version 4.1. <http://blackbridge.com/rapideye/upload/RE_Product_Specifications_ENG.pdf>.
- Richter, R., 1996a. A spatially adaptive fast atmospheric correction algorithm. *Int. J. Remote Sens.* 17 (6), 1201–1214.
- Richter, R., 1996b. Atmospheric correction of satellite data with haze removal including a haze/clear transition region. *Comput. Geosci.* 22 (6), 675–681.
- Rundquist, B.C., 2002. The influence of canopy green vegetation fraction on spectral measurements over native tallgrass prairie. *Remote Sens. Environ.* 81 (1), 129–135.
- Skamarock, W.C., Klemp, J.B., Dudhia, J., Gill, D.O., Barker, D.M., Duda, M.G., Huang, X.Y., Wang, W., Powers, J.G., 2008. A description of the advanced research WRF Version 3. NCAR Tech Notes-475 +STR.
- Smith, M.O., Ustin, S.L., Adams, J.B., Gillespie, A.R., 1990. Vegetation in deserts: I. A regional measure of abundance from multispectral images. *Remote Sens. Environ.* 31 (1), 1–26.
- Song, C., Woodcock, C.E., Seto, K.C., Lenney, M.P., Macomber, S.A., 2001. Classification and change detection using Landsat TM data: when and how to correct atmospheric effects? *Remote Sens. Environ.* 75 (2), 230–244.
- Wittich, K.-P., Hansing, O., 1995. Area-averaged vegetative cover fraction estimated from satellite data. *Int. J. Biometeorol.* 38 (4), 209–215.
- Wizemann, H.-D., Ingwersen, J., Högy, P., Warrach-sagi, K., Streck, T., Wulfmeyer, V., 2014. Three year observations of water vapor and energy fluxes over agricultural crops in two regional climates of Southwest Germany. *Meteorol. Z.*, <http://dx.doi.org/10.1127/metz/2014/0618>.
- Xiao, J., Moody, A., 2005. A comparison of methods for estimating fractional green vegetation cover within a desert-to-upland transition zone in central New Mexico, USA. *Remote Sens. Environ.* 98 (2–3), 237–250.
- Yue, Y.M., Wang, K.L., Liu, B., Li, R., Zhang, B., Chen, H.S., Zhang, M.Y., 2013. Development of new remote sensing methods for mapping green vegetation and exposed bedrock fractions within heterogeneous landscapes. *Int. J. Remote Sens.* 34 (14), 5136–5153.
- Zerger, A., Gobbett, D., Crossman, C., Valencia, P., Wark, T., Davies, M., Handcock, R.N., Stol, J., 2012. Temporal monitoring of groundcover change using digital cameras. *Int. J. Appl. Earth Obs. Geoinf.* 19 (1), 266–275.

6 Distinguishing between early and late covering crops in the land surface model Noah-MP: Impact on simulated surface energy fluxes and temperature

Kristina Bohm^a, Joachim Ingwersen^a, Josipa Milovac^b, Petra Högy^c, Thilo Streck^a

^a Institute of Soil Science and Land Evaluation, Department of Biogeophysics, University of Hohenheim, 70593 Stuttgart, Germany

^b Institute of Physics and Meteorology, University of Hohenheim, 70593 Stuttgart, Germany

^c Institute of Landscape and Plant Ecology, University of Hohenheim, 70593 Stuttgart, Germany

Chapter 6 is published with the consent of the Copernicus Publications on behalf of the European Geosciences Union under the Creative Commons Attribution 4.0 License. The original publication was in: Journal of Biogeosciences (2020), Volume 17, Pages 2791–2805. It can be found under the following link: <https://doi.org/10.5194/bg-17-2791-2020>

Biogeosciences, 17, 2791–2805, 2020
<https://doi.org/10.5194/bg-17-2791-2020>
© Author(s) 2020. This work is distributed under
the Creative Commons Attribution 4.0 License.



Distinguishing between early- and late-covering crops in the land surface model Noah-MP: impact on simulated surface energy fluxes and temperature

Kristina Bohm^{1,‡}, Joachim Ingwersen¹, Josipa Milovac², and Thilo Streck¹

¹Institute of Soil Science and Land Evaluation, Department of Biogeophysics, University of Hohenheim, 70593 Stuttgart, Germany

²Institute of Physics and Meteorology, University of Hohenheim, 70593 Stuttgart, Germany

[‡]previously published under the name Kristina Imukova

Correspondence: Kristina Bohm (imukovaks@gmail.com)

Received: 19 November 2019 – Discussion started: 11 December 2019

Revised: 16 March 2020 – Accepted: 18 March 2020 – Published: 26 May 2020

Abstract. Land surface models are essential parts of climate and weather models. The widely used Noah-MP land surface model requires information on the leaf area index (LAI) and green vegetation fraction (GVF) as key inputs of its evapotranspiration scheme. The model aggregates all agricultural areas into a land use class termed “cropland and pasture”. In a previous study we showed that, on a regional scale, the GVF has a bimodal distribution formed by two crop groups differing in phenology and growth dynamics: early-covering crops (ECC; e.g., winter wheat, winter rapeseed, winter barley) and late-covering crops (LCC; e.g., corn, silage maize, sugar beet). That result can be generalized for central Europe. The present study quantifies the effect of splitting the land use class cropland and pasture of Noah-MP into ECC and LCC on surface energy fluxes and temperature. We further studied the influence of increasing the LCC share, which in the study area (the Kraichgau region, southwest Germany) is mainly the result of heavily subsidized biomass production, on energy partitioning at the land surface. We used the GVF dynamics derived from high-resolution (5 m × 5 m) RapidEye satellite data and measured LAI data for the simulations. Our results confirm that the GVF and LAI strongly influence the partitioning of surface energy fluxes, resulting in pronounced differences between simulations of ECC and LCC. Splitting up the generic crop into ECC and LCC had the strongest effect on land surface exchange processes in July–August. During this period, ECC are at the senescence growth stage or already harvested, while LCC have a well-developed ground-

covering canopy. The generic crop resulted in humid bias, i.e., an increase in evapotranspiration by +0.5 mm d⁻¹ (latent heat flux is 1.3 MJ m⁻² d⁻¹), decrease in sensible heat flux (H) by 1.2 MJ m⁻² d⁻¹ and decrease in surface temperature by –1 °C. The bias increased as the shares of ECC and LCC became similar. The observed differences will impact the simulations of processes in the planetary boundary layer. Increasing the LCC share from 28 % to 38 % in the Kraichgau region led to a decrease in latent heat flux (LE) and a heating up of the land surface in the early growing season. Over the second part of the season, LE increased and the land surface cooled down by up to 1 °C.

1 Introduction

Within weather and climate models, land surface exchange processes are simulated by so-called land surface models (LSMs). The main role of an LSM is to partition net radiation at the land surface into sensible heat flux (H), latent heat flux (LE) and ground heat flux (G) and determine the land surface temperature. Surface energy partitioning has a significant influence on the evolution of the atmospheric boundary layer (ABL). ABL evolution strongly influences the initiation of convection, cloud formation, and ultimately the location and strength of precipitation (Crawford et al., 2001; Koster et al., 2006; Santanello et al., 2013; van Heerwaarden et al., 2009; Milovac et al., 2016).

The surface energy partitioning depends on the physical and physiological properties of the land surface (Raddatz, 2007). In LSMs, Earth's surface is subdivided into different land use classes, among them cropland. Physiological state variables of crops such as the green vegetation fraction (GVF) and leaf area index (LAI) vary significantly throughout the growing season. This alters the biophysical parameters of surface albedo, bulk canopy conductance and roughness length, leading to significant changes in surface energy fluxes (Crawford et al., 2001; Ghilain et al., 2012; Tsvetinskaya et al., 2001a; Wizemann et al., 2014). In many parts of the world, cropland covers a considerable part of the simulation area. Therefore, accurately simulating the seasonal variability in surface energy fluxes highly depends on an adequate representation of plant growth dynamics.

One of the widely used LSMs is Noah-MP. It is usually coupled with the Weather Research and Forecasting (WRF) model, which is intended for use from the large-eddy simulation (LES) scale up to the global scale. Within each grid cell, Noah-MP computes net longwave radiation as well as LE , H and G separately for the bare soil and the vegetated tile, whereas shortwave radiation is computed over the entire grid cell (semiteile approach; Lhomme and Chehbouni, 1999; Niu et al., 2011).

Noah-MP collects agricultural areas into only general land use classes such as “dryland cropland and pasture”, “irrigated cropland and pasture”, or “mixed dryland/irrigated cropland and pasture”. Vegetation dynamics and their seasonal development are described in the Noah-MP model by the plant variables of GVF and LAI. The surface energy fluxes critically depend on accurately representing GVF and LAI dynamics (Chen and Xie, 2011; Crawford et al., 2001; Refslund et al., 2014). In Noah-MP, the GVF and LAI are fixed quantities; they do not depend on the weather conditions during a simulation. The GVF is defined as the grid-cell fraction covered by a green canopy (Gutman and Ignatov, 1998). It is a function of the upper canopy (Rundquist, 2002) and represents the horizontal density of vegetation in each grid cell (Gutman and Ignatov, 1998). The LAI represents the vertical density of the canopy. Certain biophysical parameters in Noah-MP such as surface albedo, roughness and emissivity are considered linear functions of the LAI.

By default, Noah-MP derives GVF values from the normalized difference vegetation index (NDVI) obtained from the NOAA NESDIS satellite. These data have a resolution of $15 \text{ km} \times 15 \text{ km}$. Due to the mixing of croplands, forest and urban areas, the overall GVF is often positively biased. Moreover, as shown by Imukova et al. (2015), seasonal GVF data are strongly smoothed compared to the actual GVF dynamics. Milovac et al. (2016) and Nielsen et al. (2013) found that the GVF grid data used in the Noah-MP LSM are outdated and stated that these should be updated given their importance for ABL evolution.

In a previous study, we derived GVF data with a resolution of $5 \text{ m} \times 5 \text{ m}$ (Imukova et al., 2015) for a region in southwest

Germany (Kraichgau) using RapidEye satellite data. On the regional scale, the GVF shows a bimodal distribution mirroring the different phenology of crops. Crops could be grouped into two classes. Early-covering crops (ECC), such as winter wheat, winter rape, winter barley and spring barley, develop early in spring, achieve a maximum GVF usually between late May and mid-June, and become senescent in July. Late-covering crops (LCC), such as corn, silage maize, and sugar beet, are drilled in spring and develop a maximum ground-covering canopy from July to August. They are still green in September, when the ECC are already harvested. The dynamics of ECC and LCC vary to some degree from season to season and from region to region.

The shares of ECC and LCC may change over time, often reflecting economic decisions that may depend on policy interventions. In Germany, a substantial change in these shares was introduced by subsidizing biogas production. In 2005, 1.7×10^6 ha of maize was cultivated in Germany. Only 70 000 ha of this area was cropped with silage maize for biogas production (SRU Special Report, 2007). In 2009, the area cropped with maize for biogas production had increased to about 500 000 ha, while the total maize area remained almost constant (Huyghe et al., 2014). In 2012, the total acreage of maize had increased to 2.57×10^6 ha with 0.9×10^6 ha intended for biogas plants. The increase occurred mainly at the expense of grassland. Since then, the total maize crop area has remained almost constant: 2.6×10^6 ha in 2018 (Fachagentur Nachwachsende Rohstoffe e.V., 2019). From 2005 to 2018, the maize area in Germany increased by about 53 %.

The objectives of the present study were (1) to elucidate the extent to which surface energy fluxes simulated with Noah-MP are affected by aggregating early- and late-covering crops into one generic cropland class and (2) to quantify the effect of a land use change, driven by the expansion of maize cropping as a response to the increasing demand for biogas plants, on energy partitioning and surface temperature in the Kraichgau region (southwest Germany). Additionally, we tested the performance of Noah-MP on LE data measured with the eddy covariance technique.

2 Materials and methods

2.1 Study site and weather data measurements

The site under study is the agricultural field belonging to the farm Katharinentalerhof. The field is located north of the city of Pforzheim (48.92° N , 8.70° E). The central research site is a part of the Kraichgau region. The Kraichgau region covers about 1500 km^2 . Mean annual temperature ranges between 9 and 10° C , and annual precipitation ranges between 730 and 830 mm . The Neckar and Enz rivers form the borders to the east. To the north and south, the region is bounded by the low mountain ranges of the Odenwald and Black Forest. In the west, it adjoins the Upper Rhine Plain (Oberrheinisches

Tiefland). Kraichgau has a gently sloping landscape with elevations between 100 and 400 m above sea level (a.s.l.). Soils are predominantly formed from loess material. The region is intensively used for agriculture: around 46 % of the total area is used for crop production. Winter wheat, winter rapeseed, spring barley, corn, silage maize and sugar beet are the predominant crops.

Weather data used to force the Noah-MP model were acquired at an agricultural field (EC1, 14 ha) belonging to the farm Katharinentalerhof. The terrain is flat (elevation 319 m a.s.l.). The predominant wind direction is southwest. The study site has been described in detail in several studies (Imukova et al., 2015; Ingwersen et al., 2011; Wizemann et al., 2014).

An eddy covariance (EC) station was operated in the center of the EC1 field. Wind speed and wind direction were measured with a 3D sonic anemometer (CSAT3, Campbell Scientific, UK) installed at a height of 3.10 m. Downwelling longwave and downwelling shortwave radiation were measured with an NR01 four-component sensor (NR01, Hukseflux Thermal Sensors, the Netherlands). Air temperature and humidity were measured at a 2 m height (HMP45C, Vaisala Inc., USA). All sensors recorded data at 30 min intervals. Rainfall was measured using a tipping bucket (resolution at 0.2 mm per tip) rain gauge (ARG100, Campbell Scientific, UK). For further details about instrumentation and data processing see Wizemann et al. (2014).

2.2 Eddy covariance measurements

In order to test the Noah-MP performance, we used the EC measurements of latent heat flux over maize and winter wheat fields (EC2 and EC3, respectively) of the 2012 growing season. The EC2 and EC3 agricultural fields also belong to the farm Katharinentalerhof introduced above. They are 23 and 15 ha large. The winter wheat was planted in autumn 2011 and harvested on 29 July. The maize was drilled on 2 May and harvested on 20 September. The EC station was operated in the center of each field. The latent heat flux was measured at a 30 min resolution. For the maize, the *LE* data were only available till 20 September, whereas for the winter wheat field there were no missing data. Detailed information on the EC measurements is given in Imukova et al. (2016). The EC flux data were processed with TK3.1 software (Mauder et al., 2011). Surface energy fluxes were computed from 30 min covariances. For data quality analysis we used the flag system after Foken (Mauder et al., 2011). *LE* half-hourly values with flags from 1 to 6 (high- and moderate-quality data) were used to test the performance of the Noah-MP LSM. *LE* data were gap-filled using the mean diurnal variation method with an averaging window of 14 d (Falge et al., 2001). The random error of *LE*, which consists of the instrumental noise error of the EC station and the sampling error, was computed by the TK3.1 software (Mauder

et al., 2013). For more details on EC data processing, please refer to Imukova et al. (2016).

The model performance is usually tested against field measurements of sensible and latent heat flux performed with the eddy covariance (EC) technique (Ingwersen et al., 2011; El Maayar et al., 2008; Falge et al., 2005). The EC method is a widely used method for this purpose although it has one well-known problem. The energy balance of EC flux data is typically not closed, which means *LE* and/or *H* measured with the EC technique are most probably underestimated. A previous study showed the EC technique provides reliable *LE* measurements at our study site and these data can be used for model testing (Imukova et al., 2016).

2.3 The Noah-MP v1.1 land surface model

2.3.1 Model parametrization

The multiphysics options of Noah-MP were set as shown in Table 1. For the simulation we used the US Geological Survey land use dataset. The vegetation type index was set to 2 (dryland cropland and pasture) and soil type index to 4 (silt loam). The model was forced with half-hourly weather data (wind speed, wind direction, temperature, humidity, pressure, precipitation, downwelling longwave and shortwave radiation) measured at EC1 from 2011 to 2012. Simulations were initialized with a spinup period of 1 year (2011) and run with a time step of 1800 s.

2.3.2 GVF dynamics

The GVF data required by the Noah-MP model were derived from high-resolution (5 m × 5 m) RapidEye satellite data. Detailed information on the deriving of the GVF data used in the current research can be found in Imukova et al. (2015). The GVF data were calculated from the normalized difference vegetation index (NDVI) computed from the red and near-infrared bands of the satellite images. The relationship between the GVF and NDVI was established by linear regression using ground truth measurements. GVF maps for the Kraichgau region were derived at a monthly resolution.

Table 2 shows the observed and mean GVF dynamics of ECC and LCC over the growing seasons 2012 and 2013 as well as the GVF dynamics of the generic crop in the Kraichgau region. The GVF values on the 15th day of each month, as required by the Noah-MP model, were calculated by linearly interpolating the monthly values derived from the GVF maps. A generic GVF dynamic was calculated as the weighted mean of ECC and LCC from 2012 and 2013. The areal distribution of ECC and LCC was determined from the GVF maps of May 2012. All pixels with a GVF value below 0.5 were counted as LCC, whereas pixels with values above that threshold were assigned to ECC. Figure 1 shows the spatial distribution of early- and late-covering crops in Kraichgau. The estimated areal distribution of ECC and

Table 1. Settings of the multiphysics options used in the Noah-MP simulation.

Multiphysics option	Setting
Vegetation model	opt_dveg = 1: prescribed (Table LAI, shdfac = FVEG)
Canopy stomatal resistance	opt_crs = 2: Jarvis
Soil moisture factor for stomatal resistance	opt_btr = 1: Noah
Runoff and groundwater model	opt_run = 1: SIMGM
Surface layer drag coefficient (CH and CM)	opt_sfc = 1: based on Monin–Obukhov similarity theory
Supercooled liquid water	opt_frz = 1: NY06
Frozen soil permeability	opt_inf = 1: NY06
Radiation transfer	opt_rad = 3: gap = 1 – FVEG
Snow surface albedo	opt_alb = 2: CLASS
Rainfall and snowfall	opt_snf = 1: Jordan91
Lower boundary of soil temperature	opt_tbot = 2: Noah
Snow/soil temperature time scheme	opt_stc = 1: Semi-implicit

Table 2. GVF dynamics of early-covering crops (ECC) and late-covering crops (LCC) in 2012 and 2013 in the Kraichgau region, southwest Germany, as well as the GVF dynamics of the generic crop.

GVF		15 Apr	15 May	15 Jun	15 Jul	15 Aug	15 Sep
GVF 2012	ECC	– ^b	0.74	0.83	0.37	0.01 ^c	0.01
	LCC	– ^b	0.01	0.35	0.74	0.69 ^c	0.56
GVF 2013	ECC	0.54	0.80	0.57 ^c	0.29	0.01	0.01
	LCC	0.01	0.06	0.37 ^c	0.69	0.74	0.75
Mean GVF	ECC	0.54	0.77	0.70	0.33	0.01	0.01
	LCC	0.01	0.04	0.36	0.72	0.72	0.66
Generic crop GVF ^a		0.39	0.57	0.60	0.44	0.21	0.19

^a Weighted mean GVF calculated based on fractions of ECC (72%) and LCC (28%) in Kraichgau. ^b No RapidEye scenes were available for April. ^c No RapidEye scenes were available for these months; GVF values were derived by linear interpolation between adjacent months.

LCC was 72% and 28%, respectively. These results correspond well with data of the Statistisches Landesamt Baden-Württemberg (<http://www.statistik.baden-wuerttemberg.de/>, last access: November 2019).

2.3.3 LAI dynamics

Noah-MP requires prescribed LAI data for each month. Data were derived from field measurements. The LAI was measured biweekly using an LAI-2000 plant canopy analyzer (LI-COR Biosciences Inc., USA). In 2012 and 2013, the LAI of the crops was measured on five permanently marked plots of 1 m² on three different fields. Detailed information about the study plots can be found in Imukova et al. (2015). In 2009–2011, the LAI and the phenological development of the crops were measured on five permanently marked plots of 4 m² in the same three fields. The growth stages of crops were determined using the BBCH scale (Meier et al., 2009). More details on the measurements can be found in Ingwersen et al. (2011, 2015). Table 3 shows measured and mean LAI dynamics as well as generic LAI dynamics estimated by considering shares of ECC (72%) and LCC (28%) in the study

region. LAI dynamics of winter wheat and winter rape were assigned to ECC; those of maize were assigned to LCC. The mean LAI dynamics of ECC were estimated based on the measurements conducted in winter wheat and winter rape stands during the 2012 and 2013 growing seasons. Since LAI data were not available for maize in 2013, the mean LAI dynamics of LCC were assessed using field data from the same fields collected in 2009–2012.

2.4 Simulation runs

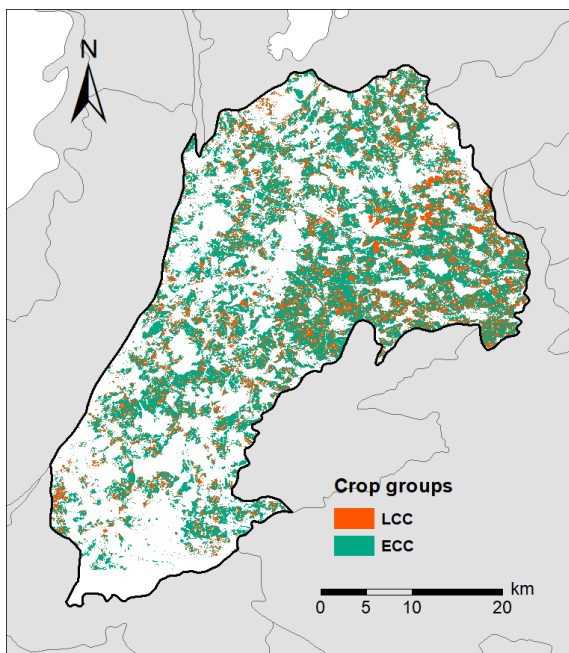
We firstly quantified the extent to which ECC and LCC differ with regard to their energy and water fluxes, surface temperature (TS) and soil temperature (TG). For this, we performed one local simulation for each crop group using the mean LAI and the mean GVF dynamics observed during the two growing seasons (see Tables 2 and 3).

Secondly, to determine the effect of splitting up the vegetation dynamics of a generic crop into that of ECC and LCC, we compared the following two local simulation runs:

Table 3. LAI dynamics of early-covering crops (ECC) and late-covering crops (LCC) in 2012 and 2013 in the Kraichgau region, southwest Germany, as well as the LAI dynamics of the generic crop.

Green LAI		15 Apr	15 May	15 Jun	15 Jul	15 Aug	15 Sep
LAI 2012	ECC	2.4	4.4	4.6	0.0	0.0	0.0
	LCC	0.0	0.1	0.9	3.2	5.0	3.7
LAI 2013	ECC	1.7	4.2	4.3	0.0	0.0	0.0
	LCC ^b	–	–	–	–	–	–
Mean LAI	ECC	2.1	4.3	4.5	0.0	0.0	0.0
	LCC ^c	0.0	0.1	0.9	3.1	4.5	3.8
Generic crop LAI ^a		1.5	3.1	3.5	0.9	1.3	1.1

^a Weighted mean LAI calculated based on fractions of ECC (72 %) and LCC (28 %) in Kraichgau. ^b LAI data for maize in 2013 were not measured. ^c Since LAI data for maize in 2013 were not available, LAI dynamics were derived from the field data of 2009–2012 for maize in the Kraichgau region.

**Figure 1.** Map of early-covering (ECC) and late-covering crops (LCC) in Kraichgau region, southwestern Germany.

- In Run 1, Noah-MP was forced with the GVF and LAI dynamics of the generic crop (Tables 2 and 3). Accordingly, in this simulation, we first computed the weighted mean of the vegetation properties (GVF and LAI) and subsequently simulated the surface energy fluxes, TS and TG.
- In Run 2, we first simulated the energy and water fluxes separately for ECC and LCC with their crop-specific vegetation dynamics. Afterward, we calculated the weighted averages of the simulated fluxes and temperatures based on the share of early-covering (72 %) and late-covering crops (28 %) in Kraichgau.

Thirdly, we studied the effect of increasing the LCC share on the surface energy fluxes and surface and soil temperatures. As mentioned in the introduction, the maize cropping area in Germany increased by 53 % over the last decade. In Kraichgau currently 46 % of the total area is covered by croplands. Taking the above fractions of ECC and LCC results in areal fractions of ECC and LCC of 33 % and 13 %, respectively, of the total area. An increase in LCC at the expense of grassland increases LCC share from 13 % to 20 % and increases the areal fraction of croplands to 53 %, which leads to a rise in the share of LCC on croplands from 28 % to 38 %. To study the effect of this land use change on the Noah-MP simulations, we performed one additional generic crop simulation, but this time the generic crop dynamics were computed with an LCC share of 38 %.

2.5 Statistical analysis

The model performance was evaluated based on the model efficiency (EF), root-mean-square error (RMSE) and bias. EF is defined as the proportion of the total variance explained by a model:

$$EF = 1 - \frac{\sum_{i=1}^N (P_i - O_i)^2}{\sum_{i=1}^N (O_i - \bar{O})^2}, \quad (1)$$

where P_i denotes predicted values and O_i and \bar{O} are observed values and their mean, respectively, while N is the number of observations. RMSE and bias were calculated as

$$RMSE = \sqrt{\frac{1}{N} \sum_{i=1}^N (P_i - O_i)^2} \quad (2)$$

and

$$bias = \frac{1}{N} \sum_{i=1}^N (P_i - O_i). \quad (3)$$

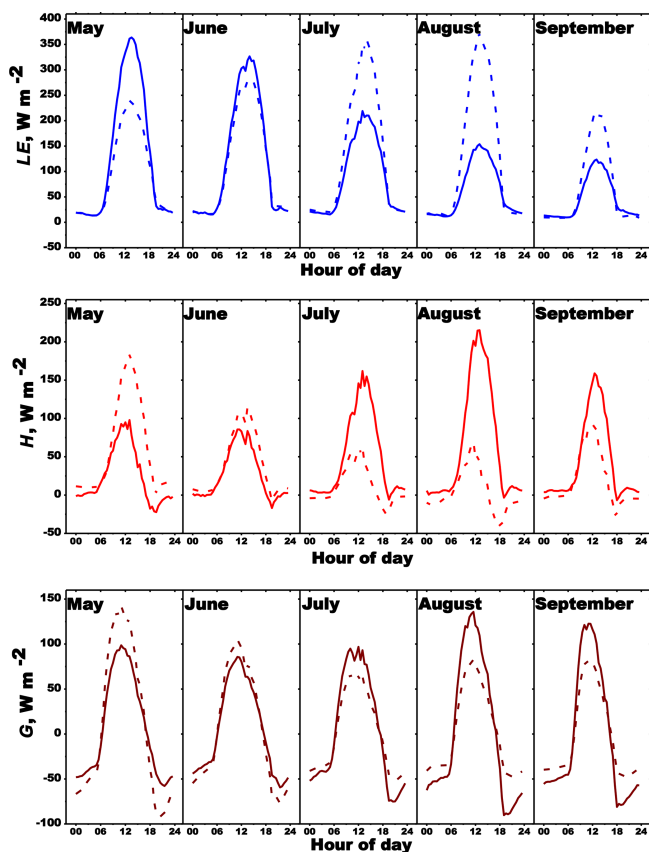


Figure 2. Simulation results of Noah-MP LSM for latent heat flux (LE), sensible heat flux (H) and ground heat flux (G). Simulations were performed for two types of crops: early covering (solid line) and late covering (dashed line). Time is local time.

3 Results

3.1 ECC vs. LCC

Over the growing season, ECC and LCC show distinct differences with regard to energy partitioning at the land surface (Fig. 2). The observed shifts were strongest for LE and H . Early-covering crops had already reached their maximum LE value in May, after which LE declined during the growing season. In contrast, LCC showed a continued increase in LE over the season, peaking 3 months later in August. The smallest difference in evapotranspiration between both crop types was on average 0.4 mm d^{-1} (LE $0.9 \text{ MJ m}^{-2} \text{ d}^{-1}$) in June, while the largest mean deviation of -2.3 mm d^{-1} (LE $-5.7 \text{ MJ m}^{-2} \text{ d}^{-1}$) occurred in August (Table 4). With regard to H , the situation was opposite (Fig. 2). In the case of ECC, H increased continuously over the course of the growing season, peaking in August. In contrast, LCC had already reached the H maximum in May. Afterward, H decreased continuously until late August. As for LE , the smallest ($-1.2 \text{ MJ m}^{-2} \text{ d}^{-1}$) and largest ($5.3 \text{ MJ m}^{-2} \text{ d}^{-1}$) mean differences in H between ECC and LCC were observed

in June and August, respectively (Table 4). Compared with LCC, the higher latent heat fluxes of ECC in May and June resulted in a cooler land surface, on average by -2.6 and -1.0°C , respectively (Table 4). From July to August the situation was reversed: because latent heat fluxes of ECC are distinctly lower than that of LCC, the surface temperature at ECC sites was up to 4°C warmer than at LCC sites (Fig. 3).

The mean difference in daily ground heat flux between ECC and LCC during the growing season ranged between -0.2 and 0.2 MJ m^{-2} (Table 4). Also for the ground heat flux, the smallest difference between both crops types was observed in June (0.05 MJ m^{-2}).

3.2 Noah-MP vs. eddy covariance measurements

The average random error of the latent heat flux measured with the EC technique for the entire growing season was about 25 % over the winter wheat field and about 21 % over the maize field.

The simulated latent heat flux based on ECC and LCC parametrization agreed fairly well with the eddy covariance data (Tables 5–6, Figs. 4–5). The model efficiency over the entire simulation period was 0.87 for ECC and 0.90 for LCC. The best agreement between the observations and the Noah-MP LSM using crop-type-specific sets was achieved for winter wheat in June and for maize in August and September. The generic crop parametrization showed less satisfying modeling results, particularly for the maize field (Tables 5–6). For the entire growing season, EF was 0.78 for winter wheat and only 0.57 for maize. Over the winter wheat field, LE was overestimated. Overestimation of LE was highest in July and August. Over the maize field, LE was overestimated in May and June and underestimated in July, August and September. Particularly in May and August, the bias increased to 68.8 and -56 W m^{-2} , respectively. The best model performance using the generic crop set was achieved for the winter wheat in June and for the maize in July.

3.3 Run 1 vs. Run 2 (generic crop vs. weighted mean of ECC and LCC)

The generic crop simulation run (Run 1) generally yielded higher LE than Run 2 (i.e., splitting up the generic crop into ECC and LCC; Fig. 6). During the growing season the mean difference in evapotranspiration between two runs was 0.1 mm d^{-1} (LE $3.7 \text{ MJ m}^{-2} \text{ d}^{-1}$; Table 7). The smallest mean monthly differences occurred in June and September: 0.02 mm d^{-1} (LE $0.4 \text{ MJ m}^{-2} \text{ d}^{-1}$) and 0.03 mm d^{-1} (LE $1 \text{ MJ m}^{-2} \text{ d}^{-1}$), respectively. The most pronounced differences in LE were recorded in late July (DOY 197–208; Fig. 7). The average difference in half-hourly fluxes over this period, between 09:00 and 18:00 LT, was 36 W m^{-2} , and the highest half-hourly deviation between both runs was 83 W m^{-2} (Fig. 7). The highest daily deviation was 0.8 mm d^{-1} (Fig. 6). Over the whole season, the cumula-

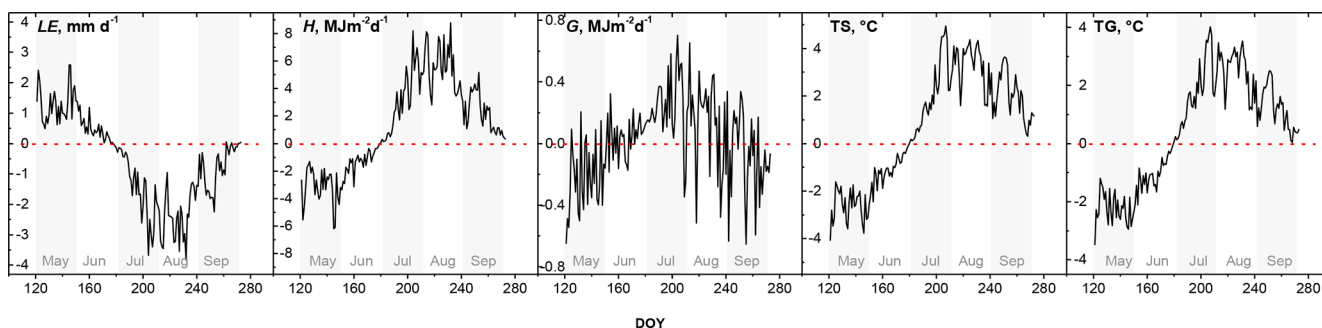


Figure 3. Differences (ECC minus LCC) in latent heat flux (LE), sensible heat flux (H), ground heat flux (G), mean surface temperature (TS) and mean ground temperature (TG) between simulations for ECC and LCC.

Table 4. Mean differences (ECC minus LCC) in latent heat flux (LE), sensible heat flux (H), ground heat flux (G), mean surface temperature (TS) and mean ground temperature (TG) between ECC and LCC simulations.

Month	DOY	LE		H	G	TS	TG
		(mm d^{-1})	($\text{MJ m}^{-2} \text{d}^{-1}$)				
May	121–151	1.3	3.3	−3.1	−0.2	−2.6	−2.2
Jun	152–181	0.4	0.9	−1.2	0.05	−1.0	−0.9
Jul	182–212	−1.5	−3.8	3.3	0.2	2.1	1.8
Aug	213–243	−2.3	−5.7	5.3	0.1	3.2	2.4
Sep	244–273	−0.7	−1.8	2.1	−0.1	1.9	1.2

DOY is day of year.

Table 5. Root-mean-square error (RMSE), bias and modeling efficiency (EF) of the latent heat flux for the simulation runs of winter wheat stand (EC3 field).

Variant	May	Jun	Jul	Aug	Sep	Overall
RMSE (Wm^{-2})						
ECC	45.4	35.4	33.0	26.3	13.5	32.5
Generic crop	36.3	33.0	59.6	63.6	20.9	45.7
Bias (Wm^{-2})						
ECC	27.3	17.9	14.2	17.1	0.8	15.5
Generic crop	20.5	15.2	33.9	41.7	7.7	23.8
EF (1)						
ECC	0.88	0.91	0.80	0.74	0.89	0.87
Generic crop	0.91	0.92	0.62	0.41	0.85	0.78

Table 6. Root-mean-square error (RMSE), bias and modeling efficiency (EF) of the latent heat flux for the simulation runs of maize stand (EC2 field).

Variant	May	Jun	Jul	Aug	Sep	Overall
RMSE (Wm^{-2})						
LCC	53.1	37.3	31.8	28.1	18.9	35.7
Generic crop	102.0	50.9	29.8	85.8	43.7	68.0
Bias (Wm^{-2})						
LCC	37.4	21.5	13.7	−14.9	−2.5	11.0
Generic crop	68.6	29.9	−10.6	−56.0	−22.9	1.8
EF (1)						
LCC	0.59	0.87	0.94	0.96	0.96	0.90
Generic crop	0.30	0.80	0.91	0.12	0.77	0.57

tive difference in evapotranspiration between two runs was 20 mm, leading to a 16% lower seasonal water balance (SWB) in Run 1 (SWB −133 mm) than in Run 2 (SWB −113 mm).

In contrast, H values of Run 1 were mostly lower over all months than those simulated in Run 2 (Fig. 6). From May to September, the mean difference in H was about $−0.4 \text{ MJ m}^{-2}$ (−13%; Table 7). The smallest difference oc-

curred again in June; the largest difference occurred again in late July (Fig. 7). During DOY 197–208 the mean differences in half-hourly H values were about $−29 \text{ W m}^{-2}$, the peak deviation being $−72 \text{ W m}^{-2}$ (09:00–18:00 LT; Fig. 7). Cumulating these differences over the day reduced the production of sensible heat on average on the order of 1.2 MJ m^{-2} , corresponding to a 46% reduction compared to Run 2 (Table 7). Ground heat fluxes as well as soil temperature were affected only moderately by the different vegetation parametrization

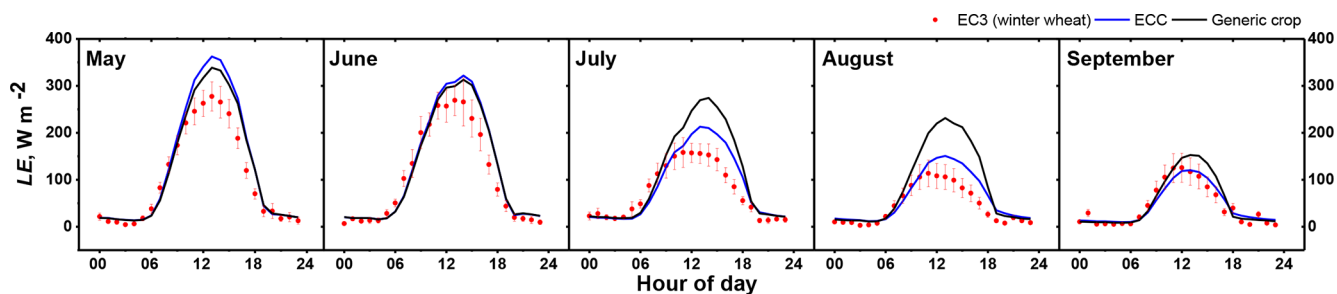


Figure 4. Monthly averaged measured and simulated diurnal latent heat flux (LE) for May–September. The Noah-MP LSM was run with two different vegetation parametrizations: early-covering crops (ECC) and generic crop.

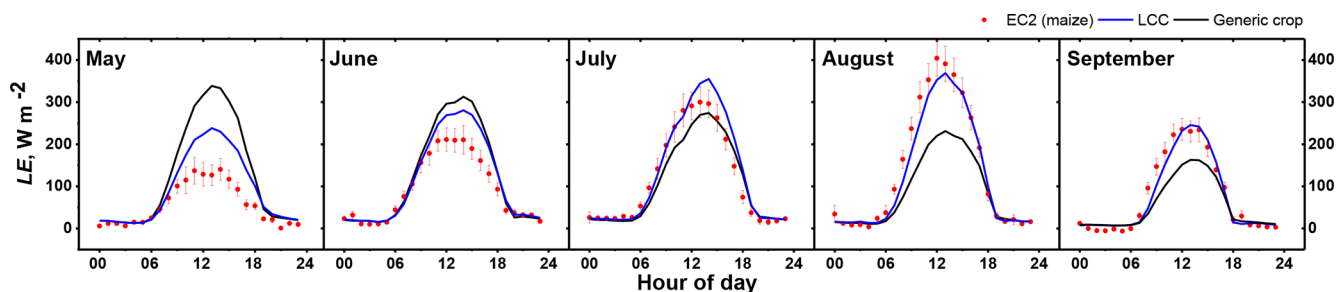


Figure 5. Monthly averaged measured and simulated diurnal latent heat flux (LE) for May–September. The Noah-MP LSM was run with two different vegetation parametrizations: late-covering crops (LCC) and generic crop.

of Run 1 and 2 (Figs. 7, 6). As for LE and H , the largest mean differences in G values were observed during DOY 197–208 ($-0.034 \text{ MJ m}^{-2} = 10\%$; Table 7).

Due to the humid bias of Run 1, the canopy surface was cooler than in Run 2 in all months. On average, the TS of Run 1 was 0.2°C ($\sim 1.4\%$) lower during the growing season than in Run 2. In late July (DOY 197–208) the mean daily difference was -1°C (Table 7, Fig. 6) and reached a daytime (09:00–18:00 LT) peak difference of up to -2.6°C (Fig. 7).

3.4 Land use change towards LCC

Increasing the LCC fraction from 28% to 38% mainly led to changes in LE and H (Table 8). That LCC increase lowered the LE value ($-0.3 \text{ MJ m}^{-2} \text{ d}^{-1}$ or $\text{ET } 0.1 \text{ mm d}^{-1}$) early in the season. This was accompanied by a higher H value ($+0.3 \text{ MJ m}^{-2} \text{ d}^{-1}$), which in turn led to a 0.3°C warmer surface temperature than for the runs with the actual ECC/LCC ratio. From July to September, increasing the LCC fraction boosted evapotranspiration by about 0.2 mm d^{-1} ($LE 0.4 \text{ MJ m}^{-2} \text{ d}^{-1}$) and decreased the H value by about $0.3 \text{ MJ m}^{-2} \text{ d}^{-1}$ (Table 8). The largest half-hourly differences occurred in August (DOY 213–243, Fig. 8), amounting to $+40$ and -30 W m^{-2} for LE and H , respectively. The smallest deviations for both fluxes were recorded in June. Over the July–September period, the higher LE value of the simulation run with the increased LCC fraction cooled the land surface by up to -1°C (Fig. 8). In general over the growing season, increasing the LCC share by 10% led

to an increase in cumulative evapotranspiration, which in turn resulted in a 10 mm lower seasonal water balance (SWB -143 mm).

With regard to the ground heat flux, increasing the LCC fraction led to an up to 10 W m^{-2} higher flux over the noon-time during the second part of the growing season (Fig. 8), whereas early in the season the differences did not exceed 0.2°C (Table 8).

4 Discussion

The comparison of the ECC and LCC simulations confirmed that the GVF and LAI significantly affect the partitioning of surface energy fluxes. The LE value increases with crop growth and peaks when the canopy is fully developed, i.e., has a maximum LAI and GVF. By contrast, the highest H and G values were observed at sparsely covered fields or on the fields with a senescent canopy. During the main growth period of crops, H and G values were quite low. ECC and LCC vary significantly in sowing and harvest date, leaf area and senescence dynamics, water use efficiency, and phenology. Their surface energy fluxes therefore differ distinctly. Our simulation results are in agreement with experimental data of Wizeman et al. (2014) as well as with modeling studies of Sulis et al. (2015), Tsvetsinskaya et al. (2001b), Xue et al. (1996) and Ingwersen et al. (2018).

Simulation results based on ECC and LCC parametrization are in complete harmony with the field observations at

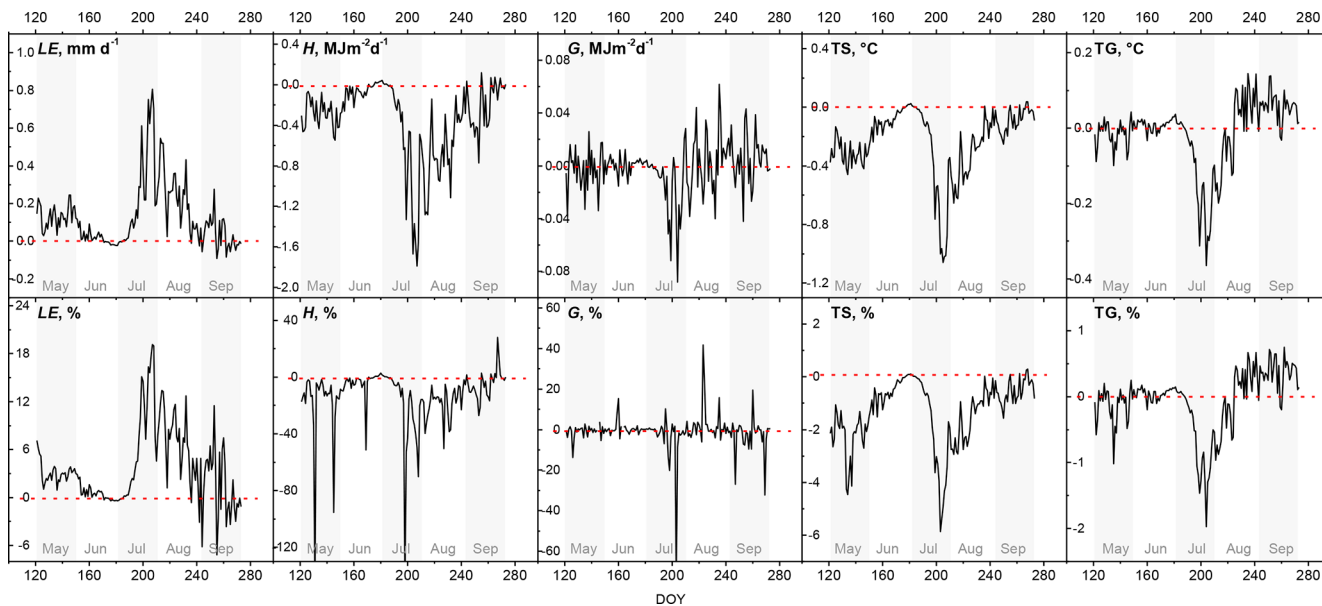


Figure 6. Differences in latent heat flux (LE), sensible heat flux (H), ground heat flux (G), mean surface temperature (TS) and mean ground temperature (TG) between Run 1 and Run 2 simulations (Run 1–Run 2). Given percentages are relative differences between Run 1 and Run 2 simulations.

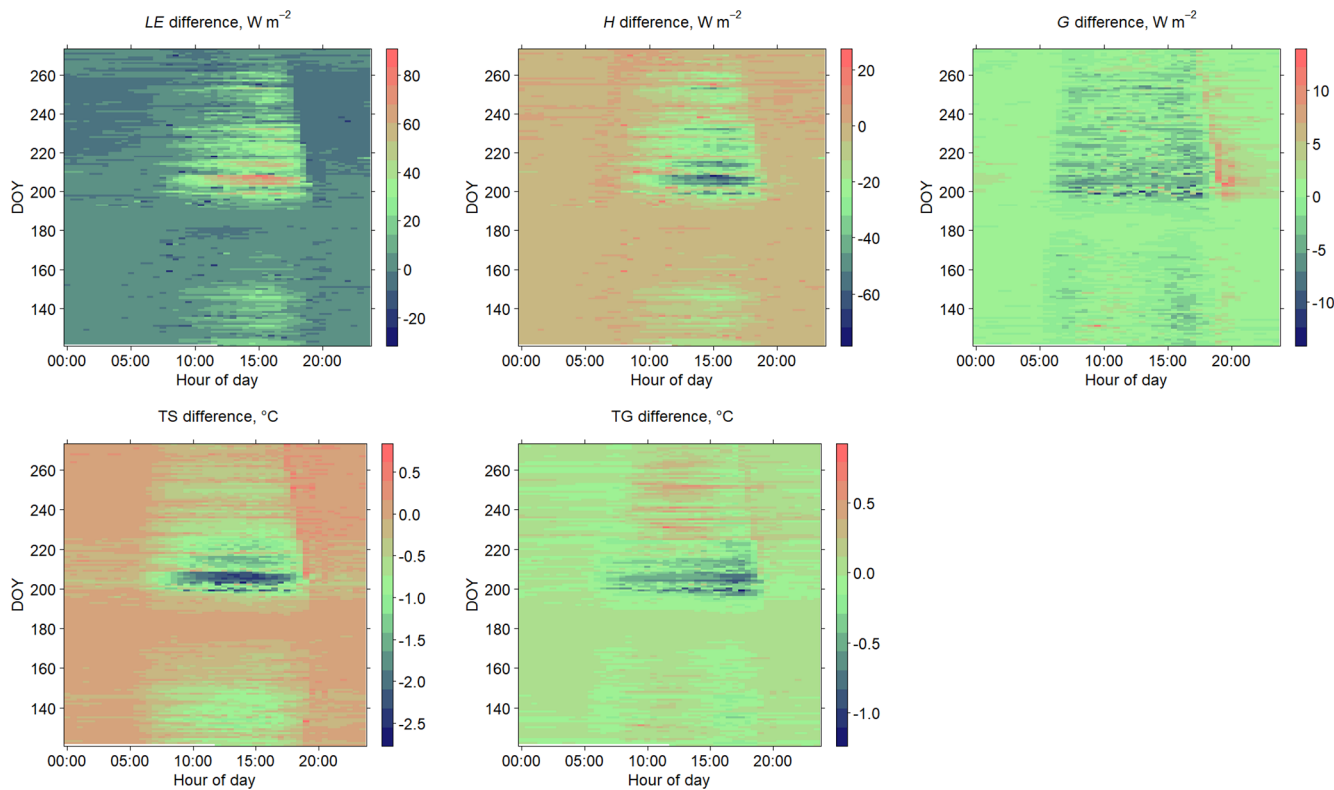


Figure 7. Differences in latent heat flux (LE), sensible heat flux (H), ground heat flux (G), mean surface temperature (TS) and mean ground temperature (TG) between Run 1 (generic crop) and Run 2 (weighted mean of early- and late-covering crops) simulations (Run 1–Run 2). Time is local time.

Table 7. Mean differences in latent heat flux (LE), sensible heat flux (H), ground heat flux (G), surface temperature (TS) and ground temperature (TG) between Run 1 and Run 2 simulations. Numbers in parentheses: the relative difference between Run 1 and Run 2 simulations as a percentage.

Month	DOY	LE		H	G	TS	TG
		(mm d^{-1})	($\text{MJ m}^{-2} \text{d}^{-1}$)				
May	121–151	0.1 (3)	0.3	−0.3 (19)	−0.003 (1)	−0.3 (2)	−0.02 (0.1)
Jun	152–181	0.02 (0.4)	0.04	−0.1 (4)	0.001 (1)	−0.1 (1)	0.01 (0.05)
Jul	182–212	0.3 (7)	0.6	−0.6 (21)	−0.016 (4)	−0.4 (2)	−0.1 (0.6)
Jul*	197–208	0.5 (14)	1.3	−1.2 (46)	−0.034 (10)	−1.0 (4)	−0.2 (1)
Aug	213–243	0.2 (7)	0.5	−0.6 (18)	0.004 (2)	−0.3 (1)	0.01 (0.03)
Sep	244–273	0.03 (1)	0.1	−0.2 (5)	0.005 (3)	−0.1 (1)	0.1 (0.4)
Mean		0.1 (3.7)	0.3	−0.4 (13.2)	−0.002 (1)	−0.2 (1.4)	−0.01 (0.1)

DOY is day of year. * 15–27 July.

Table 8. Mean differences in latent heat flux (LE), sensible heat flux (H), ground heat flux (G), surface temperature (TS) and ground temperature (TG) between simulations with the LCC fraction increased by 10% and the baseline simulation (increased LCC share minus baseline simulation). Numbers in parentheses: the relative difference between increased LCC share and baseline simulation as a percentage.

Month	DOY	LE		H	G	TS	TG
		mm d^{-1}	$\text{MJ m}^{-2} \text{d}^{-1}$				
May	121–151	−0.1 (3.3)	−0.3	0.3 (14)	0.02 (1)	0.3 (2)	0.2 (1)
Jun	152–181	−0.04 (1.0)	−0.1	0.1 (6)	−0.005 (0.5)	0.1 (1)	0.1 (1)
Jul	182–212	0.2 (4.3)	0.4	−0.3 (12)	−0.02 (6)	−0.2 (1)	−0.2 (1)
Aug	213–243	0.2 (7.6)	0.6	−0.5 (17)	−0.01 (1)	−0.3 (2)	−0.2 (1)
Sep	244–273	0.1 (3.8)	0.2	−0.2 (4)	0.01 (4)	−0.2 (1)	−0.1 (1)

DOY is day of year.

our study site. The performance test of Noah-MP on the EC data showed the crop-type-specific sets significantly improve the simulation of latent heat flux at the field scale. In contrast, generic crop parametrization showed less satisfying modeling results. In general, it performed better for winter wheat stand than for maize. Based on the generic crop set, simulation results tend to greatly overestimate the latent heat flux for maize in the beginning of the growing season when the plants are small. In August and September, the latent heat flux was in contrast distinctly underestimated; during this period the maize canopy is fully developed. For wheat, the model overestimates the latent heat flux, particularly during the July–September period, when the winter wheat stand ripened and reached senescence or was harvested.

Besides the vegetation dynamics, the simulated energy and water fluxes depend on additional model settings. Ingwersen et al. (2011) performed a sensitivity study with the Noah model for our study site. They found that among the vegetation parameters the minimum stomatal resistance (RS) and a parameter used in the radiation stress function of the Jarvis scheme (RGL) are the most sensitive parameters. Using constant RS, as it is implemented in Noah, results in the underestimation of sensible heat flux and overestimation of latent

heat flux during the ripening stage of the cereals. Considering a monthly varying RS helped to distinctly improve the simulation of the energy and water fluxes at the land surface. Ingwersen et al. (2010) concluded that integrating the crop growth model which delivers daily RS, LAI and GVF values into Noah would greatly enhance the overall performance of the land surface model. Among the soil parameters, the most sensitive parameters are the soil moisture threshold where transpiration begins to stress (REFSMC), maximum soil moisture content (MAXSMC) and soil moisture threshold where direct evaporation from the top layer ends (DRYSMC). Considering these parameters also has the potential to further improve simulation results.

The potential increase in the LCC fraction (driven by the high demand for biogas and forage production) leads to significant changes in the partitioning of the energy fluxes in croplands. In recent years the total area under maize in Germany has more than doubled. This corresponds to an approximately 10% increase in the LCC fraction for the study region. In the early vegetation period, the altered ECC/LCC ratio leads to a decrease in evapotranspiration, an increase in H and a warmer cropland surface because, during that period, a higher fraction of fields is bare or sparsely cov-

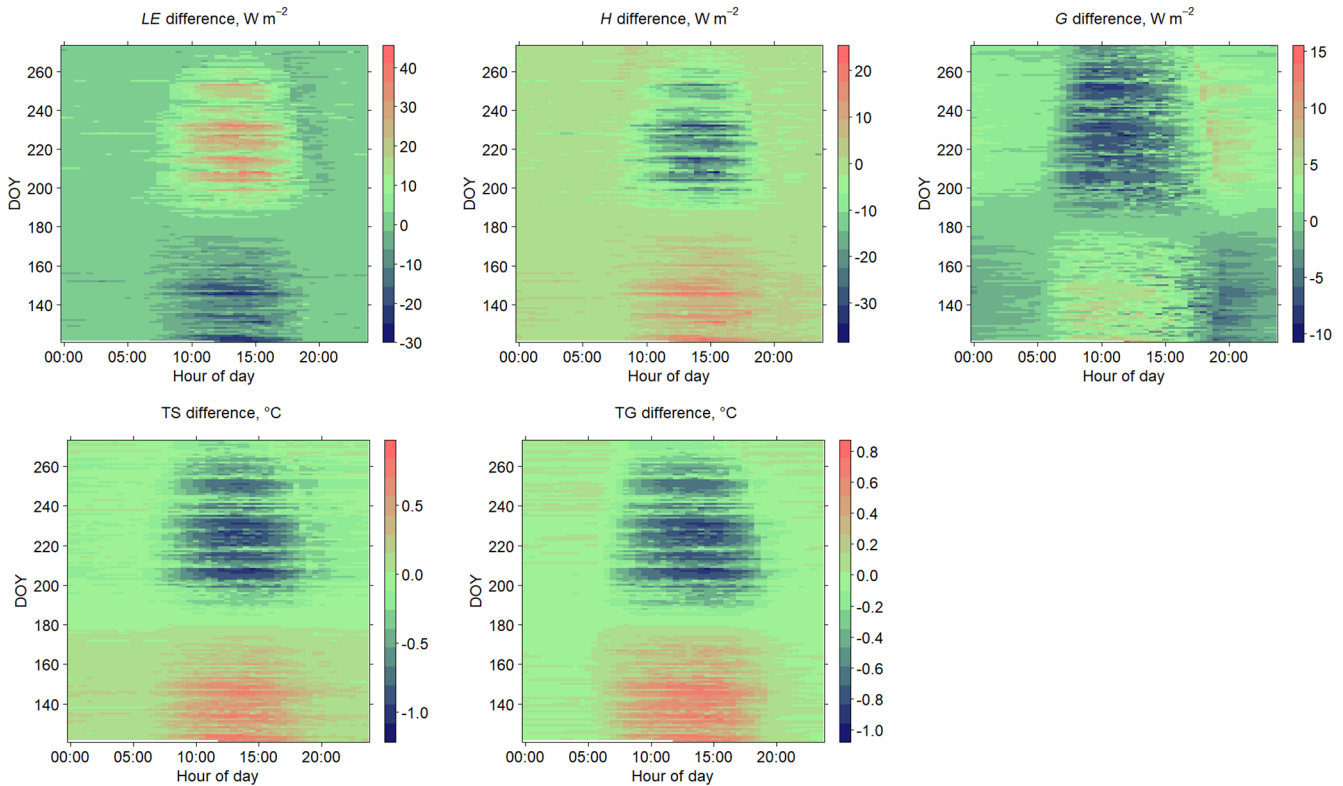


Figure 8. Impact of increasing the LCC fraction from 28 % to 38 % on latent heat flux (LE), sensible heat flux (H), ground heat flux (G), surface temperature (TS) and ground temperature (TG) (increased LCC share minus baseline simulation). Time is local time.

ered with vegetation. In mid-June, the situation reverses. The higher share of LCC boosts LE , decreases H and lowers surface temperatures. The increased evapotranspiration over the growing season, in turn, leads to a lower seasonal water balance.

Comparing the generic crop simulation (Run 1) with the weighted mean of two separate simulations for ECC and LCC (Run 2) showed the largest difference over the second half of the growing season, particularly during late July and early August. In July, ECC become senescent: GVF drops sharply and the green LAI equals zero. In early August, ECC are usually harvested. In contrast, LCC have a developed ground-covering canopy during July–August. Leaves of these crops are still green in September. This transition period is very smooth in the case of the generic crop, resulting on average in about 14 % higher LE and in about 46 %, 10 % and 4 % lower H , G and surface temperature values, respectively, compared with Run 2.

The results presented above apply to the ECC/LCC ratio within our study area. What can we expect in agricultural landscapes with different ECC/LCC ratios? The ECC/LCC ratio has nearly no effect on energy partitioning in June, whereas in May, July and August its influence on the turbulent fluxes is pronounced (Fig. 9). The weak effect in June is because, during this period, the LAI and GVF of

ECC and LCC are similar (Fig. 11). In the other months, however, the ECC/LCC ratio heavily affects the energy partitioning. For example, increasing the LCC share from 10 % to 90 % boosts daily evapotranspiration in August from 2.5 to 4.3 mm d⁻¹, decreases the H value by about 4.1 MJ m⁻² d⁻¹ and cools down the cropland surface by 2 °C. Over the growing season, the increase in the LCC share leads to a general increase in evapotranspiration, which in turn lowers the seasonal water balance (Table 9). Moreover, different ECC/LCC ratios will also affect the above-mentioned humid bias of the generic crop parametrization (Fig. 10). The bias is largest if ECC and LCC shares are balanced (ECC 50 % and LCC 50 %), whereas combinations with one predominant crop distinctly lower the bias. In August, for instance, the differences in LE between the two runs with ECC 50 %–LCC 50 % equal 0.27 mm d⁻¹, while ECC 10 %–LCC 90 % yields differences of 0.09 mm d⁻¹.

Our results show that performing simulations based on single dynamics for each type of crop (ECC and LCC) improve simulations of surface fluxes during transition periods and at the end of the growing season. Lumping ECC and LCC into one land-use class (croplands and pasture), as done in Noah-MP, is an oversimplification. Several authors have demonstrated the necessity to distinguish biophysical plant parameters in substantially different crops to obtain representative

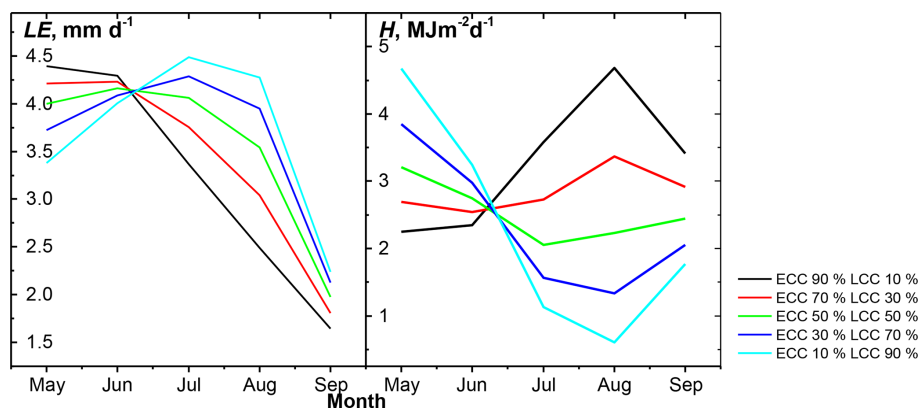


Figure 9. Simulation results of Noah-MP LSM for latent heat flux (LE) and sensible heat flux (H). Simulations were performed considering different shares of ECC and LCC.

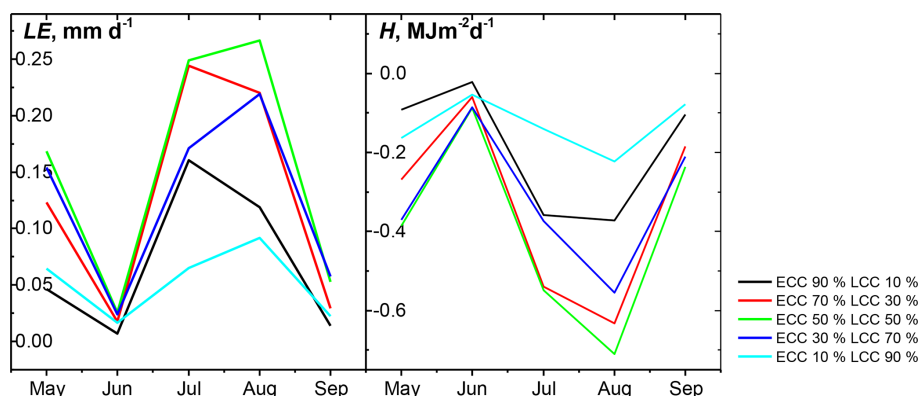


Figure 10. Differences in latent heat flux (LE) and sensible heat flux (H) between Run 1 and Run 2 simulations (Run 1–Run 2). Simulations were performed considering different shares of ECC and LCC.

Table 9. Weather data and simulation results of Noah-MP LSM for cumulative evapotranspiration for the Kraichgau region. Simulations were performed considering different shares of early-covering crops (ECC) and late-covering crops (LCC).

ECC and LCC shares	Total rainfall (R) (mm)	Cumulative evapotranspiration (ET) (mm)	Seasonal water balance ($R-ET$) (mm)
ECC 90 % LCC 10 %	388	496	-108
ECC 70 % LCC 30 %	388	522	-134
ECC 50 % LCC 50 %	388	544	-156
ECC 30 % LCC 70 %	388	557	-169
ECC 10 % LCC 90 %	388	563	-175

simulation results in the lower atmosphere (Sulis et al., 2015; Tsvetsinskaya et al., 2001b; Xue et al., 1996). They have showed that high-resolution spatial information on various croplands and associated physiological characterizations can significantly improve the simulations of land surface energy fluxes, leading to better weather and climate predictions.

Changes in the LAI and GVF with plant growth lead to changes in surface albedo, bulk canopy conductance and roughness length, which in turn alter the partitioning of surface energy fluxes (Chen and Xie, 2011, 2012; Crawford et al., 2001; Tsvetsinskaya et al., 2001a; Xue et al., 1996). Such altered energy partitioning at the land surface then changes the thermodynamic state of the atmospheric boundary layer with regard to air temperature, surface vapor pressure, relative humidity and finally rainfall (Chen and Xie, 2012; McPherson and Stensrud, 2005; Sulis et al., 2015; Tsvetsinskaya et al., 2001b). The observed differences between Run 1 and crop-type-based runs will most probably influence the simulated processes in the ABL. For instance, Sulis et al. (2015) significantly improved the simulations of land surface energy fluxes by using the crop-specific physiological characteristics of the plant. They observed a difference of about 40 % between simulated fluxes using the generic and crop-specific parameter sets. The differences in the land surface energy partitioning led to different heat and moisture budgets of the atmospheric boundary layer for the generic and specific (sugar beet and winter wheat) croplands.

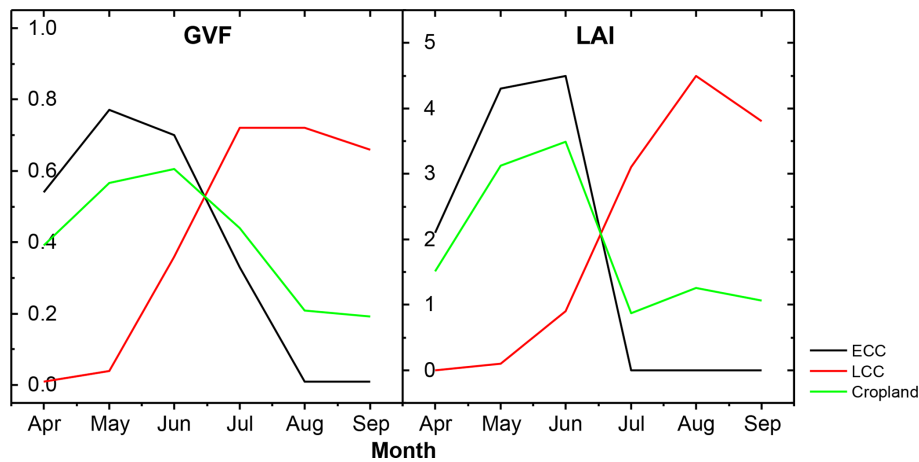


Figure 11. GVF and LAI dynamics of early-covering crops (ECC), late-covering crops (LCC) and cropland.

In the case of specific croplands, particularly sugar beet, those authors observed a larger contribution of the entrainment zone to the heat budget of the ABL as well as a shallower ABL.

McPherson and Stensrud (2005) examined the impact of directly substituting the tallgrass prairie land use class with winter wheat on the formation of the ABL. These crops have different growing seasons. In the US Great Plains, native prairie tallgrass mainly grows in summer, while winter wheat grows throughout winter and reaches maturity in late spring. Simulations showed a larger LE value and lower H value over the area with the winter wheat stand in comparison with tallgrass. By 21:00 UTC, LE ranged from 300 to 400 $W m^{-2}$ for the wheat run and from 200 to 275 $W m^{-2}$ for the tallgrass run. H ranged from 25 to 125 $W m^{-2}$ for the former and from 100 to 200 $W m^{-2}$ for the latter. Substituting tallgrass prairie with winter wheat boosted the atmospheric moisture near the surface upstream and downstream of the study area, and resulted in a shallower ABL upstream and downstream of this area. The shallower ABL reduced the entrainment of higher-momentum air into the ABL and therefore led to weaker winds within the ABL.

Milovac et al. (2016) performed six simulations at a 2 km resolution with two local and two nonlocal ABL schemes combined with two LSMs (Noah and Noah-MP) to study the influence of energy partitioning at the land surface on the ABL evolution on a diurnal scale. They observed that LE values simulated by Noah-MP were more than 50% lower than that simulated by Noah. As expected, a lower LE value resulted in a drier ABL. The ABL evolution and its features strongly influence the initiation of convection and cloud formation as well as the location and strength of precipitation. For instance, a drier and higher ABL would yield a higher lifting condensation level, leading to higher clouds and a higher probability of convective precipitation.

5 Conclusions

The GVF and LAI significantly affect the simulation of energy partitioning, yielding pronounced differences between simulated surface energy and water fluxes and temperatures of ECC and LCC. In our study area, the use of a generic crop parametrization (croplands and pasture in Noah-MP) resulted in a humid bias along with lower surface temperatures. This humid bias will be largest in landscapes with a balanced share of ECC and LCC, whereas in landscapes in which one of the two crop types predominate, the bias will be weaker. We observed the strongest effects on turbulent fluxes over the second part of the season, particularly in July–August. During this period, ECC are at the senescence growth stage or already harvested, while LCC have a fully developed ground-covering canopy. We therefore expect that the observed differences will impact the simulation of processes in the ABL. Our results show that splitting up croplands into ECC and LCC can improve LSMs, particularly during transition periods and late in the growing season.

Increasing the LCC fraction by 10% reduces evapotranspiration and increases surface temperatures over the first part of the growing season. Later in the season, this land use change leads to the opposite situation: increased evapotranspiration accompanied by a slight cooling of the land surface. Over the growing season, an increase in the LCC share by 10% leads to higher cumulative evapotranspiration, which in turn lowers the seasonal water balance.

Data availability. Data is available at <https://doi.org/10.1594/PANGAEA.916167> (Bohm et al., 2020).

Author contributions. The present study was a part of subproject P2, Soil–plant–atmosphere interactions at the regional scale, of the research unit 1695, Agricultural Landscapes under Global Climate

Change – Processes and Feedbacks on a Regional Scale. TS is the primary investigator of this project and the supervisor of the present study. KB and experienced land surface modeler JI designed the modeling study. JM provided expertise in weather and climate modeling. KB performed the Noah-MP simulations and prepared the manuscript with contributions from all coauthors.

Competing interests. The authors declare that they have no conflict of interest.

Review statement. This paper was edited by Paul Stoy and reviewed by two anonymous referees.

References

- Bohm, K., Ingwersen, J., Milovac, J., and Streck, T.: Noah-MP simulated surface energy fluxes and temperature for a generic crop, early covering crops (ECC) and late covering crops (LCC) for Kraichgau region, southwest Germany, PANGAEA, <https://doi.org/10.1594/PANGAEA.916167>, 2020.
- Chen, F. and Xie, Z.: Effects of crop growth and development on land surface fluxes, *Adv. Atmos. Sci.*, 28, 927–944, 2011.
- Chen, F. and Xie, Z.: Effects of crop growth and development on regional climate: A case study over East Asian monsoon area, *Clim. Dynam.*, 38, 2291–2305, 2012.
- Crawford, T. M., Stensrud, D. J., Mora, F., Merchant, J. W., and Wetzel, P. J.: Value of incorporating satellite-derived land cover data in MM5/PLACE for simulating surface temperatures, *J. Hydrometeorol.*, 2, 453–468, 2001.
- El Maayar, M., Chen, J. M., and Price, D. T.: On the use of field measurements of energy fluxes to evaluate land surface models, *Ecol. Model.*, 214, 293–304, 2008.
- Fachagentur Nachwachsende Rohstoffe e.V.: Anbau und Verwendung nachwachsender Rohstoffe in Deutschland, report number: FKZ 22004416, available at: <http://www.fnrserver.de/ftp/pdf/berichte/22004416.pdf> (last access: November 2019), 2019.
- Falge, E., Baldocchi, D., Olson, R., Anthoni, P., Aubinet, M., Bernhofer, C., Burba, G., Ceulemans, R., Clement, R., Dolman, H., Granier, A., Gross, P., Grünwald, T., Hollinger, D., Jensen, N., Katul, G., Keronen, P., Kowalski, A., Lai, C. T., Law, B. E., Meyers, T., Moncrieff, J., Moors, E., Munger, J. W., Pilegaard, K., Rannik, Ü, Rebmann, C., Suyker, A., Tenhunen, J., Tu, K., Verma, S., Vesala, T., Wilson, K., and Wofsy, S.: Gap filling strategies for defensible annual sums of net ecosystem exchange, *Agr. Forest Meteorol.*, 107, 43–69, 2001.
- Ghilain, N., Arboleda, A., Sepulcre-Cantó, G., Batelaan, O., Ardö, J., and Gellens-Meulenberghs, F.: Improving evapotranspiration in a land surface model using biophysical variables derived from MSG/SEVIRI satellite, *Hydrol. Earth Syst. Sci.*, 16, 2567–2583, <https://doi.org/10.5194/hess-16-2567-2012>, 2012.
- Gutman, G. and Ignatov, A.: The derivation of the green vegetation fraction from NOAA/AVHRR data for use in numerical weather prediction models, *Int. J. Remote Sens.*, 19, 1533–1543, 1998.
- Huyghe, C., De Vlieghe, A., van Gils, B., and Peeters, A.: Grassland and herbivore production in Europe and effects of common policies, Editions Quae, Versailles, 323 pp., <https://doi.org/10.35690/978-2-7592-2157-8>, 2014.
- Imukova, K., Ingwersen, J., and Streck, T.: Determining the spatial and temporal dynamics of the green vegetation fraction of croplands using high-resolution RapidEye satellite images, *Agr. Forest Meteorol.*, 206, 113–123, 2015.
- Imukova, K., Ingwersen, J., Hevart, M., and Streck, T.: Energy balance closure on a winter wheat stand: comparing the eddy covariance technique with the soil water balance method, *Biogeosciences*, 13, 63–75, <https://doi.org/10.5194/bg-13-63-2016>, 2016.
- Ingwersen, J., Steffens, K., Högy, P., Warrach-Sagi, K., Zhunusbayeva, D., Poltoradnev, M., Gäbler, R., Wizemann, H.-D., Fangmeier, A., Wulfmeyer, V., and Streck, T.: Comparison of Noah simulations with eddy covariance and soil water measurements at a winter wheat stand, *Agr. Forest Meteorol.*, 151, 345–355, 2011.
- Ingwersen, J., Imukova, K., Högy, P., and Streck, T.: On the use of the post-closure methods uncertainty band to evaluate the performance of land surface models against eddy covariance flux data, *Biogeosciences*, 12, 2311–2326, <https://doi.org/10.5194/bg-12-2311-2015>, 2015.
- Ingwersen, J., Högy, P., Wizemann, H. D., Warrach-Sagi, K., and Streck, T.: Coupling the land surface model Noah-MP with the generic crop growth model Gecros: Model description, calibration and validation, *Agr. Forest Meteorol.*, 262, 322–339, <https://doi.org/10.1016/j.agrformet.2018.06.023>, 2018.
- Koster, R. D., Guo, Z., Dirmeyer, P. A., Bonan, G., Chan, E., Cox, P., Davies, H., Gordon, C. T., Kanae, S., Kowalczyk, E., Lawrence, D., Liu, P., Lu, C. H., Malyshev, S., McAvaney, B., Mitchell, K., Mocko, D., Oki, T., Oleson, K. W., Pitman, A., Sud, Y. C., Taylor, C. M., Verseghy, D., Vasic, R., Xue, Y., and Yamada, T.: GLACE: The Global Land-Atmosphere Coupling Experiment, Part I: Overview, *J. Hydrometeorol.*, 7, 590–610, 2006.
- Lhomme, J. T. and Chehbouni, A.: Comments on dual-source vegetation-atmosphere transfer models, *Agr. Forest Meteorol.*, 94, 269–273, 1999.
- Margulis S. A. and Entekhabi, D.: Feedback between the Land Surface Energy Balance and Atmospheric Boundary Layer Diagnosed through a Model and Its Adjoint, *J. Hydrometeorol.*, 2, 599–620, 2001.
- Mauder M. and Foken. T.: Documentation and Instruction Manual of the Eddy-Covariance Software Package TK3, Arbeitsergebnisse Nr. 46, Universität Bayreuth, Abteilung Mikrometeorologie, Bayreuth, 60 pp., 2011.
- Mauder, M., Cuntz, M., Drüe, C., Graf, A., Rebmann, C., Schmid, H. P., Schmidt, M., and Steinbrecher, R.: A strategy for quality and uncertainty assessment of long-term eddy-covariance measurements, *Agr. Forest Meteorol.*, 169, 122–135, 2013.
- McPherson, R. A. and Stensrud, D. J.: Influences of a winter wheat belt on the evolution of the boundary layer, *Mon. Weather Rev.*, 133, 2178–2199, 2005.
- Meier, U., Bleiholder, H., Buhr, L., Feller, C., Hack, H., Hess, M., Lancashire, P. D., Schnock, U., Staus, R., Van Den Boom, T., Weber, E., and Zwerger, P.: The BBCH system to coding the phenological growth stages of plants—history and publications, *Journal für Kulturpflanzen*, 61, 41–52, 2009.
- Milovac, J., Warrach-Sagi, K., Behrendt, A., Späth, F., Ingwersen, J., and Wulfmeyer, V.: Investigation of PBL schemes combining the WRF model simulations with scanning water vapor differ-

- ential absorption lidar measurements, *J. Geophys. Res.-Atmos.*, 121, 624–649, 2016.
- Nielsen, J. R., Ebba, D., Hahmann, A. N., and Boegh, E.: Representing vegetation processes in hydrometeorological simulations using the WRF model, DTU Wind Energy, (Riso – PhD; No. 0016(EN)), 128 pp., 2013.
- Niu, G.-Y., Yang, Z.-L., Mitchell, K. E., Chen, F., Ek, M. B., Barlage, M., Kumar, A., Manning, K., Niyogi, D., Rosero, E., Tewari, M., and Xia, Y.: The community Noah land surface model with multiparameterization options (Noah-MP): 1. Model description and evaluation with local-scale measurements, *J. Geophys. Res.-Atmos.*, 116, D12109, <https://doi.org/10.1029/2010JD015139>, 2011.
- Raddatz, R. L.: Evidence for the influence of agriculture on weather and climate through the transformation and management of vegetation: Illustrated by examples from the Canadian Prairies, *Agr. Forest Meteorol.*, 142, 186–202, 2007.
- Refslund, J., Dellwik, E., Hahmann, A. N., Barlage, M. J., and Boegh, E.: Development of satellite green vegetation fraction time series for use in mesoscale modeling: Application to the European heat wave 2006, *Theor. Appl. Climatol.*, 117, 377–392, 2014.
- Rundquist, B. C.: The influence of canopy green vegetation fraction on spectral measurements over native tallgrass prairie, *Remote Sens. Environ.*, 81, 129–135, 2002.
- Santanello Jr., J. A., Peters-Lidard, C. D., Kennedy, A., and Kumar, S. V.: Diagnosing the nature of land-atmosphere coupling: A case study of dry/wet extremes in the U.S. southern Great Plains, *J. Hydrometeorol.*, 14, 3–24, 2013.
- SRU Special Report: Climate Change Mitigation by Biomass, Special Report, The German Advisory Council on the Environment, available at: http://www.umweltrat.de/SharedDocs/Downloads/EN/02_Special_Reports/2007_Special_Report_Climate_Change.pdf?__blob=publicationFile (last access: November 2019), 2007.
- Sulis, M., Langensiepen, M., Shrestha, P., Schickling, A., Simmer, C., and Kollet, S. J.: Evaluating the influence of plant-specific physiological parameterizations on the partitioning of land surface energy fluxes, *J. Hydrometeorol.*, 16, 517–533, 2015.
- Tsvetsinskaya, E. A., Mearns, L. O., and Easterling, W. E.: Investigating the effect of seasonal plant growth and development in three-dimensional atmospheric simulations. Part I: Simulation of surface fluxes over the growing season, *J. Clim.*, 14, 692–709, 2001a.
- Tsvetsinskaya, E. A., Mearns, L. O., and Easterling, W. E.: Investigating the effect of seasonal plant growth and development in three-dimensional atmospheric simulations. Part II: Atmospheric response to crop growth and development, *J. Clim.*, 14, 711–729, 2001b.
- van Heerwaarden, C. C., de Arellano, J. V.-G., Moene, A. F., and Holtslag, A. A. M.: Interactions between dry-air entrainment, surface evaporation and convective boundary-layer development, *Q. J. R. Meteorol. Soc.*, 135, 1277–1291, 2009.
- Wizemann, H.-D., Ingwersen, J., Högy, P., Warrach-sagi, K., Streck, T., and Wulfmeyer, V.: Three year observations of water vapor and energy fluxes over agricultural crops in two regional climates of Southwest Germany, *Meteorol. Z.*, 24, 39–59, 2014.
- Xue, Y., Fennessy, M. J., and Sellers, P. J.: Impact of vegetation properties on U.S. summer weather prediction, *J. Geophys. Res.-Atmos.*, 101, 7419–7430, 1996.

7 General Discussion and Conclusions

The present PhD study was part of the DFG RU 1695 “Regional Climate Change”. The RU framework included plans to develop a land system model in order to study the effects of global climate change on the structure and functions of agricultural landscape at the regional scale. The present PhD study was designed to improve certain aspects of the land surface modeling part of this land system model. The following major problems were investigated: a) the nature of the energy imbalance of EC data over a winter wheat stand and identifying the appropriate post-closure method for the study region; b) improving the GVF parametrization of cropland in the Noah-MP LSMs and c) studying the effect of merging different crop types with various shares into a single generic cropland class on the simulation of land surface exchange processes.

As already discussed in numerous studies, the widely used EC method fails to close the energy balance, which hampers using EC data to parameterize and test LSMs (Charuchittipan et al. 2014, Stoy et al. 2013, Panin and Bernhofer 2008, Foken, 2008, Oncley et al. 2007, Wilson et al. 2002, Twine et al. 2000). Our study region is no exception. From year to year, high energy residuals (>20%) were recorded at the study site. We therefore performed additional independent experiments and tested various post-closure methods to verify and correct the EC turbulent fluxes for use in the Noah-MP LSMs. The results demonstrate that, in our study region, the EC method provides reliable data on latent heat flux and that the measured *LE* flux can therefore be used without adjustments to calibrate and parametrize Noah-MP LSM. Our findings echo the results of several experimental studies in which good agreement was shown between evapotranspiration measured by the EC technique and other independent methods (Schume et al. 2005, Wilson et al. 2001). Based on the current state of knowledge, we suggest adding the missing energy to the sensible heat flux (the *H* post-closure method) at our study site. Discussions are ongoing on the problem of EBC, and numerous experiments have been performed to find the most suitable post-closure method. Nonetheless, the components of the energy residual remain unknown and the recommendation is to investigate this at each study site separately (Gebler et al. 2015, Barr et al. 2012, Wohlfahrt et al. 2010, Cuenca et al. 1997). Closing the energy balance gap can significantly improve the accuracy of Noah-MP, and my thesis therefore recommends a thorough investigation of the nature of the energy balance gap. Several studies have already demonstrated the importance of photosynthetic energy flux, air heat

storage and biomass heat storage in energy balance closure. Considering these minor energy fluxes can improve the EBC by up to 15% (Eshonkulov et al. 2019, Guo et al. 2009, Jacobs et al. 2008, Meyers and Hollinger 2004). The results of my study prompted follow-up research on the energy balance gap at our study site. In the next phase of the RU 1695, more attention was paid to measuring previously neglected energy storage terms such as air heat storage, energy storage in the canopy and energy consumption by photosynthesis. Furthermore, G was determined at various locations within the EC footprint and a harmonic analysis was applied to the measured G data. Results are summarized in Eshonkulov et al. (2019). The authors showed that considering minor storage terms help to increase EBC on average by up to 6.8% in the Kraichgau region. Nonetheless, at least 11% of the available energy was still missing. Eshonkulov also concluded that minor storage terms can contribute substantially to closing the energy balance gap and recommended performing year-round measurements of these terms because some loss of the stored energy is possible during the nongrowing season.

The disadvantages of the coarse resolution of the default GVF grid data of Noah-MP are well-known and are discussed in detail in the literature (Milovac et al. 2016, Nielsen et al. 2013). My thesis presents, for the first time, high-resolution GVF maps derived from RapidEye satellite data for use with Noah-MP. Based on these maps and ground measurements, we studied the GVF dynamics of various crops. At the regional scale, the GVF has a bimodal distribution during the growing seasons due to differences in crop phenology. Crops can be divided into two classes. Early covering crops (ECC), e.g. winter wheat, winter rape, winter barley and spring barley, develop early in spring, achieve maximum green canopy cover by mid-June and are harvested in late summer. Late covering crops (LCC), e.g. corn, silage maize, and sugar beet, are planted in spring, exhibit maximum GVF in July-August and are harvested in autumn. The GVF dynamics as well as LAI dynamics of ECC and LCC vary seasonally and regionally. Moreover, the shares of these crop groups differ from region to region and may change over time, for instance as a result of different economic strategies and decisions.

The present thesis shows that integrating ECC and LCC into a generic cropland class as implemented in Noah-MP is an oversimplification. Generic crop parameterization results in a humid bias along with lower surface temperatures for our study site. The strongest effects on the

turbulent fluxes is observed over the second part of the growing season, particularly in July-August. The results show that the computation of surface energy and water fluxes is improved by considering each group of crops. The performance test of Noah-MP on the EC data showed the generic crop parametrization gives poor modeling results whereas simulated fluxes based on ECC and LCC parametrization were in a complete harmony with the EC measurements at study site. The results echo the finding of other experimental and modeling studies showing that different crop types result in a different partitioning of surface energy fluxes (Wizeman et al. 2014, Ingwersen et al. 2018, Sulis et al. 2015, Tsvetsinskaya et al. 2001, Xue et al. 1996). The use of crop-specific physiological characteristics in the LSMs can significantly improve the computation of the surface energy and water fluxes and therefore ultimately improve the precision of weather and climate models (Sulis et al. 2015, McPherson and Stensrud 2005).

This thesis emphasizes the importance of thoroughly investigating soil-plant-atmosphere interactions. These interactions are the basis for all land surface models. Accordingly, the quality of weather and climate simulations depends on their adequate representation. My thesis underlines that much work has been done to improve our understanding of land surface process, but that many challenges remain to be overcome. I believe this thesis can inspire more people to further investigate soil-plant-atmosphere interactions. Those who accept this challenge should think very critically because there are no ideal models. Moreover, there are no ideal experimental data to validate and parameterize these models. The take-home message: keep paying attention to the results of the models and experiments and continue the important mission of improving our LSMs!

8 References

- Barr, A. G., King, K. M., Gillespie, T. J., den Hartog, G. and Neumann, H. H.: A comparison of Bowen ratio and eddy correlation sensible and latent heat flux measurements above deciduous forest, *Boundary-Layer Meteorol.*, 71, 21-41, 1994.
- Charuchittipan, D., Babel, W., Mauder, M., Leps, J., and Foken, T.: Extension of the Averaging Time in Eddy-Covariance Measurements and Its Effect on the Energy Balance Closure, *Boundary-Layer Meteorol.*, 152, 303-327, 2014.
- Chen, f. and Dudhia, J.: Coupling and advanced land surface-hydrology model with the Penn State-NCAR MM5 modeling system. Part I: Model implementation and sensitivity. *Monthly Weather Review*, 129(4), pp. 569-585, 2001.
- Chen, F. and Xie, Z.: Effects of crop growth and development on land surface fluxes, *Adv. Atmos. Sci.*, 28, 927-944, 2011.
- Cuenca, R. H., Stangel, D. E. and Kelly, S. F.: Soil water balance in a boreal forest, *J. Geophys. Res. D Atmos.*, 102, 29355-29365, 1997.
- Crawford, T. M., Stensrud, D. J., Mora, F., Merchant, J. W. and Wetzell, P. J.: Value of incorporating satellite-derived land cover data in MM5/PLACE for simulating surface temperatures, *J. Hydrometeorol.*, 2, 453-468, 2001.
- Dudhia, J.: A nonhydrostatic version of the Penn State-NCAR mesoscale model: validation tests and simulation of an Atlantic cyclone and cold front. *Monthly Weather Review*, 121(5), pp. 1493-1513, 1993.
- El Maayar, M., Chen, J. M. and Price, D. T.: On the use of field measurements of energy fluxes to evaluate land surface models, *Ecol. Model.*, 214, 293-304, 2008.
- Eshonkulov, R., Poyda, A., Ingwersen, J., Pulatov, A., Streck, T.: Improving the energy balance closure over a winter wheat field by accounting for minor storage terms. *Agricultural and Forest Meteorology*. 264. Pages 283-296, 2019.
- Falge, E., Reth, S., Brüggemann, N., Butterbach-Bahl, K., Goldberg, V., Oltchev, A., Schaaf, S., Spindler, G., Stiller, B., Queck, R., Köstner, B. and Bernhofer, C.: Comparison of surface energy exchange models with eddy flux data in forest and grassland ecosystems of Germany, *Ecol. Model.*, 188, 174-216, 2005.
- Foken, T.: The energy balance closure problem: An overview, *Ecol. Appl.*, 18, 1351-1367, 2008.
- Gayler, S., Ingwersen, J., Priesack, E., Wöhling, T., Wulfmeyer, V. and Streck, T.: Assessing the relevance of subsurface processes for the simulation of evapotranspiration and soil moisture dynamics with CLM3.5: Comparison with field data and crop model simulations, *Environ. Earth Sci.*, 69, 415-427, 2013.

- Gebler, S., Hendricks Franssen, H.-J., Pütz, T., Post, H., Schmidt, M. and Vereecken, H.: Actual evapotranspiration and precipitation measured by lysimeters: A comparison with eddy covariance and tipping bucket, *Hydrol. Earth Syst. Sci.*, 19, 2145-2161, 2015.
- Guo, J. X., Bian, L. G. and Dai, Y. J.: Multiple time scale evaluation of the energy balance during the maize growing season, and a new reason for energy imbalance, *Sci. China Ser. D Earth Sci.*, 52, 108-117, 2009.
- Gutman, G. and Ignatov, A.: The derivation of the green vegetation fraction from NOAA/AVHRR data for use in numerical weather prediction models, *Int. J. Remote Sens.*, 19, 1533-1543, 1998.
- Ingwersen, J., Imukova, K., Högy, P. and Streck, T.: On the use of the post-closure methods uncertainty band to evaluate the performance of land surface models against eddy covariance flux data, *Biogeosciences*, 12, 2311-2326, 2015.
- Ingwersen, J., Steffens, K., Högy, P., Warrach-Sagi, K., Zhunusbayeva, D., Poltoradnev, M., Gäbler, R., Wizemann, H. -D., Fangmeier, A., Wulfmeyer, V. and Streck, T.: Comparison of Noah simulations with eddy covariance and soil water measurements at a winter wheat stand, *Agric. For. Meteorol.*, 151, 345-355, 2011.
- Ingwersen, J., Högy, P., Wizemann, H.-D., Warrach-Sagi, K., Streck, T.: Coupling the land surface model Noah-MP with the generic crop growth model Gecros: Model description, calibration and validation. *Agric. Forest Meteorol.*, in print. 2018
- Jacobs, A. F. G., Heusinkveld, B. G. and Holtslag, A. A. M.: Towards closing the surface energy budget of a mid-latitude grassland, *Boundary-Layer Meteorol.*, 126, 125-136, 2008.
- Koster, R. D., Guo, Z., Dirmeyer, P. A., Bonan, G., Chan, E., Cox, P., Davies, H., Gordon, C. T., Kanae, S., Kowalczyk, E., Lawrence, D., Liu, P., Lu, C., Malyshev, S., McAvaney, B., Mitchell, K., Mocko, D., Oki, T., Oleson, K. W., Pitman, A., Sud, Y. C., Taylor, C. M., Versegny, D., Vasic, R., Xue, Y. and Yamada, T.: GLACE: The Global Land-Atmosphere Coupling Experiment. Part I: Overview, *J. Hydrometeorol.*, 7, 590-610, 2006.
- Mauder, M. and Foken, T.: Impact of post-field data processing on eddy covariance flux estimates and energy balance closure, *Meteorol. Z.*, 15, 597-609, 2006.
- Meyers, T. P. and Hollinger, S. E.: An assessment of storage terms in the surface energy balance of maize and soybean, *Agric. For. Meteorol.*, 125, 105-115, 2004.
- McPherson, R. A. and Stensrud, D. J.: Influences of a winter wheat belt on the evolution of the boundary layer, *Mon. Weather Rev.*, 133, 2178-2199, 2005.
- Milovac, J., Warrach-Sagi, K., Behrendt, A., Späth, F., Ingwersen, J., Wulfmeyer, V.: Investigation of PBL schemes combining the WRF model simulations with scanning water vapor differential absorption laser measurements, *J. Geophys. Res. Atmos.*, 121, 2016.

- Nielsen, J. R., Ebba, D., Hahmann, A. N., Boegh E.: Representing vegetation processes in hydrometeorological simulations using the WRF model, DTU Wind Energy, 128 p., 2013.
- Niu, G., Yang, Z., Mitchell, K. E., Chen, F., Ek, M. B., Barlage, M., Kumar, A., Manning, K., Niyogi, D., Rosero, E., Tewari, M. and Xia, Y.: The community Noah land surface model with multiparameterization options (Noah-MP): 1. Model description and evaluation with local-scale measurements, *J. Geophys. Res. D Atmos.*, 116, 2011.
- Oncley, S. P., Foken, T., Vogt, R., Kohsiek, W., DeBruin, H. A. R., Bernhofer, C., Christen, A., van Gorsel, E., Grantz, D., Feigenwinter, C., Lehner, I., Liebenthal, C., Liu, H., Mauder, M., Pitacco, A., Ribeiro, L. and Weidinger, T.: The energy balance experiment EBEX-2000. Part I: Overview and energy balance, *Boundary-Layer Meteorol.*, 123, 1-28, 2007.
- Panin, G. N. and Bernhofer, C.: Parametrization of turbulent fluxes over inhomogeneous landscapes, *Izv. Atmos. Ocean Phys.*, 44, 701-716, 2008.
- Refslund, J., Dellwik, E., Hahmann, A. N., Barlage, M. J. and Boegh, E.: Development of satellite green vegetation fraction time series for use in mesoscale modeling: Application to the European heat wave 2006, *Theor. Appl. Climatol.*, 117, 377-392, 2014.
- Rundquist, B.C.: The influence of canopy green vegetation fraction on spectral measurements over native tallgrass prairie. *Remote Sensing of Environment*, 81(1), pp. 129-135, 2002.
- Santanello Jr., J. A., Peters-Lidard, C. D., Kennedy, A. and Kumar, S. V.: Diagnosing the nature of land-atmosphere coupling: A case study of dry/wet extremes in the U.S. southern Great Plains, *J. Hydrometeorol.*, 14, 3-24, 2013.
- Schume, H., Hager, H. and Jost, G.: Water and energy exchange above a mixed European Beech - Norway Spruce forest canopy: A comparison of eddy covariance against soil water depletion measurement, *Theor. Appl. Climatol.*, 81, 87-100, 2005.
- Skamarock, W.C., Klemp, J.B., Dudhia, J., Gill, D.O., Barker, D.M., Duda, M.G., Huang, X.Y., Wang, W. and Powers, J.G.: A description of the Advanced Research WRF Version 3. NCAR Tech Notes-475+STR, 2008.
- Stoy, P. C., Mauder, M., Foken, T., Marcolla, B., Boegh, E., Ibrom, A., Arain, M. A., Arneth, A., Aurela, M., Bernhofer, C., Cescatti, A., Dellwik, E., Duce, P., Gianelle, D., van Gorsel, E., Kiely, G., Knohl, A., Margolis, H., Mccaughey, H., Merbold, L., Montagnani, L., Papale, D., Reichstein, M., Saunders, M., Serrano-Ortiz, P., Sottocornola, M., Spano, D., Vaccari, F. and Varlagin, A.: A data-driven analysis of energy balance closure across FLUXNET research sites: The role of landscape scale heterogeneity, *Agric. For. Meteorol.*, 171-172, 137-152, 2013.
- Sulis, M., Langensiepen, M., Shrestha, P., Schickling, A., Simmer, C. and Kollet, S. J.: Evaluating the influence of plant-specific physiological parameterizations on the partitioning of land surface energy fluxes, *J. Hydrometeorol.*, 16, 517-533, 2015.

Tsvetsinskaya, E. A., Mearns, L. O. and Easterling, W. E.: Investigating the effect of seasonal plant growth and development in three-dimensional atmospheric simulations. Part I: Simulation of surface fluxes over the growing season, *J. Clim.*, 14, 692-709, 2001a.

Tsvetsinskaya, E. A., Mearns, L. O. and Easterling, W. E.: Investigating the effect of seasonal plant growth and development in three-dimensional atmospheric simulations. Part II: Atmospheric response to crop growth and development, *J. Clim.*, 14, 711-729, 2001b.

van Heerwaarden, C. C., de Arellano, J. V. -, Moene, A. F. and Holtslag, A. A. M.: Interactions between dry-air entrainment, surface evaporation and convective boundary-layer development, *Q. J. R. Meteorol. Soc.*, 135, 1277-1291, 2009.

Twine, T. E., Kustas, W. P., Norman, J. M., Cook, D. R., Houser, P. R., Meyers, T. P., Prueger, J. H., Starks, P. J. and Wesely, M. L.: Correcting eddy-covariance flux underestimates over a grassland, *Agric. For. Meteorol.*, 103, 279-300, 2000.

Wilson, K., Goldstein, A., Falge, E., Aubinet, M., Baldocchi, D., Berbigier, P., Bernhofer, C., Ceulemans, R., Dolman, H., Field, C., Grelle, A., Ibrom, A., Law, B. E., Kowalski, A., Meyers, T., Moncrieff, J., Monson, R., Oechel, W., Tenhunen, J., Valentini, R. and Verma, S.: Energy balance closure at FLUXNET sites, *Agric. For. Meteorol.*, 113, 223-243, 2002.

Wilson, K. B., Hanson, P. J., Mulholland, P. J., Baldocchi, D. D. and Wullschleger, S. D.: A comparison of methods for determining forest evapotranspiration and its components: Sap-flow, soil water budget, eddy covariance and catchment water balance, *Agric. For. Meteorol.*, 106, 153-168, 2001.

Wizemann, H.-D., Ingwersen, J., Högy, P., Warrach-Sagi, K., Streck, T. and Wulfmeyer, V.: Three year observations of water vapor and energy fluxes over agricultural crops in two regional climates of Southwest Germany. *Meteorol. Z.*, 2014.

Wohlfahrt, G., Irschick, C., Thalinger, B., Hörtnagl, L., Obojes, N. and Hammerle, A.: Insights from independent evapotranspiration estimates for closing the energy balance: A grassland case study, *Vadose Zone J.*, 9, 1025-1033, 2010.

Xue, Y., Fennessy, M. J. and Sellers, P. J.: Impact of vegetation properties on U.S. summer weather prediction, *J. Geophys. Res. D Atmos.*, 101, 7419-7430, 1996.

Acknowledgments

I am very grateful to:

The Iamonet Erasmus Mundus Scholarship Program and personally Jochem Gieraths, who chose me among other Russian students to do research at the University of Hohenheim, and Prof. Dr. Stekolnikov K.Y., who supervised me at VSAU and encouraged me to participate in this program.

Prof. Dr. Thilo Streck for giving me an opportunity to work in the subproject P2 of the DFG Research Unit 1695 “Global Climate Change”, for encouraging and supervising the work this thesis is based upon.

Dr. Joachim Ingwersen for the endless support, patient guidance and encouragement. During my years in Hohenheim, I have improved my research skills considerably and mostly thanks to Dr. Joachim Ingwersen. Joachim, thank you for everything: from bringing cold water on a hot day during a soil sampling campaign up to guiding me through all research processes and introducing me to an incredible world of programming!

Prof. Dr. Volker Wulfmeyer and Prof. Dr. Andreas Fangmeier for investing their time.

Sybille Schulz for helping with numerous administrative issues.

Benedikt Prechter, our technical assistant, who visited with me weekly the study site and helped to keep the EC stations running.

Maxim Poltoradnev and Benedikt Prechter for the great help in conducting the soil sampling campaigns and installing the soil moisture network.

Michael Stachowitsch, for English language editing my manuscripts and the present thesis.

All my Hohenheim colleagues from all over the world throughout the years for a warm working atmosphere, helpful discussions and delicious food.

My family and friends for supporting me all these years. I am especially thankful to my dear husband, Sascha: without you, I would probably never have gotten this far, thank you for believing in me and supporting me all these years. And finally, I would like to thank my little boy. My dear son, you are my greatest motivation to move further, love you!

Curriculum Vitae

Name: Kristina Bohm (born Imukova)
 City: Schwetzingen, Germany
 Date of birth: 20.10.1988
 Marital status: Married

Education

Sep 2011 – May 2015 PhD student
Institute of Soil Science and Land Evaluation, Biogeophysics, University of Hohenheim, Stuttgart, Germany

Sep 2005 – Jun 2010 Diploma in Agrochemistry and Soil Science
Voronezh State Agricultural University, Voronezh, Russia

Publications

Publications, included in the doctoral thesis:

Bohm, K., Ingwersen, J., Milovac, J., Högy, P., Streck, T.; 2020. Distinguishing between early and late covering crops in the land surface model Noah-MP: Impact on simulated surface energy fluxes and temperature. *Biogeosciences*, 17, 2791–2805. <https://doi.org/10.5194/bg-17-2791-2020>

Imukova, K., Ingwersen, J., Hevart, M., Streck, T.; 2016. Energy balance closure on a winter wheat stand: comparing the eddy covariance technique with the soil water balance method. *Biogeosciences* 13, 63–75. <https://doi.org/10.5194/bg-13-63-2016>.

Imukova, K., Ingwersen, J., Streck, T.; 2015. Determining the spatial and temporal dynamics of the green vegetation fraction of croplands using high-resolution RapidEye satellite images. *Agric.For.Meteorol.* 206, 113–123. <https://doi.org/10.1016/j.agrformet.2015.03.003>.

Other publications:

Poltoradnev, M., Ingwersen, J., Imukova, K., Högy, P., Wizemann, H., Streck, T.; 2018: How Well Does Noah-MP Simulate the Regional Mean and Spatial Variability of Topsoil Water Content in Two Agricultural Landscapes in Southwest Germany? *Journal of Hydrometeorology*, 19, 555–573. <https://journals.ametsoc.org/doi/10.1175/JHM-D-17-0169.1>

Ingwersen, J., Imukova, K., Högy, P., Streck, T.; 2015. On the use of the post-closure methods uncertainty band to evaluate the performance of land surface models against eddy covariance flux data. *Biogeosciences* 12, 2311–2326. <https://doi.org/10.5194/bg-12-2311-2015>

Oral presentations

Imukova, K., Ingwersen, J., Streck, T. (2014) Estimating Green Vegetation Fraction (GVF) of croplands in Southwest Germany using high-resolution RapidEye satellite data. Bodenkundliches Kolloquium SS 2014, Institut für Bodenkunde und Standortslehre (310), Stuttgart, Germany

Imukova, K., Ingwersen, J., Streck, T. (2014) Determining the green vegetation fraction from RapidEye data for use in regional climate simulations. 6 RESA (RapidEye Science Archive) Workshop 2014, 05-06 May 2014, Deutsches Zentrum für Luft- und Raumfahrt, Bonn, Germany

Imukova, K., Ingwersen, J., Streck, T. (2013) Remote sensing of the Green Vegetation Fraction based on high-resolution RapidEye satellite images for use in regional climate simulations. Jahrestagung der Deutschen Bodenkundlichen Gesellschaft, 7-12 September 2013, University of Rostock, Germany

Imukova, K., Ingwersen, J., Streck, T. (2013) An energy balance closure experiment on a winter wheat stand: Eddy covariance technique compared with the soil water balance method. International Symposium on Patterns in SiVegetation-Atmosphere-Systems: Monitoring, Modeling and Data Assimilation. 11-14 March 2013, University of Bonn, Germany

Poster presentations

Imukova, K., Ingwersen, J., Streck, T. (2015) An improved parametrization of the green vegetation fraction of croplands for the application in regional climate simulations. Conference, Integrated Hydrosystem Modeling, 7-10 April 2015, University of Tübingen, Germany

Imukova, K., Ingwersen, J., Streck, T. (2014) Monitoring of the Spatial Distribution and Temporal Dynamics of the Green Vegetation Fraction of Croplands in Southwest Germany Using High-Resolution RapidEye Satellite Images. European Geosciences Union General Assembly 2014. 27 April – 02 May 2014, Vienna, Austria

Schwetzingen 19.11.19